PHYSIOLOGICAL CONSEQUENCES OF INCREASED PHOSPHORYLATION-DEPENDENT ACTIVATION OF GUANYLYL CYCLASE-A AND -B

A Dissertation
SUBMITTED TO THE FACULTY OF
UNIVERSITY OF MINNESOTA
BY

Brandon Mark Wagner

IN PARTIAL FULFILLMENT OF THE REQUIRMENTS
FOR THE DEGREE OF
DOCTOR OF PHILOSOPHY

Advisor: Dr. Lincoln R. Potter

March 2022

ACKNOWLEDGEMENTS

My parents, you have always supported me and my decisions. You encouraged me to think for myself and cautioned against idealizing others. You enabled the development of my own curiosity and taught me the importance of retaining my imagination that is too often lost in adulthood. Mom and dad, your genetics and parenting created the mold with which I could become the scientist I am today.

Lincoln, thank you for being the mentor I needed. Our conversations and my experience in your lab made me a better scientist. I am not certain about anything in life, but because of you I am most confident in my ability to look at the data and (eventually) get the right answer. In the words of Richard Feynman, you instilled in me this lesson: “The first principle is that you must not fool yourself and you are the easiest person to fool.”

Jerid, you were the mentor and friend I did not know I needed. I cannot tell how much I appreciate the time we shared together, both in and out of the lab. Without your mentorship, I would have been incredibly unproductive. Without your friendship, I would have been lost. Every coffee, beer, or meal we shared means more to me than you thought it did.

O’Connell Lab, my time as an undergraduate in your lab only strengthened my desire to pursue my PhD. Tim, thank you for always speaking your honest opinion and making yourself available to talk with. Chastity, everything solid piece of data I have collected was a direct result of the instruction I received from you at the bench.

Blake, Devin, and Ryan, you have been my closest friends since high school. I am so grateful to have had your support throughout the last 10 years. Although we have all chosen different paths in life, it is extremely comforting to know that we can all get together and find that we have not grown apart.

Janne, as my wife you have had to put up with me the most. You believed in me from the very beginning since we met 10 years ago. I cherish our conversations and have the upmost love and respect for you. I cannot even begin to imagine what graduate school or life would be like without you by my side. You challenge me every day and because of that, I am a better person in all aspects of my life. I am so fortunate to be able to come home to you and our beloved cats, Izzy and Louis, after every great or terrible day in the lab. I cannot wait to see what life has in store for us.

Finally, there is one special acknowledgment I feel would be disingenuous of me to not include here. All the inspiration and motivation I have received from my friends, mentors, professors, and the research of others, pales in comparison to that of which I received from coffee. Every good piece of data or sentence I have written in pursuit of my PhD was preceded by a good cup of coffee.

ABSTRACT

Guanylyl Cyclase (GC)-A and GC-B are homologous, cell surface, enzyme receptors that catalyze the formation of the second messenger cyclic guanosine monophosphate (cGMP) from guanosine triphosphate (GTP). Atrial natriuretic peptide (ANP) and B-type NP (BNP) bind and activate GC-A, whereas C-type NP (CNP) binds and activates GC-B. GC-A primarily regulates cardiovascular function, which includes decreasing blood pressure, blood volume, and cardiac hypertrophy, but also regulates metabolism, immune function, and hearing. In contrast, GC-B is best known for regulating the female reproductive system and long bone growth, strength, and density.

Both GC-A and GC-B contain an extracellular ligand-binding domain, a single membrane-spanning region, and an intracellular region that consists of a kinase homology regulatory domain (KHD), a helix-loop-helix dimerization domain and C-terminal GC catalytic domain. The KHD is phosphorylated on multiple, conserved serine and threonine residues. Phosphorylation is absolutely required to transduce the ligand-binding activation signal to the catalytic domains of GC-A and GC-B. Dephosphorylation of the KHD inactivates the enzymes and renders them unresponsive to ligand. When I began my studies, little was known about how phosphorylation of these GC receptors regulate physiological processes in animals. In close collaboration with Dr. Laurinda Jaffe's laboratory, our group generated novel, knock-in mouse models that express mutated forms of either GC-A or GC-B that are activated like the phosphorylated wild-type (WT) enzymes but cannot be inactivated by dephosphorylation. These enzymes contain glutamate substitutions for the known phosphorylation sites, which mimic the negative charges of the phosphorylated residues on the WT receptors. However, unlike the WT receptors, the negative charges cannot be enzymatically removed. Hence, the glutamate-substituted enzymes exhibit increased and prolonged natriuretic peptide-dependent GC activity compared to the WT enzymes. Because the GC-A mutant has 8 glutamate substitutions, and the GC-B mutant has 7 glutamate substitutions, the mutated enzymes are called GC-A-8E and GC-B-7E, respectively. Standard double allele screening technology was used to knock in the GC-B-7E construct into each WT locus for the two GC-B alleles to produce the GC-B$^{7E/7E}$ mice. In contrast, CRISPR-CAS9 technology was used to knock in the GC-A-8E construct into the two endogenous alleles for GC-A to make the GC-A$^{8E/8E}$ mice.

My research on these mice revealed demonstrable, physiological consequences of increased phosphorylation-dependent activation of GC-A and GC-B. GC-A$^{8E/8E}$ mice exhibit increased and prolonged cGMP synthesis in the presence ANP and/or BNP, which led to reduced ERK1/2 phosphorylation, reduced cardiomyocyte cross-sectional area, reduced cardiac hypertrophy, and increased systolic function in male, but not female, mice. Regarding GC-B, previous work in the Potter and Jaffe laboratories showed in cell culture that dephosphorylation is required for FGFR3-dependent inhibition of GC-B. My research on the GC-B$^{7E/7E}$ mice indicates that dephosphorylation of GC-B is required for FGFR3-dependent achondroplasia. Furthermore, my work suggests that GC-B-dependent increases in bone formation and bone strength in mice require decreases in osteoclasts as well as increases in osteoblasts and that this only occurs during an early developmental window, which may have significant clinical implications for the treatment of achondroplasia in children and osteoporosis in adults.

TABLE OF CONTENTS

LIST OF TABLES

LIST OF FIGURES

CHAPTER 1: INTRODUCTION TO PHYSIOLOGICAL CONSEQUENCES OF INCREASED PHOSPHORYLATION-DEPENDENT ACTIVATION OF GUANYLYL CYCLASE-A AND -B

NATRIURETIC PEPTIDES AND THEIR MEMBRANE RECEPTORS

The first evidence that cyclic guanosine monophosphate (cGMP) exists in biological systems was reported in 1963 when Ashman and colleagues identified it in rat urine (1). Six years later, the enzymes that catalyze the conversion of guanosine triphosphate (GTP) to cGMP were characterized and purified by multiple investigators (2-5). These enzymes were originally referred to as guanylate cyclases but were later renamed guanylyl cyclases (GC) (6). By 1975, two major categories of GCs were purified. The first category are soluble, heterodimeric-heme-binding forms that are activated by nitric oxide, whereas the second are insoluble, particulate forms that are activated by peptides (7, 8). Two alpha subunits and two beta subunits of the soluble enzyme have been identified, but the function, if any, for the beta2 subunit is unknown. Seven membrane GCs (GC-A, GC-B, GC-C, GC-D, GC-E, GC-F, and GC-G) have been discovered to date in mammals (9).

In 1981, De Bold et al. reported that intravenous injection of atrial homogenates into rats elicited a rapid and remarkable decrease in blood pressure that was accompanied by increased renal excretion of sodium and water (10). This seminal observation led to the purification of several peptides from atrial tissue that possess both natriuretic and smooth-muscle relaxing activity (11-14). These peptides were given several names including atrial natriuretic factor, cardionatrin, cardiodilatin, and atriopeptin. However, the name most often used today is atrial natriuretic peptide (ANP). B-type natriuretic peptide (BNP), originally called brain natriuretic peptide (15), and C-type natriuretic peptide (CNP) (16) were subsequently purified from porcine brain extracts based on their ability to relax smooth muscle. All three peptides contain a highly conserved, 17 amino acid disulfide-linked ring that is required for biological activity (11).

In 1984, ANP was shown to elevate cGMP concentrations in rat tissues, primary cell cultures, and urine (17). That same year, ANP was reported to stimulate particulate, but not soluble, GC activity in various rat tissue homogenates in a manner that correlated with vascular smooth muscle relaxation (18, 19). Subsequently, photoaffinity and/or chemical cross-linking to whole cells or membrane preparations and subsequent fractionation by SDS-PAGE revealed the binding of ^{125}I-labeled ANP to proteins of 60 and 120-140 kDa (20-23). Purification of the smaller 60 kDa protein and cloning of its cDNA predicted a homodimeric receptor with a large extracellular binding domain, a

single membrane-spanning region, and a small 37 amino acid intracellular domain (24, 25). This receptor is known today as the natriuretic peptide clearance receptor (NPR-C) or natriuretic peptide receptor 3 (NPR3). Purification of the larger 120-140 kDa protein revealed that the ANP binding activity cofractionated with GC activity (26-29). This receptor is referred to today as natriuretic peptide receptor-A (NPR-A), natriuretic peptide receptor 1 (NPR1), or most commonly, GC-A. Cloning of the cDNA for GC-A was achieved by probing a rat brain cDNA library with a sea urchin receptor GC homolog and sequence analysis suggested that the ANP-binding and GC domain resided within the same polypeptide (30, 31). A second GC-linked receptor was identified from the same library screen and was named GC-B but is also called natriuretic peptide receptor-B (NPR-B) or natriuretic peptide receptor 2 (NPR2) (32, 33). Subsequently, ligand specificity determined in transfected cells indicated that ANP and BNP bind and stimulate GC-A, whereas CNP binds and stimulates GC-B (34, 35).

Natriuretic peptides

In general, there are three major natriuretic peptides in mammals: ANP, BNP, and CNP. All natriuretic peptides are synthesized as preprohormones. Human preproANP is 151 amino acids in length and cleavage of the N-terminus produces the 126-amino acid proANP. ProANP is the predominant form stored in atrial granules. Upon its secretion, proANP is rapidly cleaved at the cardiomyocytes' surface by the transmembrane cardiac protease corin to form the biologically active carboxyl terminal 28-amino acid peptide (36). Corin-deficient mice have elevated levels of proANP, no detectable levels of ANP, and exhibit spontaneous hypertension (37).

Low amounts of ANP are continuously secreted from atrial myocytes under baseline conditions, however atrial wall stretch resulting from increased intravascular volume stimulates a rapid release of ANP into the coronary sinus where it is efficiently distributed to its various target organs through the circulatory system (38, 39). Additionally, hormones such as endothelin, angiotensin II (ANGII), and arginine-vasopressin have been shown to directly stimulate the release of ANP (40-42). Significantly, plasma ANP levels are elevated 10- to 30-fold in heart failure patients (43). In 1995, mice lacking ANP were generated by Oliver Smithies and colleagues. These mice exhibited hypertension with blood pressures elevated by 27 mmHg, which was initially suggested to be salt-sensitive (44). However, one year later the same group

reported that the blood pressures of the same ANP knock out (KO) mice were not influenced by dietary salt intake (45).

BNP was initially purified from porcine brain extracts and called brain natriuretic peptide based on its ability to relax smooth muscle (15). However, the original name was deemed a misnomer because it was subsequently found in much higher concentrations in cardiac ventricles from patients and animals undergoing cardiac stress. Hence, it is now most often referred to as B-type natriuretic peptide (46). Like ANP, human BNP is synthesized as a 134-amino acid preprohormone that is then cleaved to produce a 108-amino acid prohormone, from which the additional cleavage by an unknown protease results in the 32-residue carboxyl-terminal, biologically active BNP (47, 48).

While BNP is stored in atrial granules with ANP, it is most abundant in ventricles from stressed hearts, such as those from patients with heart failure. BNP is not stored in significant quantities in ventricular granules, but rather is continually secreted and transcriptionally regulated by cardiac wall stretch (46). Plasma BNP concentrations in healthy individuals are low and are approximately one-tenth that of ANP. In contrast, plasma BNP is elevated 200- to 300-fold in patients with heart failure, which makes it a more sensitive diagnostic marker for cardiac stress than ANP (46). Interestingly, mice with genetic deletion of BNP are normotensive, but display exaggerated cardiac fibrosis in response to pressure overload (49). This finding suggests that BNP plays less of an endocrine role in the regulation of blood pressure compared to ANP and functions more as a paracrine regulator of cardiac remodeling under pathological conditions in mice.

CNP was also purified from porcine brain extracts and induced smooth muscle relaxation, but the natriuretic and hypotensive effects were found to be about 100-fold less potent than that of ANP and BNP (16). CNP is the most abundant natriuretic peptide in the brain and is highly expressed in chondrocytes and endothelial cells (50-52). Of the three natriuretic peptides described above, CNP is the most highly conserved, being completely identical at the amino acid level in mice, rats, and humans.

Biologically active CNP exists in both 22- and 53-amino acid forms, which appear to elicit identical responses, although the lengthier version has a longer half-life (53). ProCNP has been shown to be converted to CNP-53 by the intracellular endoprotease furin (54). CNP-53 is the predominant form in the brain, endothelial cells, and heart (55-57). In some tissues, CNP-53 is cleaved to produce CNP-22 by an unknown extracellular protease and is the most abundant form in plasma and cerebral spinal fluid

(56, 58). Plasma CNP levels are low under physiological conditions and, like ANP and BNP, are elevated in patients with heart failure but to a much lesser degree (56, 59). Mouse and human genetic studies have demonstrated that CNP is most critical in the skeleton. For instance, mice lacking CNP are normotensive but display severe dwarfism as a result of impaired endochondral ossification (60), whereas mice with transgenic CNP overexpression exhibit enhanced skeletal growth and possibly accelerated fracture healing (61, 62). In humans, autosomal dominant loss-of-function mutations in CNP result in short stature (63). Conversely, humans with mutations that cause CNP overexpression (64, 65) or bi-allelic loss of function mutations in NPR-C that lead to increased plasma CNP concentrations result in tall stature and skeletal overgrowth (66).

Natriuretic peptide clearance and degradation

All three natriuretic peptides are degraded through two known processes: 1) NPR-C-mediated internalization and subsequent lysosomal degradation, and 2) degradation by neprilysin and other unknown proteases. NPR-C is a disulfide-linked homodimer that is homologous to the extracellular domains of GC-A and GC-B, but contains only 37 intracellular amino acids (67), whereas neprilysin is a membrane-bound enzyme that has broad substrate specificity (68).

The first demonstration of NPR-C-mediated natriuretic peptide clearance was in 1987, which used a ring-deleted ANP analog known as C-ANF$^{4\text{-}23}$ (69). C-ANF$^{4\text{-}23}$ preferentially binds NPR-C over GC-A such that infusion of the analog into anesthetized rats increases endogenous plasma ANP levels by blocking NPR-C-mediated clearance of ANP (69, 70). Since NPR-C binds ANP, BNP, and CNP but has no GC activity, it was hypothesized that the major function of NPR-C is to clear natriuretic peptides from the circulation through receptor-mediated degradation (25). Indeed, mice with NPR-C loss of function mutations display phenotypes associated with increased GC-A activity (dilute urine) and increased GC-B activity (increased skeletal length) (71, 72).

Extracellular proteases have been shown to degrade natriuretic peptides as well. Early studies using renal brush border membranes observed rapid degradation of ANP (73, 74). Subsequent studies identified neprilysin as the major ANP degrading enzyme in the kidney (75). A report comparing the hydrolysis of the three natriuretic peptides by neprilysin found that initial cleavage sites of human ANP and CNP were between the conserved cysteine and phenylalanine residues at the beginning of the ring structures

(76). In contrast, the same report found that human BNP was insensitive to the same enzymatic cleavage between the cysteine and phenylalanine residues and was shown to be a poorer substrate for neprilysin compared to ANP or CNP (76, 77). It is worth noting here that BNP varies greatly between species, whereas ANP and CNP do not exhibit the same degree of interspecies variation (78). The significant variation of BNP between species was shown to be particularly consequential in regard to its degradation by neprilysin. For instance, Dickey and Potter demonstrated that the neprilysin inhibitor phosphoramidon failed to block human BNP degradation by human or rat kidney membranes, whereas the degradation of rat BNP by either membrane preparation was significantly reduced by inhibition of neprilysin (79). This suggests that neprilysin is not a major degrading enzyme of BNP in humans. Consistent with the *in vitro* evidence of neprilysin-mediated degradation of natriuretic peptides, neprilysin inhibitors increase circulating natriuretic peptides in humans and animal models, as well as increase sodium excretion in heart failure patients (80-84). However, with respect to neprilysin-inhibitors in humans, the increase in circulating BNP is likely due to the indirect effects of increased ANP and CNP competing with BNP for NPR-C-mediated clearance and other protease pathways, rather than the direct inhibition of BNP degradation by neprilysin.

Guanylyl cyclase-A and -B

Natriuretic peptides exert their physiological functions through GC-A and GC-B (85). As stated above, GC-A and GC-B are homologous membrane-bound receptor enzymes that exist as homodimers with a large extracellular ligand-binding domain, a single membrane spanning region, and an intracellular kinase homology domain (KHD) and C-terminal GC catalytic domain (86-88). The intracellular regions of the rat forms of GC-A and GC-B are 78% identical at the amino acid level (89), which is consistent with their similar regulation by ATP and phosphorylation (9). Since GC-A was the first mammalian membrane GC cloned, it is the archetypal membrane GC and is the best characterized receptor for natriuretic peptides.

GC-A is highly expressed in kidney, lung, adrenal, brain, liver, vasculature, testis, and adipose tissues (31, 33, 90-93). GC-A protein expression has also been observed at lower, but significant, levels in the heart (94). GC-B is abundantly expressed in brain, lung, bone, heart, and ovary tissue (33, 91, 95). Despite the similarities in structure, function and expression pattern of GC-A and GC-B, early genetic studies demonstrated

diverse physiological effects between the two receptors. For instance, genetic ablation of GC-A in mice results in hypertension and severe cardiac hypertrophy and fibrosis (96, 97). In contrast, mice with GC-B loss of function mutations are normotensive but display achondroplastic-like dwarfism (98, 99).

Activation of guanylyl cyclase-A and -B

In the absence of natriuretic peptides, the GC activity of GC-A and GC-B is tightly repressed. Natriuretic peptide binding to the extracellular domain increases enzyme activity, causing an increase in the rate of intracellular cGMP production. The extracellular domains of both GC-A and GC-B are highly glycosylated and some groups report that glycosylation affects ligand binding and receptor trafficking (100, 101), whereas other groups have found that it does not (102-104). Our group has suggested that glycosylation is required for proper folding, conformation, and phosphorylation of GC-B (105). Although GC-A and GC-B have a growth factor receptor-like topology, ligand binding does not lead to further oligomerization of the receptors (86, 106). Crystallographic studies on the ANP-bound extracellular domain of GC-A indicate that natriuretic peptides bind to their receptors in a 1:2 stoichiometry, which causes an intermolecular twist (107). How the extracellular ligand binding signal is propagated through the intracellular domains is not known.

The ligand binding signal must travel through the membrane and KHD to activate the intracellular GC catalytic domain. While the KHD shares identity with known kinases, our lab has been unable to detect any intrinsic kinase activity for GC-A or GC-B, and mutations of amino acids in these GCs that are known to inactivate most protein kinases, failed to affect the phosphorylation status of GC-A and GC-B (108). Early studies suggested that the KHD represses the activity of the enzyme because receptors lacking the KHD display constitutive GC activity and do not respond to natriuretic peptides (109, 110). Constructs lacking both the extracellular and KHD are also constitutively active (111). Thus, in the absence of ligand, the KHD suppresses enzyme activity and ligand binding to the extracellular domain induces a conformational change that relieves the inhibitory effect of the KHD on the catalytic domains, which results in increased cGMP synthesis. Further investigation on the role of the KHD in GC-A and GC-B established that it is highly phosphorylated and that phosphorylation of the KHD is

required to transmit the hormone binding signal to the catalytic domain, which will be discussed in depth in the next section.

PHOSPHORYLATION-DEPENDENT REGULATION OF MEMBRANE GUANYLYL CYCLASES

Membrane GCs were first shown to be phosphorylated in sea urchin sperm, which was also the first species from which transmembrane GCs were molecularly cloned (112). In 1983, Ward and Vacquier observed that an abundant 160 kDa membrane protein in sea urchin sperm flagellum was constitutively phosphorylated and was rapidly dephosphorylated upon exposure to sea urchin egg jelly (113). Two years later, Garbers and colleagues reported that the GC activity in sea urchin sperm decreased when exposed to an egg jelly-associated peptide and this decrease in activity was associated with a shift in the apparent molecular weight an abundant membrane protein from 160 kDa to 150 KDa. Importantly, the shift in MW was associated with a loss of ^{32}P label from the 160 kDa band (114). However, the conclusion that the activity of the GC was reduced when exposed to the egg jelly peptide was wrong because the initial experiments failed to measure GC activity at very early time points that contained the phosphorylated and more active form of the enzyme. Subsequent back-to-back publications from the same group identified the major 160 kDa protein as a GC and discovered that adding the egg jelly peptide to isolated membrane preparations bound to and, in contrast to their earlier report, activated the enzyme when examined at earlier timepoints (115, 116). This led to the conclusion that the peptide-induced activation of the GC was transient such that initial GC activity was high but rapidly decreases after addition of the peptide if measured at later timepoints. Furthermore, they observed that the peptide-induced increase in GC activity preceded dephosphorylation of the enzyme and that the decrease in enzyme activity was associated with dephosphorylation. As a result of these biochemical studies, a novel paradigm was proposed in which the activation of the enzyme was peptide-mediated, and the extent of its activation was dependent on its phosphorylation state. This was a novel mechanism that opposed the more common, highly reported mechanism of inactivation of the beta-adrenergic receptor studied intensely by the Lefkowitz group (117-121). In 1988, Ramarao and Garbers confirmed the inactivation by dephosphorylation paradigm by demonstrating that purified, phosphorylated enzyme exhibited egg peptide-dependent GC activity that was 5-fold greater than the purified, dephosphorylated form of the enzyme (122).

Phosphorylation-dependent regulation of guanylyl cyclase-A and -B

Shortly thereafter, multiple laboratories began to purify, characterize, and molecularly clone mammalian membrane-bound GCs. Although investigations of the sea urchin membrane GC established that phosphorylation positively regulates the activity of the enzyme, it was not clear whether the mammalian GCs were regulated in the same manner. In fact, initial studies suggested that phosphorylation of GC-A inhibited ANP-dependent activity of the enzyme. Between 1988 and 1990, the group of Rameshwar K. Sharma published four studies suggesting that phosphorylation of GC-A inactivated the enzyme (123-126). The conclusions of these studies were based principally on the correlation between the addition of protein kinase C (PKC) activators, or PKC itself, and decreases in ANP-dependent GC activity in isolated membranes, as well as the ability of phorbol esters to decrease ANP-dependent cGMP elevations in intact cells. These studies either completely failed to (123) or never directly measured GC-A phosphorylation in intact cells (124-126). Importantly, all these studies assumed that phosphorylation mediated the decrease in GC activity since the addition of PKC to isolated membrane preparations reduces ANP-dependent GC activity but again, none of these studies measured receptor phosphate content. Similarly, Larose et al. reported that incubation of purified GC-A from bovine adrenal tissue with the serine/threonine kinases, PKA, PKG and PKC increased the incorporation of ^{32}P into GC-A. They went on to demonstrate that treatment of bovine adrenal zona glomerulosa cells with phorbol esters to activate PKC also increased incorporation of ^{32}P into GC-A, which was associated with a decrease in ANP-dependent GC activity (127). These meretricious studies were published at the time when it was becoming clear that many of the more common seven-membrane-spanning cell surface receptors were desensitized by phosphorylation (128, 129). Hence, their conclusions were harmonious with the existing precedent. However, the initial desensitization of GC-A by phosphorylation model was completely inconsistent with reports of GC regulation in the sea urchin sperm.

In 1992, in contrast to all previous reports, Potter and Garbers published the first study where receptor phosphate content and enzymatic activity were measured in the same enzyme preparation at the same time. They observed that in resting human embryonic kidney (HEK) 293 cells that were stably overexpressing rat GC-A, the enzyme was highly phosphorylated with the majority of phosphate on serines and less phosphate on threonines with no detectable phosphate on tyrosine (130). In membranes

prepared from these overexpressing HEK 293 cells that were exposed to 1 μM ANP for 1 hour, there was a 50% decline in ANP-dependent GC activity that was tightly correlated with a loss in receptor phosphate. The loss of phosphate was not explained by receptor degradation since similar experiments performed on ^{35}S-methionine labeled receptors demonstrated that ANP exposure had little effect on GC-A protein (130). Importantly, no change in enzyme activity was observed in the absence of natriuretic peptide, which indicated that phosphorylation was correlated with ANP-dependent activity but not basal enzymatic activity. In a critical experiment, addition of protein phosphatase A2 catalytic subunit to ^{32}P-labeled membranes revealed a time-dependent decrease in ANP-dependent GC activity that was tightly correlated with reductions in GC-A ^{32}P content. Importantly, both loses in ^{32}P-content and ANP-dependent GC activity were blocked by the specific PP2A inhibitor okadaic acid. This was the first time that the hormonal activation and phosphate content of the enzyme were measure concurrently. The combined data from this report strongly suggested that in the basal state, GC-A is highly phosphorylated and highly active when stimulated with ANP. Additionally, this report provided the first data to indicate that homologous desensitization of GC-A is correlated with dephosphorylation as was previously described for membrane GCs in sea urchin sperm.

Less than a year later, Koller et al. reported that GC-A expressed in COS cells is phosphorylated on serines and threonines prior to ANP-stimulation and that phosphorylation of the receptor decreased after stimulation with ANP (103). Furthermore, the authors observed that alanine substitutions for amino acids in the KHD of GC-A that are highly conserved with known protein kinases produced enzymes with undetectable ^{32}P content and very low ANP-dependent GC activity. Again, these mutations did not affect enzyme protein concentrations, which suggested that phosphorylation of the KHD is required for natriuretic peptide activation of GC-A. Subsequently, Joubert et al. (131) determined that incubation of HEK 293 cells overexpressing GC-A with ANP resulted in a time-dependent decrease in GC-A phosphorylation that was consistent with initials reports by Potter and Garbers (130) and Koller et al. (103). In addition, Joubert et al. provided data that supported the notion that dephosphorylation of GC-A in response to ANP exposure results from reduced kinase activity as opposed to increased phosphatase activity.

In 1994, another study showed that NIH3T3 cells expressing GC-A displayed a marked reduction in ANP-dependent cGMP elevations and GC activity after incubation with the phorbol ester PMA, a known activator of PKC, which coincided with reductions in GC-A phosphate content (132). Further experimentation revealed that the PMA-dependent, but not ANP-dependent, dephosphorylation and desensitization of GC-A was completely blocked by PKC inhibitors, which suggested that the heterologous, phorbol ester-mediated desensitization of GC-A is associated with PKC activation. These data directly dispute earlier claims that activation of PKC inhibits the activity of the enzyme by direct phosphorylation of GC-A (125-127). Moreover, the same report found that PMA and ANP desensitization of GC-A are distinct events mediated by dephosphorylation of unique residues that are PKC-dependent and PKC-independent, respectively. Thus, through rigorous experimentation it became clear that dephosphorylation, not phosphorylation, was a mechanism of GC-A inactivation, as predicted by the studies initially conducted on the highly conserved GC in sea urchin sperm.

Although an understanding of the phosphorylation-dependent regulation of GC-A was beginning to emerge, it was unknown whether GC-B was regulated in the same fashion. Similar to the initial reports on GC-A, one publication suggested that GC-B is directly phosphorylated by PKC, which reduces CNP-dependent cGMP production (133). However, the authors failed to determine the phosphorylation state of the receptor and assumed that the reduction in CNP-dependent cGMP production was a direct result of PKC phosphorylation of GC-B. Gilkes et al. also showed that PMA inhibited CNP-dependent cGMP elevations in AtT-20 cells, which provided further evidence that PKC inhibits GC-B activity (134). In 1998, Potter reported that GC-B is highly phosphorylated on serines with lessor amounts of phosphate on threonines when overexpressed in NIH3T3 cells (135). As with GC-A, prior exposure to whole cells overexpressing GC-B to its specific peptide activator CNP, resulted in time-dependent decreases in CNP-dependent GC activity that were associated with decreases in GC-B phosphate content (135). In the same experiment, the CNP-dependent GC activity was measured concomitantly with the phosphate content of the enzyme and were positively correlated at every timepoint examined. Critically, membranes from metabolically labeled cells were incubated with purified protein phosphatase 2A catalytic subunit with or without the inhibitor okadaic acid. Again, a direct positive correlation was observed between GC-B phosphate content and CNP-dependent GC activity. These data suggest that the CNP-

dependent enzyme activity of GC-B is regulated by phosphorylation and is analogous to that described for GC-A, which is consistent with the similarity at the amino acid level between the two enzymes as well as the conservation of phosphorylation sites as described below. Furthermore, these data provided additional support for the hypothesis that these mammalian GC receptors are positively, and not negatively, regulated by phosphorylation.

Hormones or growth factors that stimulate vasoconstriction, cellular growth, or proliferation decrease natriuretic peptide-stimulated cGMP accumulation. Initial experiments showed that ANGII inhibited ANP-dependent cGMP elevations in rat aortic smooth muscle cells by stimulating cGMP hydrolysis via a calcium-activated phosphodiesterase (PDE) (136). In cultured glomerular mesangial cells, ANGII was reported to reduce ANP-dependent cGMP elevations through activation of a calcium-dependent PDE in the initial phase, whereas PKC activation was required for inhibition during the maintenance phase (137). Endothelin was also shown to inhibit ANP-dependent cGMP production in smooth muscle cells in a PKC-dependent manner (138). Experiments by Müller et al. demonstrated that desensitization of GC-A by pretreatment with ANP or lysophosphatidic acid (LPA) were similar and time-dependent in MA-10 Leydig cells (139). Interestingly, they found that ANP-induced desensitization was blocked by various PKA inhibitors, whereas LPA-induced desensitization was not. These data contrast with prior data by Potter and Garbers who reported that PKC inhibitors do not block ANP-dependent dephosphorylation of GC-A (132). While the authors did not directly measure GC-A phosphorylation in their study, they suggested that the similarity between the ANP- and LPA-induced desensitization provides compelling evidence that the LPA-induced reduction in GC-A activity was mediated by dephosphorylation as well. One general hypothesis is that ANGII, endothelin, and/or LPA decrease ANP-dependent cGMP production through dephosphorylation-dependent heterologous desensitization of GC-A. However, no data directly showing that these inhibitory factors dephosphorylate GC-A has been published to our knowledge.

In contrast to GC-A, heterologous desensitization of GC-B has been clearly demonstrated. Chrisman and Garbers first demonstrated that platelet-derived growth factor (PDGF), fetal bovine serum (FBS), or fibroblast growth factor (FGF) inhibit CNP-dependent cGMP elevations in fibroblasts (140). Subsequently, LPA and S1P were found to be the serum factors responsible for FBS-induced cGMP inhibition (141).

Similarly, Abbey et al. demonstrated that pretreatment with vasopressin (142), LPA (143), or S1P (144) inhibit CNP-dependent cGMP elevations. Importantly, the observed inhibition by LPA or S1P was dose-dependent and did not require decreases in GC-B protein expression, which suggests that they exert their effects through receptor-mediated heterologous desensitization of GC-B. Subsequent reports from the Potter Lab found that LPA (145) and S1P (146) also decrease the phosphate content of GC-B.

Identification and characterization of the phosphorylation sites of guanylyl cyclase-A and -B

The initial studies by Garbers and Potter, Koller et al., Joubert et al., and Chrisman et al. suggested that GC-A and GC-B are phosphorylated in the basal state and that dephosphorylation is a mechanism of desensitization of these receptors. However, to further investigate the role of dephosphorylation in the inactivation of these receptors, the identification of the actual phosphorylated residues was required. Initial attempts to narrow down the phosphorylated regions of GC-A and GC-B used tryptic phosphopeptide mapping analysis of deleted or chimeric constructs that were originally perfected in Tony Hunter's laboratory at the Salk Institute. Using this approach, Potter and Hunter determined that the phosphorylation sites are located within the first 132 intracellular amino acids of each receptor (147). Since previous data showed that GC-A contained phosphoserine and phosphothreonine (103, 130, 132), the authors generated mutant constructs containing either single serine or threonine to alanine substitutions, or a combination of these alanine substitutions. Alanine was chosen because it cannot be phosphorylated and contains a small side chain like serine or threonine that is unlikely to affect protein confirmation. Expression of the mutant constructs in HEK 293 cells followed by metabolic ^{32}P labeling revealed that individual alanine substitutions at S497, T500, S502, S506, S510, and T513 resulted in receptors with decreased phosphate content compared to the WT receptor. Furthermore, these single mutants had altered tryptic phosphopeptide maps. Constructs containing four or five of the phosphorylation site substitutions lost most of the tryptic phosphopeptides observed in the maps of the WT receptor and had very low levels of ^{32}P, suggesting that these six residues in the KHD are *bona fide* phosphorylation sites within GC-A. Importantly, mutants that exhibited reduced phosphorylation had significantly reduced ANP-dependent GC activity, and GC-A mutants containing four or five alanine substitutions for suspected

phosphorylation sites had no detectable increases in GC activity after stimulation with ANP, making this the first demonstration that phosphorylation is absolutely required for ANP-dependent activation of GC-A.

Within the same year of identifying the phosphorylation sites of GC-A, Potter and Hunter published a similar set of experiments identifying five clear phosphorylation sites of GC-B. They initially showed that single serine or threonine to alanine mutations at S513, T516, S518, S522, S523, and S526 within the KHD of GC-B reduced the phosphorylation state of the receptor when expressed in HEK 293 cells (148). Alanine substitutions at all seven potential phosphorylation sites, including the six above and T529, resulted in a completely dephosphorylated receptor. Unlike the GC-A study, alanine substitutions for individual serines or threonines in GC-B resulted in the disappearance of specific individual phosphopeptides on tryptic phosphopeptide maps, which confirmed that all of the specifically mutated serines and threonines described above, except S522, were actually phosphorylated. Comigration of synthetically synthesized phosphopeptides with ^{32}P-labeled phosphopeptides isolated from metabolically labeled cells, confirmed that the identification of many of the individual phosphorylation sites. Importantly, enzyme assays determined that CNP-dependent GC activity was reduced in all mutants containing single serine or threonine to alanine substitutions for *bona fide* phosphorylation sites. Furthermore, a GC-B mutant containing seven alanine substitutions for putative phosphorylation sites only exhibited 6% of the activity of the WT receptor. Thus, similar to GC-A, phosphorylation of GC-B was shown to be essential for activation of the enzyme by CNP.

The identification of the phosphorylation sites of GC-A and GC-B enabled further testing of the role of dephosphorylation in the desensitization these receptors. In contrast to the alanine-substituted receptor, a GC-A mutant containing glutamate substitutions that mimic the negative charge of the phosphorylated residues (149, 150) for the first six identified phosphorylation sites in GC-A called GC-A-6E, yielded an enzyme that was activated by ANP and resistant to ANP-dependent desensitization. However, this initial glutamate-substituted mutant was only activated by ANP to about 20% to 25% of the level as the phosphorylated WT enzyme (151), which suggested that either additional phosphorylation sites had yet to be identified and/or that the single negative charge of each glutamate substitution was not sufficient to compensate for -1 to -2 negative charge associated with the phosphorylation of serine and threonine residues *in vivo*.

Nonetheless, these new glutamate-substituted constructs provide additional evidence supporting the desensitization by dephosphorylation hypothesis for natriuretic peptide stimulated GC receptors. Additionally, the phosphatase inhibitor microcystin that prevented both the dephosphorylation and inactivation of WT-GC-A, failed to increase the activity of the GC-A-6E enzyme as expected if the appropriate phosphorylation sites were identified correctly (151).

The initial tryptic phosphopeptide mapping experiments identified several phosphorylation sites within GC-A and GC-B, however given the limitations of this technique, it was possible that more sites remained to be discovered. In 2010, Schröter et al. used mass spectrometry to identify a new phosphorylation site in GC-A at position S487 as well as confirming the six initially characterized phosphorylation sites (152). In agreement with Schröter et al., new mass spectrometry studies conducted by Potter and colleagues detected the same phosphorylation sites in GC-A and also identified T529 as a new phosphorylation site in GC-B along with confirming the five originally identified sites of GC-B (153). In a separate report, a functional screen based on whether glutamate substitutions increased natriuretic peptide-stimulated GC activity, suggested that S473 in GC-A and S489 in GC-B may also be phosphorylated (154). In fact, the same study reported that the mutation of the six chemically identified and the one functionally identified phosphorylation sites in GC-B to glutamates produced an enzyme called GC-B-7E that is activated by CNP just like the phosphorylated WT enzyme, but unlike the phosphorylated WT receptor, GC-B-7E was resistant to inactivation by dephosphorylation. In similar studies reported in 2017, Otto et al. described a mutant form of GC-A containing single glutamate substitutions for the seven chemically determined sites (S487, S497, T500, S502, S506. S510, T513) as well as the functionally identified site (S473) called GC-A-8E that mimics the enzymatic activity of the phosphorylated WT GC-A and is resistant to dephosphorylation-dependent desensitization (155). Hence, the engineered, glutamate-substituted versions of GC-A and GC-B provided a novel approach to test the desensitization by dephosphorylation hypothesis for the first time.

Although the GC-A-8E and GC-B-7E mutants mimic their WT counterparts, these mutants contain glutamate substitutions at S473 and S489, respectively, for which there is a lack of chemical evidence indicating that these residues are phosphorylated in biological systems. In fact, we currently think that these amino acids are not

phosphorylated *in vivo*. However, even if these residues are not *bona fide* phosphorylation sites, it makes sense that more than one glutamate substitution may be needed to reproduce the functional effect of each phosphorylated residue because phosphates can carry up to two negative charges depending on the pH of the milieu surrounding the site. This argument is consistent with the hypothesis that phosphorylation is required for hormonal activation of GC-A and GC-B solely due to charge interactions. Thus, we proposed a model in which the negative charges of phosphorylated residues form salt bridges between positively charged arginine and lysine residues within the KHD. As a result, an ordered and rigid structure is formed, which is required to transmit the natriuretic peptide binding signal from the extracellular domain through the transmembrane domain and KHD to the catalytic domain. Specifically, this model predicts that the rigid KHD allows the rotational force caused by natriuretic peptide binding to be transmitted to the catalytic domain to bring the catalytic subunits closer together, which will increase substrate affinity. Conversely, when GC-A and GC-B are dephosphorylated, the lack of negatively charged residues produces an unordered KHD structure that cannot propagate the natriuretic peptide activation signal to the catalytic domain (Figure 1).

The identification and characterization of the phosphorylation sites in GC-A and GC-B was a critical step in understanding how phosphorylation regulates the enzyme activity of these receptors and helped resolve decades-long controversies. Moreover, it directly led to the design of receptor constructs that could be used to investigate the role of phosphorylation-dependent regulation *in vivo*. The identities of the kinase(s) and phosphatase(s) that phosphorylate and dephosphorylate these receptors, respectively, remain unknown. Hence, GC-A-8E and GC-B-7E are alternative approaches to understanding the physiological consequences of increased phosphorylation-dependent activation of GC-A and GC-B.

PHYSIOLOGICAL EFFECTS OF GUANYLYL CYCLASE-A AND -B

Natriuretic peptides are often described simply as peptides that act to lower blood pressure and volume by promoting natriuresis. However, the effects of these peptides are ubiquitous and they have been shown to regulate numerous physiological and pathological conditions as documented by thousands of papers. As stated above, ANP and BNP bind and activate GC-A, whereas CNP binds and activates GC-B. The vast majority of the actions associated with these peptides are mediated through their respective receptor by stimulating the synthesis of cGMP, a classical intracellular second messenger signaling molecule. There are three primary cGMP binding proteins: cGMP-dependent protein kinases, or commonly referred to as protein kinase G (PKG), cGMP-binding PDEs, and cyclic nucleotide-gated ion channels.

The best-characterized downstream cGMP signaling is mediated through PKGs. PKGs are serine/threonine kinases consisting of an amino-terminal regulatory domain and carboxyl-terminal catalytic domain (156). The binding of two cGMP molecules to the regulatory domain induces a conformational change that derepresses the kinase activity. Mammalian PKGs exist as two major forms, PKGI is a soluble enzyme that consists of an alpha and beta form and is found in the cytosol, whereas PKGII is a mostly bound to the inner membrane leaflet due to lipid linkage (157). PKGI is widely expressed and is abundant in brain, cardiomyocytes, platelets, and smooth muscle (158). Genetic deletion of PKGI in mice results in loss of cGMP-dependent vascular smooth muscle relaxation and develop hypertension at 4 weeks of age but this condition does not persist into adulthood (159). In contrast, PKGII expression is much more restricted, but is highly expressed in the intestine, kidney, brain, chondrocytes, and bone (160). Rodents lacking PKGII are normotensive and dwarfed due to well characterized effects on the proliferative and hypertrophic zones of the growth plate (161, 162).

The degradation of cyclic nucleotides by PDEs is a crucial component in the regulation of cyclic nucleotide signaling. PDEs are organized into 11 different families based on their ability to degrade cAMP, cGMP, or both, in addition to how they are activated or inhibited (163). For example, some degrade both cGMP and cAMP (PDE1, -2, -3, -10, and -11), whereas others specifically hydrolyze cAMP (PDE4, -7, and -8) or cGMP (PDE5, -6, and -9) (164). Through modulation of PDE activity, cGMP can

influence cAMP signaling. For instance, binding of cGMP to PDE2 or PDE3 allosterically stimulates or inhibits the degradation of cAMP in cardiomyocytes, respectively (165).

Lastly, cGMP directly binds and regulates cyclic nucleotide-gated ion channels. Cyclic GMP produced by photoreceptors GC-E and GC-F is an essential regulator of phototransduction mediated by cGMP-gated sodium and calcium channels in the retina. These channels are best known for their ability to mediate the adaptation to low-light environments in photoreceptor cells (166). Whereas GC-A and GC-B are activated by peptides binding to the extracellular domain, photoreceptor GCs are activated by GC-activating proteins (GCAPs) (167). GCAPs activate photoreceptor GCs through interaction with their intracellular domains (168). Using the phosphorylation sites of GC-A and GC-B as a template, multiple, conserved phosphorylation sites within the KHD of GC-E were identified by mass spectroscopy (169). However, unlike GC-A and GC-B, GC-E phosphorylation does not appear to regulate the enzyme activity of the photoreceptor. Parenthetically, similar conserved sites were subsequently identified in a sea urchin membrane GC as well (170).

GC-A regulation of blood pressure

Genetic studies in animal models have provided clear evidence that ANP and GC-A are critical for normal cardiovascular function. Initial studies found that ANP knockout mice have blood pressures 20 to 30 mmHg higher compared to WT littermates (44, 45). The laboratories of David L. Garbers and Oliver Smithies independently generated GC-A KO mice. Consistent with genetic deletion of ANP, both groups found that GC-A KO mice exhibited elevated blood pressures up to 40 mmHg higher than WT animals (96, 97). Conversely, transgenic overexpression of ANP (171) or BNP (172) in mice reduces blood pressure by 20 to 30 mmHg. These data clearly demonstrate that GC-A regulates basal blood pressures in mice. However, the most impressive data demonstrating the relationship between GC-A and blood pressure came from Oliver et al., who demonstrated that ANP-dependent GC activities and blood pressures are directly proportional to GC-A gene dosage over a range of 0 to 4 WT-GC-A alleles (173).

Insightful studies by Michaela Kuhn and colleagues revealed cell-specific functions mediating the regulation of blood pressure and volume by GC-A activation. Mice with selective GC-A deletion in smooth muscle cells displayed normal chronic arterial blood pressure but were unable to maintain normal blood pressures in response

to acute vascular volume expansion (174). Conversely, inactivation of GC-A specifically in endothelial cells resulted in mice with blood pressures elevated 10-15 mmHg and a 11-13% increase in total plasma volume, however, the acute vasodilating effects ANP were preserved in these mice (175). Together, these data indicate that GC-A expressed in smooth muscle cells mediates the acute, direct vasodilating effects of ANP, whereas GC-A expression in endothelial cells, and perhaps other cells, is critical in the maintenance of long-term, chronic regulation of intravascular volume and blood pressure.

GC-A regulation of cardiac hypertrophy

ANP and BNP have been shown to have direct effects on the heart under physiological conditions. Mice with genetic deletion of ANP (44) or GC-A (97, 176) display severe cardiac hypertrophy. In contrast, mice overexpressing ANP display reduced cardiac hypertrophy (177). One obvious explanation for the cardiac hypertrophy observed in the KO animals is that the prolonged exposure to systemic hypertension necessitated an increase in ventricular mass to overcome the increase in arterial blood pressure. However, three key studies demonstrated that GC-A exerts a direct, local effect on cardiac hypertrophy. The first report showed that cardiomyocyte-specific overexpression of GC-A decreases cardiomyocyte size in both WT and GC-A KO mice without altering blood pressure (178). Second, Knowles et al. found that chronic administration of 4 different antihypertensive drugs from weaning to 4 months of age decreased the blood pressures of GC-A KO mice to WT levels but had no effect on cardiac hypertrophy (179). The third study used mice with loxP/Cre-mediated cardiomyocyte-restricted deletion of GC-A. These mice had reduced cardiac ANP-dependent GC activity as well as slightly reduced blood pressure, while displaying increased cardiac hypertrophy due to increased cardiomyocyte size (180). The decreased blood pressures observed in these mice are likely a result of their elevated plasma levels of ANP and BNP. Together, these elegant studies established that GC-A locally regulates physiological cardiac hypertrophy independently of its effects on blood pressure.

GC-B regulation of the female reproductive system

Mammalian oocytes are held in the prophase of meiosis by a signal from the surrounding granulosa cells in the ovarian follicle that requires elevated cAMP levels in the oocyte (181). Laurinda Jaffe's group first identified cGMP as the inhibitory signal from the granulosa cells and showed that cGMP passes through gap junctions into the oocyte, where it functions to maintain elevated cAMP levels by inhibition of PDE3, thus preventing the transition of the oocyte from prophase to metaphase (182). Furthermore, the Jaffe group showed that luteinizing hormone (LH) causes the resumption of meiosis by lowering cGMP levels in the ovarian follicle by closing gap junctions on the granulosa cells. This causes a decrease in cGMP within the ovarian follicle, thus relieving the inhibition of PDE3 degradation of cAMP in the oocyte that prevents the resumption of meiosis. A subsequent report found that CNP and GC-B were required to sufficiently elevate cGMP levels in the granulosa cells to prevent precocious meiotic maturation of the oocyte (183). These observations indicate that cGMP produced by GC-B in the ovarian follicle is a crucial component in the regulation of oocyte meiosis.

Collaborations between the Jaffe and Potter Labs investigated the involvement of GC-B-dependent cGMP elevations in the resumption of meiosis in oocytes. They first showed that LH rapidly (within 20 min) reduces CNP-dependent GC-B activity in follicle membrane preparations, which correlated with a similarly rapid decrease in follicle cGMP (184). The rapid LH-induced reductions in follicle cGMP were not explained by decreases in GC-B protein or decreases in CNP, however LH did eventually reduce CNP in the follicle after 2 hours. Subsequently, they demonstrated that LH rapidly decreases follicle cGMP through dephosphorylation and inactivation of GC-B, which was attenuated by pretreatment with a phosphoprotein phosphatase (PPP)-family phosphatase inhibitor (185). Further collaboration between the two labs led to the generation of GC-B$^{7E/7E}$ mice, which globally express the GC-B-7E mutant described above. GC activity assays on ovarian follicle membranes from GC-B$^{7E/7E}$ mice showed that LH failed to decrease the activity of the mutant enzyme (186). Importantly, cGMP-sensing FRET experiments on living ovarian follicles revealed that the LH-induced decreases in cGMP were attenuated in follicles from GC-B$^{7E.7E}$ mice and as a result, meiotic resumption was delayed GC-B$^{7E/7E}$ oocytes. Despite this delay, GC-B$^{7E/7E}$ mice display no obvious defect in fertility, which is consistent with the reported redundant processes that work to ensure the resumption of meiosis (187). Together, these results

indicate that dephosphorylation of GC-B is required for rapid, LH-induced resumption of meiosis in oocytes and was the first demonstration that the phosphorylation state of a membrane GC regulates a physiological process. Recently, the two labs reported that elevations in cAMP by forskolin cause a similar dephosphorylation and inactivation of GC-B to that seen in response to LH in ovarian follicles, suggesting that cAMP may mediate the rapid, dephosphorylation-dependent inactivation of GC-B by LH (188).

GC-B regulation of long bone growth

The CNP/GC-B system is critical for normal bone growth. Early studies on cultured rat chondrocytes demonstrated that addition of CNP to the medium elevates cGMP and suggested that GC-B may modulate chondrocyte proliferation (50). Further studies on cultured fetal mouse tibias revealed that CNP induced endochondral ossification (189). However, some of the most striking data demonstrating the necessity of GC-B for normal bone growth comes from human and animal studies. In humans, inactivating mutations in both alleles of GC-B cause acromesomelic dysplasia Maroteaux-type (AMDM-type) dwarfism (98, 99, 190-192), and heterozygous carriers display short stature (193-195). In contrast, humans with mutations that cause CNP overexpression (64, 65) or constitutive activation of GC-B (196-198), display skeletal overgrowth. Furthermore, mice lacking CNP (60, 199) or GC-B (99) are dwarfed. Similarly, mice expressing a mutant form of GC-B containing alanine residues for the phosphorylated serine and threonine residues that mimics a constitutively dephosphorylated enzyme (148) are also dwarfed due to smaller growth plates (200). Conversely, mice with transgenic overexpression of CNP have longer bones compared to WT littermates (61).

GC-B is also a central component in fibroblast growth factor receptor 3 (FGFR3)-dependent achondroplasia (ACH). ACH is the most common form of human skeletal dwarfism that is characterized by narrower proliferative and hypertrophic zones in the growth plate that results in disproportionate reductions in long bone length (201). The vast majority of ACH cases result from gain of function mutations in FGFR3 that inhibit bone growth (202-204). Mice expressing any of the gain of function FGFR3 mutants exhibit bone defects associated with ACH (205-207). Mugniery et al. reported that dwarfism was only observed in mouse models of FGFR3-dependent ACH when the mutant receptor was expressed in the cartilage, which suggests that the defects in bone

growth are due to an effect on chondrocytes (208). In a seminal study, Yasoda et al. reported that overexpression of CNP in chondrocytes rescues FGFR3-mediated inhibition of endochondral ossification in mice (209). A subsequent report from the same group found that exogenous administration or overexpression of CNP also prevents impaired bone growth caused by FGFR3 gain of function mutations (210). Moreover, the long-lived 39 amino acid CNP analog BMN-111 has also been shown to improve long bone growth in mouse models of ACH (211, 212). Clinically, phase 3 clinical trials demonstrated that BMN-111 injections increase long bone length in children with ACH (213). These results are consistent with *in vitro* studies demonstrating that FGF and GC-B signaling are reciprocally antagonistic (140, 214, 215). Interestingly, the reduced bone length caused by activating mutations of FGFR3 closely resemble that seen with inactivating mutations of GC-B. In fact, Robinson et al. demonstrated that FGF-dependent inhibition of GC-B requires receptor dephosphorylation in rat chondrosarcoma cells (216). Laurinda Jaffe's group, in collaboration with the Potter Laboratory, published a follow-up report showing that mice expressing two alleles of GC-B-7E (GC-B$^{7E/7E}$ mice) have longer bones and that FGF reduces GC-B activity in cultured growth plate chondrocytes from WT but not GC-B$^{7E/7E}$ mice, which is consistent with the inactivation by dephosphorylation hypothesis (217). Together, these data suggest that GC-B dephosphorylation contributes to FGF-dependent inhibition of long bone growth.

GC-B regulation of bone mass and strength

Although the involvement of GC-B in long bone growth is well established, the ability of GC-B to regulate bone mass or bone strength is poorly understood. One study reported that CNP is secreted from and stimulates alkaline phosphatase activity and mineralization, as well as increases mRNA expression for osteocalcin in osteoblast-like cells from rat calvariae (218). In MC3T3-E1 osteoblastic cells, exogenous CNP elevated cGMP and decreased ^{3}H-thymidine uptake (219). Together these results suggested for the first time that GC-B regulates osteoblasts. Another group reported CNP-production in mouse bone marrow cultures and observed that addition of CNP stimulated bone resorption by activating osteoclasts (220). However, a subsequent report showed that CNP increased cGMP production in mixed avian bone cells but not in purified osteoclast, suggesting that osteoclasts do not respond directly to CNP (221). In primary cultures of

fetal rat calvarial cells, CNP enhanced osteogenic protein-1-induced osteoblastic cell differentiation (222). CNP also increases the proliferation of cultured human osteoblasts (223). RNA-seq data from the murine tibia diaphyses (224) or bone marrow-derived mouse osteoclasts (225) indicated high GC-B mRNA expression in osteoblasts and/or osteocytes, and very low or undetectable levels in osteoclasts. Hence, these functional and mRNA expression studies indicate that GC-B is expressed in osteoblasts and/or osteocytes, but not in osteoclasts. Additionally, they suggest that activation of GC-B in osteoblasts may regulate bone mass and strength.

In some patients with constitutively activating GC-B mutations that exhibit skeletal overgrowth, increased serum markers of bone resorption and incidence of bone fractures, as well as reductions in bone mineral density have also been observed (197, 198). Similarly, femurs and vertebra from mice with transgenic overexpression of CNP have decreased bone mineral density by 9 weeks of age compared WT (61). Femurs from these mice were also reported to have decreased bone mass and strength by 8 weeks (62). In contrast, femurs from mice overexpressing osteocrin, which specifically binds NPR-C thereby increasing circulating CNP concentrations, were longer but bone mass did not differ compared to femurs from WT mice. (226). However, a recent report from the same group demonstrated that tibias from 8-week-old mice lacking osteocrin, which would presumably decrease CNP levels, have less bone mass and reduced bone formation compared to WT (227). The authors went on to show that osteocrin primarily functions to potentiate CNP-dependent osteoblast differentiation, which may explain why osteocrin is required for normal bone formation but its overexpression is not sufficient to increase bone mass.

In contrast to mutations that lead to constitutive activation of GC-B, either through supraphysiological expression of CNP or through activation of GC-B in the absence of CNP, our group recently demonstrated for the first time that elevated GC-B activity increases bone mass and bone mineral density, which results in stiffer and stronger bones. Robinson et al. showed that lumbar vertebra and tibias from 9-week-old GC-B$^{7E/7E}$ mice have greater trabecular bone mass and bone mineral density compared to age-matched WT mice (228). Similarly, tibial cortical bone indices were also increased in the GC-B$^{7E/7E}$ mice. Specifically, the cortical bone fraction from GC-B$^{7E/7E}$ tibias had significantly greater cross-sectional moment of inertia (CSMI), which is an important structural parameter that determines bone strength. Consistent with the greater CSMI,

biomechanical testing revealed that femurs and tibias from GC-B$^{7E/7E}$ mice have increased ultimate load, stiffness, energy absorbed to failure and energy absorbed to ultimate load compared to WT. In agreement with the previous reports that demonstrate CNP/GC-B effects in osteoblasts, static histomorphometric analysis showed that GC-B$^{7E/7E}$ tibias had more osteoblasts than tibias from WT control mice. Furthermore, serum procollagen type 1 N-terminal propeptide (P1NP) and osteocalcin concentrations were elevated in the GC-B$^{7E/7E}$ mice, suggesting that these mice have increased osteoblast activity and bone formation. However, dynamic histomorphometry indexes indicated that neither mineral apposition rate nor bone formation rate differed between GC-B$^{7E/7E}$ and WT tibias. To our knowledge, it would be unprecedented if bones from GC-B$^{7E/7E}$ mice exhibited greater bone mass without an increase in bone formation. Therefore, our current hypothesis is that the anabolic effect on bone that results from the increased CNP-dependent GC-B activity must precede 9 weeks of age.

As mentioned above, the results from Robinson et al. contrasts with all previous reports from humans and mice with persistent activation of GC-B due to overexpression of CNP or mutations that constitutively activate GC-B in the absence of CNP. Unlike the chronic GC-B activation observed in previous studies, the GC-B-7E enzyme is not constitutively active and responds to endogenous, physiological levels of CNP. Thus, like the WT enzyme, GC-B-7E is transiently activated by CNP but because it cannot be inactivated by dephosphorylation, it exhibits elevated CNP-dependent cGMP production. This highlights the significance and uniqueness of the GC-B$^{7E/7E}$ model in studying the effects of increased GC-B activity in animal models.

CONCLUSIONS

It has been nearly 50 years since membrane GCs were first discovered and purified from mammalian tissues (2-5). Similarly, it has been over 40 years since Adolfo José de Bold's seminal observations that led to his discovery and isolation of ANP (10, 12), which led to the purification of BNP (15) and CNP (16) and the realization that these natriuretic peptides are the endogenous ligands for GC-A and GC-B, respectively (34, 35). Additionally, the current year marks the 30th anniversary of my advisor's critical report that first demonstrated that dephosphorylation of GC-A causes desensitization of the enzyme (130). From then on, the work of our group, together with many other groups, led to the identification of the phosphorylation sites of GC-A and GC-B and refined the field's understanding of how the activity of these enzymes is increased and decreased by phosphorylation and dephosphorylation in cell culture, respectively.

However, whether or not phosphorylation-dependent activation of GC-A or GC-B would prove to be of significant physiological consequence *in vivo* was unclear when I began my graduate research. Our lab, in collaboration with Dr. Laurinda Jaffe's group, generated novel knock-in mice that globally express either GC-A-8E or GC-B-7E in place of both their respective WT alleles. Historically, studies investigating the physiological functions of GC-A and GC-B have consisted of KO or transgenic overexpression mouse models. In these models the enzymes are either completing absent or chronically active. In contrast to previous gain of function models, the GC-A-8E and GC-B-7E enzymes are active only in the presence of endogenously produced and secreted natriuretic peptides, which mimics physiological conditions. These mutant enzymes contain glutamate substitutions for the known phosphorylation sites, which mimic the negative charges of the phosphorylated serines and threonines on the WT receptors. Because the negative charge of the glutamate cannot be enzymatically removed like that of a phosphorylated residue, GC-A-8E and GC-B-7E cannot be inactivated by dephosphorylation, which produces more active enzymes as well as enzymes that are active for longer periods of time. Importantly, the expression and the basal activity of the mutant enzymes do not differ from their WT receptor counterparts, thus they only exhibit increased and prolonged cGMP synthesis in the presence of natriuretic peptides. Therefore, the GC-A$^{8E/8E}$ and GC-B$^{7E/7E}$ mice are unique models to investigate the physiological functions of GC-A and GC-B.

My work on the GC-A$^{8E/8E}$ and GC-B$^{7E/7E}$ described below demonstrates that the phosphorylation-dependent modulation of these enzymes affects their physiological functions *in vivo*. We found that male, but not female, GC-A$^{8E/8E}$ had reduced cardiac hypertrophy, decreased cardiomyocyte cross-sectional area, and increased ejections fractions. Mechanistically, in response to acute natriuretic peptide stimulation, male GC-A$^{8E/8E}$ mice exhibit increased and prolonged cGMP synthesis, which was tightly correlated with sustained reductions in cardiac ERK1/2 phosphorylation compared to WT mice. Using the GC-B$^{7E/7E}$ mice, we showed that the primary mechanism for how FGFR3 gain of function mutations cause ACH is by stimulating the dephosphorylation and inactivation of GC-B. Furthermore, we showed this process occurs as early as two-weeks of age. Lastly, my research suggests that increased bone formation and bone strength resulting from increased GC-B activity requires decreases in osteoblasts in addition to increases in osteoblasts, which is associated with an early developmental period and may have clinical implications for the treatment of ACH in children and osteoporosis in adults.

FIGURES

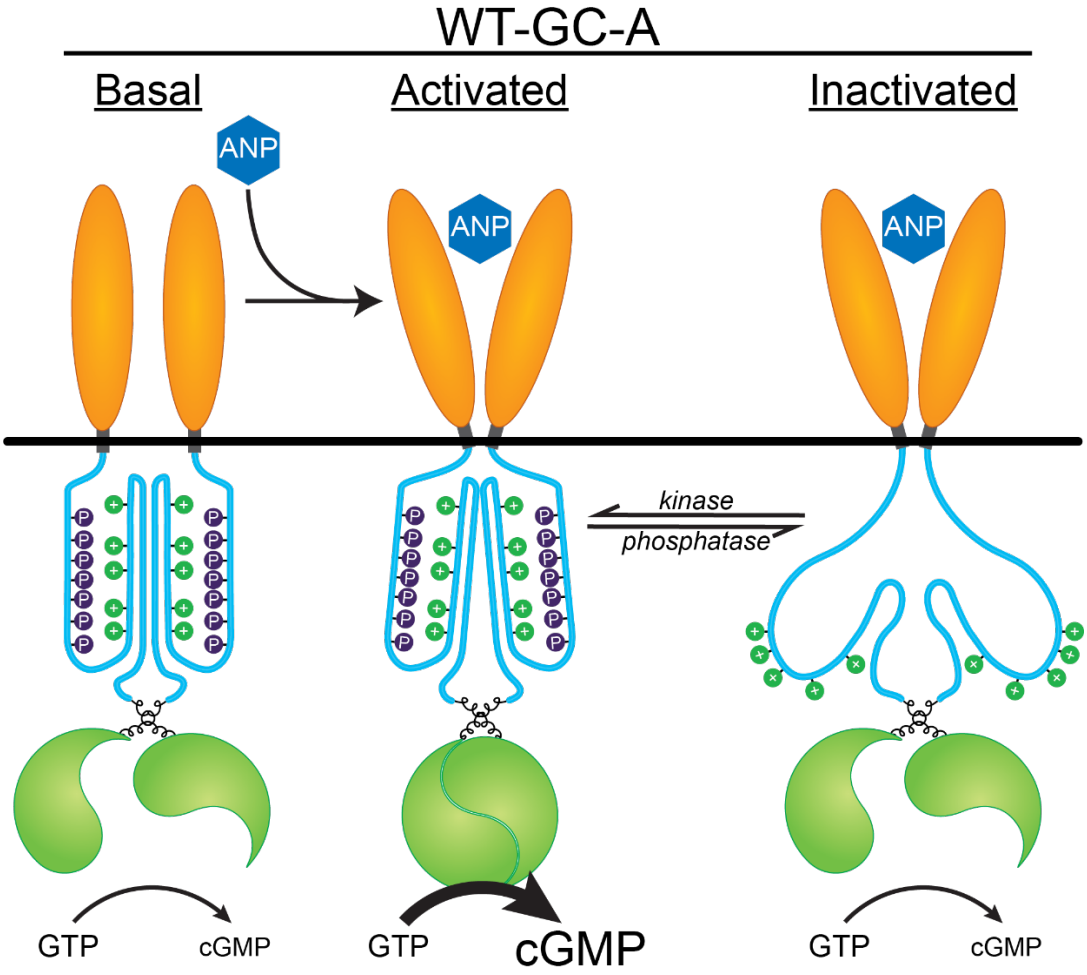

Figure 1. Model depicting the salt-bridge hypothesis for phosphorylation-dependent ANP-stimulation of GC-A

In the basal state, the KHD of GC-A is phosphorylated on multiple serine and threonine residues (represented by purple circles with the letter “P”) and, in the absence of ANP, the catalytic activity of the GC repressed and cGMP production is low. The negative charges associated with the phosphates form salt bridges with positively charged arginine and lysine resides in the KHD (green circles with “+”), which produce a rigid and ordered structure. ANP binding to the extracellular ligand binding domain causes a conformation change and a rotational force is transmitted through the rigid KHD to the GC domain to increase substrate affinity, thereby increasing cGMP production. Dephosphorylation of the KHD results in an unordered structure that does not allow transmission of the ANP activation signal; thus GC activity is low even when ANP is bound to the receptor.

CHAPTER 2: GUANYLYL CYCLASE-A PHOSPHORYLATION DECREASES CARDIAC HYPERTROPHY AND IMPROVES SYSTOLIC FUNCTION IN MALE, BUT NOT FEMALE, MICE

Brandon M. Wagner[a], Jerid W. Robinson[b], Chastity L. Healy[a], Madeline Gauthier[a], Deborah M. Dickey[b], Siu-Pok Yee[d], John W. Osborn[c], Timothy D. O'Connell[a,] and Lincoln R. Potter[a,b,]

Departments of Integrative Biology and Physiology[a], Biochemistry, Molecular Biology, and Biophysics[b], and Surgery[c] at the University of Minnesota, Medical School, Minneapolis, MN 55455 USA, and Department of Cell Biology[d] at the University of Connecticut Health Center, Farmington, CT 06030 USA

Published in:

Federation of American Societies for Experimental Biology (FASEB) Journal. 2021, 36:e22069.

SUMMARY

Atrial natriuretic peptide (NP) and BNP increase cGMP, which reduces blood pressure and cardiac hypertrophy by activating guanylyl cyclase (GC)-A, also known as NPR-A or Npr1. Although GC-A is highly phosphorylated, and dephosphorylation inactivates the enzyme, the significance of GC-A phosphorylation to heart structure and function is unknown. To identify *in vivo* processes that are regulated by GC-A phosphorylation, we substituted glutamates for known phosphorylation sites to make GC-$A^{8E/8E}$ mice that express an enzyme that cannot be inactivated by dephosphorylation. GC-A activity, but not protein, was increased in heart and kidney membranes from GC-$A^{8E/8E}$ mice. Activities were 3-fold higher in female compared to male cardiac ventricles. Plasma cGMP and testosterone were elevated in male and female GC-$A^{8E/8E}$ mice, but aldosterone was only increased in mutant male mice. Plasma and urinary creatinine concentrations were decreased and increased, respectively, but blood pressure and heart rate were unchanged in male GC-$A^{8E/8E}$ mice. Heart weight to body weight ratios for GC-$A^{8E/8E}$ male, but not female, mice were 12% lower with a 14% reduction in cardiomyocyte cross sectional area. Subcutaneous injection of fsANP, a long-lived ANP analog, increased plasma cGMP and decreased aldosterone in male GC-$A^{WT/WT}$ and GC-$A^{8E/8E}$ mice at 15 minutes, but only GC-$A^{8E/8E}$ mice had elevated levels of plasma cGMP and aldosterone at 60 minutes. fsANP reduced ventricular ERK1/2 phosphorylation to a greater extent and for a longer time in the male mutant compared to WT mice. Finally, ejection fractions were increased in male but not female hearts from GC-$A^{8E/8E}$ mice. We conclude that increased phosphorylation-dependent GC-A activity decreases cardiac ERK activity, which results in smaller male hearts with improved systolic function.

INTRODUCTION

In response to volume overload, atrial natriuretic peptide (ANP) and B-type NP (BNP) are released from the heart into the blood, where they decrease blood pressure by stimulating vasorelaxation, natriuresis, diuresis and endothelial permeability (229, 230). All of these responses are mediated through direct activation of guanylyl cyclase (GC)-A because GC-A knock out mice do not respond to cardiac NPs, are hypertensive, and display cardiac hypertrophy, whereas mice lacking the NP clearance receptor (NPR-C), the other receptor for ANP and BNP, display phenotypes associated with increased NP-stimulated GC activity (72, 96, 97, 231, 232). Although GC-A-dependent reductions in blood pressure were initially hypothesized to indirectly decrease cardiac hypertrophy (97), elegant pharmacologic and genetic studies demonstrated that GC-A reduces cardiac hypertrophy independently of blood pressure (178-180, 233) by an unknown mechanism that occurs early in development (234).

Both GC-A and GC-B, a homologous receptor that is activated by C-type NP (33), are phosphorylated on multiple conserved serines and threonines under basal conditions (130, 131, 135, 147, 148, 151, 152). However, prolonged exposure to NPs or acute exposure to luteinizing hormone (185, 186) or fibroblast growth factor for GC-B (216, 217), or possibly angiotensin II for GC-A (136, 137, 233), cause the dephosphorylation and inactivation of these receptors. Multiple homologous phosphorylation sites were first identified in GC-A and GC-B (130, 132, 135, 147, 148, 151-154), but were later identified in the retinal GC known as GC-1 or GC-E (169) and a receptor GC expressed in sea urchin sperm (170). Alanine substitutions that mimic uncharged, dephosphorylated residues, result in reduced NP-dependent GC activities (147, 148, 153), and the mutation of four or more phosphorylated GC-A residues to alanine produced an enzyme that was not activated by ANP (147). In contrast, glutamate substitutions for the individual phosphorylation sites to mimic the negative charge of phosphate preserves the ability of the enzymes to transmit the NP binding signal to the catalytic domain (151, 154, 155). Importantly, unphosphorylated versions of GC-A and GC-B containing glutamate substitutions for known phosphorylation sites have the same basal and NP-stimulated activities as the WT phosphorylated enzymes but are not inactivated by dephosphorylation (154, 155, 216).

Changes in GC-B phosphorylation regulates the resumption of meiosis in the ovarian follicle (184-187, 235) as well as longitudinal bone growth (217, 236) and skeletal bone mineral density (228) in mice, but little is known about how phosphorylation of GC-A regulates physiology *in vivo*. To date, genetically modified mice examining the physiological roles of GC-A have consisted of knock out, loss of function, or transgenic overexpression, gain of function, models (45, 49, 73, 96, 97, 173, 237-239). In these mice, GC-A is either always “on” or always “off.” Here, we created a novel knock-in mouse model called GC-A$^{8E/8E}$ that globally expresses GC-A-8E in place of both WT alleles. These mice exhibit increased and prolonged cGMP synthesis only in the presence of ANP and/or BNP, which mimics physiologic conditions. Using this model, we investigated how GC-A affects cardiac morphology and function by measuring cardiomyocyte (CM) cross-sectional area (CSA) and performing echocardiography on GC-A$^{WT/WT}$ and GC-A$^{8E/8E}$ mice of both sexes. We furthered our investigations into this process by determining if the increased NP-dependent GC-A activity observed with GC-A-8E mice resulted in a greater and more sustained reductions in the phosphorylation of the extracellular regulated kinases (ERK) 1 and 2, well-known activators of cardiac hypertrophy in mice.

METHODS

Animals. GC-A$^{8E/8E}$ mice that express GC-A-8E in a global manner were created by CRISPR-Cas9 technology at the University of Connecticut Center for Mouse Genome Modification. Primer design and the overall approach to making the GC-A$^{8E/8E}$ mice is described in Supplemental Figure 1A and is based on characterization studies of rat GC-A-8E expressed in transfected cells (155). Male and female GC-A$^{WT/WT}$ and GC-A$^{8E/8E}$ mice were genotyped as shown in Supplemental Figure 1 and maintained on a C57BL/6 background as previously described (186). Mice were fed standard chow under specific-pathogen-free conditions. All mice were 12 weeks old unless otherwise indicated. Animal care and use was compliant with the University of Minnesota and University of Connecticut Institutional Animal Care and Use Committees.

Reagents. Antibodies were from the following sources: anti-ERK1/2 P-thr 202 and P-tyr 204 #9101, anti-ERK1/2 #9102, anti-MEK1/2 P-ser 217 and P-ser 221 #9121, anti-MEK1/2 #9122 (Cell Signaling, Danvers, MA, USA), and anti MKP-1/DUSP1 (E-6)(Santa Cruz Biotechnology, Dallas, TX, USA). Antibodies to GC-A were generated and used as described (142). ELISA kits for cGMP and aldosterone were from ENZO Lifesciences, Inc. (Farmingdale, New York, USA). The testosterone ELISA was from Cayman Chemical (Ann Arbor, MI56t). ELISAs for mouse ANP and mouse BNP were from RayBiotech (Peachtree Corners, GA, USA). fsANP was from Anaspec (Fremont, CA, USA) as previously described (240). The mouse creatinine assay kit was from Crystal Chem (Elk Grove Village, IL, USA).

Guanylyl Cyclase Activity Assays. Heart and kidney tissue were homogenized in phosphatase inhibitor buffer (PIB) at 4°C (108). Assays were performed at 37 °C in a buffer containing 25 mM HEPES, pH 7.4, 50 mM NaCl, 0.1% BSA, 0.5 mM isobutylmethylxanthine, 1 mM EDTA, 0.5 μM microcystin, 5 mM $MgCl_2$, 0.1 μg/ml creatine kinase, 5 mM creatine phosphate, 1 mM ATP, and 1 mM GTP in the absence or presence of 1 μM ANP for the indicated periods of time. Assays were terminated with 0.5 ml of 110 mM ZnOAc followed by 0.5 ml 110 mM Na_2CO_3, which was centrifuged to separate the GTP from cGMP. Cyclic GMP from the eluate was purified on acidified alumina columns as previously described (241). The cGMP was eluted with 3 ml of 200 mM ammonium formate and added undiluted to the ELISA assay as described (108).

Immunoprecipitation and western blotting of GC-A. 0.15-0.25 g of membrane protein from whole kidneys or 0.08-0.10 g of membrane protein from cardiac ventricles were prepared in 0.5 to 1.0 ml of PIB from WT and GC-A$^{8E/8E}$ mice and immunoprecipitated with 2 □l of serum from rabbit #6326 that was immunized with a peptide corresponding to the last 17 C-terminal amino acids of rat GC-A (147). Samples were fractionated on an 8% gel by SDS-PAGE and blotted to a polyvinylidene difluoride membrane. The membrane was blocked with Odyssey LI-COR blocking buffer (Li-Cor Biosciences, Lincoln, NE) for 1 h at room temperature and then incubated overnight at 4°C with the same antiserum at a dilution of 1:10,000 in 1:1 blocking buffer/PBS with 0.1% Tween. The membrane was washed 4 x 5 min with TBST and then incubated with IRDye 680 goat anti-rabbit antibody with a dilution of 1:15,000 for 1 h at room temperature in 1:1 blocking buffer/PBST and 0.01% SDS. The membrane was washed 4 x 5 min with TBST and once with PBS before imaging on a Li-Cor infrared imaging device. The relative amount of GC-A protein was determined using NIH ImageJ software.

Telemetry implantation. 16-week-old male GC-A$^{WT/WT}$ and GC-A$^{8E/8E}$ mice were implanted with Data Science International Inc. (St. Paul, MN, USA) transmitters (model HD-X11) for continuous monitoring of arterial pressure and heart rate as previously described (242). The surgical area was shaved and disinfected with iodine and cleaned with 70% isopropyl alcohol. The mice were placed on a heated surgical pad and a midline back incision was made to subcutaneously implant the body of the transmitter and a second incision was made in the interior side of the left leg to access the femoral artery for placement of the catheter of the transmitter. Mice were then allowed to recover for 1 week before telemetry data was collected during the period of 17-20 weeks of age.

Heart Histology. Hearts from GC-A$^{WT/WT}$ and GC-A$^{8E/8E}$ mice were arrested in diastole with 200 µl of PBS supplemented with 60mM KCl, excised, cleaned, and weighed. Hearts were cannulated through the aorta and perfused with PBS supplemented with 60 mM KCl, followed by 4% paraformaldehyde. Fixed hearts were embedded in paraffin and then sectioned transversely at the midpoint of the ventricles. Sections were stained with wheat germ agglutinin (WGA) and DAPI, imaged at 10X magnification, and analyzed for cardiomyocyte (CM) cross sectional area (CSA) using ImageJ by averaging the area of at least 250 CMs per heart (243, 244).

Subcutaneous fsANP injections. Frameshift (fs) ANP was dissolved in water at a concentration of 1 mM and frozen at -80^{o}C until used as previously described (240). Mice were subcutaneously injected with 2 mg/kg fsANP or with an equal volume of saline as vehicle control.

Plasma and urine analysis. Plasma ANP, BNP, aldosterone, testosterone, and cGMP concentrations were determined by ELISA according to the manufacturer's instructions. Plasma and urine creatinine was determined by an enzymatic assay according to manufacturer's instructions.

ERK analysis. Ventricular lysates were prepared from GC-A$^{WT/WT}$ and GC-A$^{8E/8E}$ mice by homogenizing with a Polytron in ice-cold RIPA buffer containing 50 mM Tris HCl, pH 7.4, 150 mM NaCl, 1% Triton X-100, 0.5% sodium deoxycholate, 0.1% SDS, 1 mM EDTA, and 10 mM NaF with Roche (San Francisco, CA, USA) complete protease inhibitor tablet and microcystin added fresh followed by agitation for 30 min at 4°C. The lysates were then centrifuged at 14,000g for 10 minutes at 4°C and the supernatant was collected. Thirty micrograms of ventricular lysates were fractionated on a 10% gel by SDS-PAGE and transferred for 1 h at 100 V to a polyvinylidene difluoride membrane. The membrane was blocked with LI-COR blocking buffer for 1 h at room temperature and then incubated overnight at 4°C with primary antibody. The membrane was washed 3 x 5 min with TBST and then incubated with IRDye 680 goat anti-rabbit antibody with a dilution of 1:15,000 for 1 h at room temperature in LI-COR blocking buffer. The membrane was washed 3 × 5 min with TBST and then once with TBS and then visualized and quantified on a Li-Cor infrared imaging device.

Echocardiography. Echocardiography was performed using the Vevo 2100 (FujiFilm VisualSonics Inc. Toronto, ON, Canada) with a MS550 transducer on anesthetized mice that were gently restrained in the supine position on the prewarmed monitoring pad. Echocardiographic images were captured as mice were recovering from anesthesia to achieve a heart rate (HR) of 400 - 500 bpm. Parasternal long axis M-mode images of the left ventricle were captured to measure left ventricular posterior wall thicknesses during systole (LVPW;s) and diastole (LVPW;d), left ventricular internal diameters (LVID;s and LVID;d), left ventricular end systolic volume (ESV: (7.0/(2.4 + LVIDs))*LVIDs^3) and end diastolic volume (EDV: (7.0/(2.4 + LVIDd))*LVIDd^3), fractional shortening (FS: 100*((LVIDd – LVIDs)/LVIDd)), ejection fraction (EF: 100*((EDV – ESV)/EDV)), stroke volume (SV: EDV – ESV), and cardiac output (CO: SV*HR). Pulsed-wave Doppler

images of the aortic arch were recorded to measure peak aortic velocity (AoV). Pulsed-wave Doppler images of the apical four-chamber view were taken to measure mitral flow velocities (E wave and A wave to calculate E/A ratio).

Statistics. Statistics and graphs were generated with Prism 9 software (GraphPad Software, La Jolla, CA, USA). p-values were obtained using either an unpaired, two-tailed student's t-test, Mann-Whitney test (panels A and B of figure 4), or two-way ANOVA with or without repeated-measures followed by Turkey's post-hoc test where $p \leq 0.05$ was considered significant.

RESULTS

Generation and validation of the GC-A$^{8E/8E}$ mice. Cell culture studies indicated that a rat GC-A variant containing glutamate substitutions for the eight confirmed phosphorylation sites is activated by ANP like the phosphorylated WT receptor (155). Here, glutamates were substituted for Ser-473, Ser-487, Ser-497, Thr-500, Ser-502, Ser-506, Ser-510 and Thr-513 using amino acid numbering based on the rat cDNA as initially described by Otto et al. (155). All substitutions were confirmed by DNA sequencing (Supplemental Fig. 1B). PCR-based genotyping indicated that heterozygous breeding produced the GC-A$^{WT/WT}$, GC-A$^{8E/+}$ and GC-A$^{8E/8E}$ lines at the expected mendelian ratios (Supplemental Fig. 1C). At 12 weeks of age, there was no difference in body weight between the GC-A$^{WT/WT}$ and GC-A$^{8E/8E}$ mice. Additionally, no differences in the mass of livers, lungs, or kidneys that express high levels of GC-A were observed between the GC-A$^{WT/WT}$ and GC-A$^{8E/8E}$ mice (Supplemental Table 1A). No obvious differences were observed in fertility between WT or mutant mice as well.

Plasma cGMP concentrations are elevated in GC-A$^{8E/8E}$ mice. Plasma was isolated between 4:00PM and 6:00PM from male and female GC-A$^{WT/WT}$ and GC-A$^{8E/8E}$ mice and analyzed for ANP, BNP and cGMP by ELISA. Plasma ANP and BNP concentrations did not differ between GC-A$^{WT/WT}$ and GC-A$^{8E/8E}$ mice of either sex (Fig. 1A-D). However, cGMP levels were elevated 95.1% and 80.1% in male and female GC-A$^{8E/8E}$ mice, respectively, compared to their WT littermates (Fig. 1E and F).

GC-A$^{8E/8E}$ mice have greater ANP-dependent guanylyl cyclase activity but not GC-A protein. Membranes from cardiac ventricles and whole kidneys of male and female mice of both genetic lines were assayed for GC-A activity in the presence of saturating amounts of ANP as a function of time. As anticipated, both male and female GC-A$^{8E/8E}$ mice had two to four times more ANP-dependent GC-A activity in these tissues compared to GC-A$^{WT/WT}$ mice (Fig. 2A and B). The difference in activity was not explained by variances in protein concentrations because GC-A protein levels measured by sequential immunoprecipitation-western blot analysis from hearts and kidneys were similar between GC-A$^{WT/WT}$ and GC-A$^{8E/8E}$ mice (Fig. 2C and D). Plausible explanations for the increased ANP-dependent GC activity in tissues from the GC-A$^{8E/8E}$ mice are that more of the translated GC-A protein from the GC-A$^{8E/8E}$ mice is active since it does not require post-translational phosphorylation and/or a significant amount of the WT GC-A

protein is not completely phosphorylated at any one time (147). Unexpectedly, both GC-A$^{WT/WT}$ and GC-A$^{8E/8E}$ female mice had approximately three-fold more ventricular ANP-dependent GC-A activity than males of the same genotype, whereas renal GC-A activity was similar between sexes. Again, these sex-dependent differences in cardiac activity were not explained by variances in GC-A protein concentrations based on western blots (Fig. 2C).

Blood pressure is unchanged between male GC-A$^{WT/WT}$ and GC-A$^{8E/8E}$ mice. To investigate potential blood pressure differences between the GC-A$^{WT/WT}$ and GC-A$^{8E/8E}$ mice, 16-week-old male mice of both lines were implanted with telemetry sensors that monitor blood pressure and heart rate continuously (242). One week after sensor implant surgery, the mice were sequentially fed diets containing varying NaCl content for approximately one week during the 17-week-old to 20-week-old time period, which resulted in a 40-fold range in NaCl intake. However, regardless of the dietary salt content, neither mean arterial pressure (MAP) (Fig. 3A) nor heart rate (Fig. 3B) differed between mice of the two genotypes.

The release of creatinine into the urine is increased in male GC-A$^{8E/8E}$ mice. To determine if renal function was changed in the mutant mice, we measured plasma and urine creatinine concentrations. Plasma creatinine levels for the male GC-A$^{WT/WT}$ mice were about 0.2 mg/dL, which is consistent with previously reported mouse plasma creatinine levels (Fig. 4A)(245). In contrast, creatinine levels from several of the male GC-A$^{8E/8E}$ mice were below the limit of detection of our assay. This is not unexpected since in the absence of renal dysfunction, plasma creatinine is low. Given that plasma creatinine levels in 6 of the 10 male GC-A$^{8E/8E}$ mice were below the assay's level of detection, the most conservative analysis of this data is to assign values for the samples that were below the last standard on the curve to the lowest value that was on the curve and use the nonparametric, Mann-Whitney test to assess statistical differences. When applied, this approach yielded a statistically significant decrease ($p = 0.0018$) in male GC-A$^{8E/8E}$ creatinine concentrations compared to the GC-A$^{WT/WT}$ mice. Creatinine levels in urine were also measured in male mice of both genotypes and found to be significantly elevated in the male GC-A$^{8E/8E}$ mice (Fig. 4C). In contrast, no differences in urine creatinine concentrations were observed between the female WT and mutant mice. Taken together, these data provide strong evidence that the male GC-A$^{8E/8E}$ mice

release more creatinine into the urine than GC-A$^{WT/WT}$ mice, which is consistent with the well-known ability of GC-A to increase the glomerular filtration rate (246).

Male GC-A$^{8E/8E}$ mice have smaller hearts and cardiomyocytes. Hearts from GC-A$^{8E/8E}$ male mice were 8% smaller by weight (Fig. 5A and C), but body weights were not different (Fig. 5D), which resulted in heart weight-to-body weight ratios that were 12% lower compared to GC-A$^{WT/WT}$ male mice (Fig. 5E). No differences were observed between the female GC-A$^{8E/8E}$ and GC-A$^{WT/WT}$ mice (Fig. 5B and F-H). To further investigate the reduced cardiac hypertrophy in males, ventricles were sectioned and stained to determine the cross-sectional area (CSA) of individual CMs (Fig. 5I). Male GC-A$^{8E/8E}$ mice had a 14% decrease in CM CSA compared to the GC-A$^{WT/WT}$ male mice (Fig. 5J), consistent with the known cardiac anti-hypertrophic effects of GC-A (97, 178). Hence, this reduction in CM CSA accounts for the reduction in heart size in the GC-A$^{8E/8E}$ male mice. Consistent with the lack of differences in female heart size, CM CSA did not differ in hearts from female GC-A$^{8E/8E}$ or GC-A$^{WT/WT}$ mice (Fig. 5K).

Plasma aldosterone levels are elevated in male, but not female, GC-A$^{8E/8E}$ mice. Because mice with mutations that increase plasma aldosterone concentrations have higher blood pressure (247), and the GC-A$^{8E/8E}$ mice do not have reduced blood pressure as expected due to the increased GC-A activity, we measured aldosterone levels in our GC-A$^{WT/WT}$ and GC-A$^{8E/8E}$ mice that were fed normal chow diets with no added NaCl. Aldosterone concentrations were 78% higher in male GC-A$^{8E/8E}$ mice (557.8 pg/ml) compared to male GC-A$^{WT/WT}$ mice (312.5 pg/ml) (Fig. 6A). In contrast, no significant difference in plasma aldosterone concentrations was observed between the female GC-A$^{WT/WT}$ (264.8 pg/ml) and GC-A$^{8E/8E}$ (249.5 pg/ml) mice (Fig. 6B).

Plasma testosterone levels are elevated in male and female GC-A$^{8E/8E}$ mice. Previous reports correlated changes in cardiac hypertrophy and hypertension in genetic models with increased GC-A-dependent blood testosterone concentrations (248, 249). Therefore, we measured plasma testosterone levels in male and female GC-A$^{WT/WT}$ and GC-A$^{8E/8E}$ mice. We found that male GC-A$^{WT/WT}$ mice had plasma testosterone levels of 3.68 ng/ml compared to 5.4 ng/ml for male GC-A$^{8E/8E}$ mice, whereas female GC-A$^{WT/WT}$ mice had plasma testosterone levels of 0.08 ng/ml compared to 0.12 ng/ml for female GC-A$^{8E/8E}$ mice. For both sexes, plasma testosterone levels were significantly elevated in the mutant mice (Fig. 6C and D).

Analysis of cardiac ERK phosphorylation in male GC-A$^{8E/8E}$ mice. Cardiac hypertrophy is positively regulated by the ERK1/2 pathway (250-252), and ANP and BNP have been shown to decrease ERK1/2 phosphorylation in cultured cells (253-255). Therefore, we investigated whether ERK1/2 activity is reduced in male GC-A$^{8E/8E}$ mice. Hearts were removed from male GC-A$^{8E/8E}$ and GC-A$^{WT/WT}$ mice and ventricular extracts were fractionated by SDS-PAGE and transferred to a PVDF membrane. Western blots were probed with an antibody against phosphorylated ERK1/2, then stripped and re-probed with an antibody against ERK1/2 protein and GAPDH. The amount of phospho-ERK and total ERK protein were quantified and used to determine the stoichiometry of ERK1/2 phosphorylation. Although ventricular ERK1/2 phosphorylation trended lower in extracts from the GC-A$^{8E/8E}$ mice, the difference was not statistically significant (Supplemental Fig. 2A and B). We also measured protein expression of MKP-1/DUSP1, a phosphatase known to reduce ERK1/2 phosphorylation, but observed no significant differences (Supplemental Fig. 2C). We then examined ERK1/2 phosphorylation in younger, 4-week-old mice, and again found that ERK1/2 phosphorylation trended lower in the male GC-A$^{8E/8E}$ mice, but that the decrease was not statistically significantly different from the WT mice (Supplemental Fig. 3).

fsANP injections result in higher and more sustained plasma cGMP concentrations in male, but not female, GC-A$^{8E/8E}$ mice. Since GC-A activity is not increased without NP stimulation in our GC-A$^{8E/8E}$ model (155), we subcutaneously injected mice with saline or fsANP, a C-terminally extended, long-lived ANP analog (240, 256) as performed by Chen et al. in rats (257). Plasma cGMP concentrations were elevated more than three-fold 15 minutes after injection of fsANP in the GC-A$^{WT/WT}$ mice and declined to basal levels by 60 minutes. Saline did not increase plasma cGMP concentrations at any time period (Fig. 7A). Injections of fsANP into male GC-A$^{WT/WT}$ mice and GC-A$^{8E/8E}$ mice resulted in similar plasma cGMP elevations at 5 minutes. However, while cGMP concentrations peaked 10 to 15 minutes after fsANP injection for the male GC-A$^{WT/WT}$ mice, plasma cGMP concentrations in the male GC-A$^{8E/8E}$ mice continued to climb for 20 minutes, at which point the plasma cGMP concentrations plateaued (Fig. 7B). Elevated plasma cGMP concentrations in the GC-A$^{8E/8E}$ mice are consistent with the GC-A$^{8E/8E}$ mice not undergoing dephosphorylation-dependent homologous desensitization (103, 130, 131, 152, 154, 155). As a result of the prolonged cGMP production in the GC-A$^{8E/8E}$ mice, plasma cGMP concentrations were more than

two-fold higher in the male GC-A$^{8E/8E}$ mice compared to male GC-A$^{WT/WT}$ mice during the 15-to-30-minute time period. In contrast, little difference was observed between fsANP-dependent plasma cGMP elevations in female GC-A$^{WT/WT}$ and GC-A$^{8E/8E}$ mice (Fig. 7C).

fsANP injection decreases plasma aldosterone similarly in male GC-A$^{8E/8E}$ and GC-A$^{WT/WT}$ mice at 15, but not at 60 minutes. Plasma aldosterone concentrations from both male GC-A$^{WT/WT}$ and GC-A$^{8E/8E}$ mice taken 15 minutes after subcutaneous injection with fsANP were reduced to similar levels (WT fsANP: 53% of vehicle, 8E fsANP: 62% of vehicle)(Supplemental Fig. 4A), which is consistent with previous reports showing that ANP decreases plasma aldosterone concentrations (258). However, while plasma aldosterone concentrations from male GC-A$^{WT/WT}$ mice taken 1 hour after subcutaneous injection with fsANP were back to vehicle control levels, plasma aldosterone levels from GC-A$^{8E/8E}$ mice were significantly elevated above vehicle control levels (Supplemental Fig. 4B). These data are consistent with a dysregulation of the GC-A/aldosterone regulatory axis in the GC-A$^{8E/8E}$ mice.

fsANP injection decreases ventricular ERK1/2 phosphorylation to a greater extent and for a longer period in GC-A$^{8E/8E}$ compared to GC-A$^{WT/WT}$ mice. ERK1/2 regulatory phosphorylation was determined by Western blot in ventricular extracts from male GC-A$^{WT/WT}$ and male GC-A$^{8E/8E}$ mice 5-, 15-, 30-, and 60-minutes after injection with fsANP (Fig. 8A-B and Supplemental Fig. 5A-H). The phospho-ERK/total-ERK values were normalized to mean values from saline-injected control mice and plotted as a function of time after injection (Fig. 8D). For the male GC-A$^{WT/WT}$ mice, the maximum decrease in ERK1/2 activity was 57%, which occurred at the earliest time period of 5-minutes and recovered to 89% of the unstimulated control value by the 60-minute timepoint. In contrast, cardiac ERK1/2 activities in the male GC-A$^{8E/8E}$ mice reached a nadir of 40% 30 minutes after the fsANP injection, which remained significantly depressed at 57% of the control value 60-minutes after the fsANP injection. Importantly, no difference in ERK1/2 phosphorylation in ventricular extracts from female GC-A$^{8E/8E}$ and GC-A$^{WT/WT}$ mice was observed 30 minutes after fsANP injection (Fig. 8C). Finally, no change in MEK activity in these same cardiac extracts was detected (Supplemental Fig. 6). Together, these data indicate that acute NP activation of GC-A reduces ERK1/2 activity in cardiac ventricles to a greater extent and for a longer period of time in male GC-A$^{8E/8E}$ compared to male GC-A$^{WT/WT}$ mice.

Male GC-A$^{8E/8E}$ mice have improved systolic function. To determine if increased NP-dependent GC-A activity affects cardiac function, we performed echocardiography on male and female mice of both lines (Fig. 9 and Supplemental Table 1B). Despite their smaller hearts, male GC-A$^{8E/8E}$ mice had increased ejection fractions and fractional shortening compared to the male GC-A$^{WT/WT}$ mice (Fig. 9A and Supplemental Table 1B). End systolic volume was also decreased in the mutant male mice (Fig. 9B). However, the E/A ratio did not differ between the WT and mutant mice, indicating that the GC-A$^{8E/8E}$ male mice had normal diastolic function (Fig. 9D). In contrast, none of the measured heart functions were significantly different between the mutant and WT female mice (Fig. 9E-H and Supplemental Table 1B). Together, these data indicate that the male GC-A$^{8E/8E}$ mice have improved systolic function despite having smaller hearts.

DISCUSSION

Using a novel mouse model that exhibits increased GC-A activity only in the presence of endogenous levels of ANP and/or BNP, we investigated how prevention of GC-A dephosphorylation regulates physiology in a live animal. The GC-$A^{8E/8E}$ mice have greater and longer lasting NP-dependent GC activity, but normal basal activity, which provides a new perspective for examining the effects of increased GC-A activity *in vivo*. This increased GC-A activity was associated with decreased heart size in male, but not female, GC-$A^{8E/8E}$ mice, which is consistent with more severe cardiac hypertrophy observed in male compared to female GC-$A^{-/-}$ mice. (97). The smaller heart phenotype was not explained by changes in blood pressure since the blood pressure between male GC-$A^{WT/WT}$ and GC-$A^{8E/8E}$ mice did not differ over a 40-fold change in dietary NaCl content. These data are harmonious with reports demonstrating pressure-independent effects of GC-A on cardiac hypertrophy (178-180). Microscopy studies indicated that the decreased heart size in male GC-$A^{8E/8E}$ mice was explained by reduced CM CSA, which is in agreement with increased CM CSA in male GC-$A^{-/-}$ mice (97). Importantly, male but not female GC-$A^{8E/8E}$ mice had improved systolic function compared to GC-$A^{WT/WT}$ mice, despite having smaller hearts. These data are consistent with that of mice expressing four GC-A alleles ($Npr1^{++/++}$) that had reduced heart weight to body weight ratios and increased fractional shortening (259) as well as with GC-$A^{-/-}$ mice that had cardiac hypertrophy and increased left ventricular end diastolic and systolic dimensions (97). Hence, the totality of data indicate that gain of function GC-A models result in smaller male hearts with improved systolic function, whereas loss of function models result in larger male hearts with reduced systolic function.

Unexpectedly, there was no significant difference in blood pressure between male GC-$A^{8E/8E}$ and GC-$A^{WT/WT}$ mice, even when measured over a wide range of salt intake. The GC-A knock out mice have chronically elevated blood pressure that is unresponsive to changes in salt-intake (96, 97), whereas the $Npr1^{++/++}$ mice that express four GC-A alleles exhibit increased GC-A activity and are hypotensive (173). Increased urinary creatinine indicates that at least one known renal function of GC-A is elevated in the GC-$A^{8E/8E}$ mice as expected. One potential explanation for the lack of reduction in blood pressure in the male GC-$A^{8E/8E}$ mice is that the elevated plasma aldosterone concentrations observed in the GC-$A^{8E/8E}$ mice may compensate for the increased GC-A

activity to normalize blood pressure. Why aldosterone was unchanged in the original GC-A$^{-/-}$ mice (96) and increased in the same mice many years later is not known (260).

A previous study reported that mice with increasing numbers of GC-A alleles have proportionally increased GC-A activity, proportionally increased blood testosterone levels, and proportionally decreased blood pressure (249). Hence, it was suggested that the GC-A dependent increases in testosterone levels contribute to the hypotension observed in mice with increased GC-A activity. However, in our model, where GC-A activity is only increased in response to natural ligand activation, we observed no change in blood pressure despite significant increases in blood testosterone levels in male mice. Additionally, Li et al suggested that male mice exhibit more cardiac hypertrophy than female mice because they have higher testosterone levels (248). However, in our model where the male mice exhibit increased GC-A activity and testosterone levels, these mice display reduced cardiac hypertrophy. Similarly, the female GC-A$^{8E/8E}$ mice have 48% higher serum testosterone levels as the female GC-A$^{WT/WT}$ mice but show no signs of hypertrophy. Hence, increased testosterone levels are neither associated with hypotension in male mice nor cardiac hypertrophy in mice of either sex in our GC-A$^{8E/8E}$ model.

Cyclic GMP stimulated by NPs, but not nitric oxide, counteracts cardiac hypertrophy in murine knock out hypertension models by directly acting on CMs (96, 178-180, 261, 262), and reductions in NP-dependent cGMP concentrations by phosphodiesterase 9A result in pathologic cardiac hypertrophy (263). Significantly, GC-A has been shown to decrease ERK1/2 activity in cultured cells by many investigators through a mechanism that is usually mimicked by cGMP analogs and requires protein kinase G (209, 253-255, 264), although Hofmann and colleagues have shown that protein kinase G I is not required for reductions in transaortic constriction (TAC)-dependent or angiotensin II-dependent cardiac hypertrophy in mice (265-267).

Cardiac hypertrophy can be physiologic as occurs during development and exercise, or pathologic as occurs with hypertension and chemotherapy (252, 268). ERK1/2 activation is more closely associated with physiologic as opposed to pathologic cardiac hypertrophy (268). Genetic studies involving ERK1$^{-/-}$ and ERK2$^{+/-}$ mice, or studies using mice overexpressing dual specificity phosphatase 6 that dephosphorylates and inactivates ERK1/2 (252, 268), suggest that increased ERK1/2 activity is not required for pathological cardiac hypertrophy (269, 270).

Regarding the physiologic consequences of GC-A inhibition of ERK1/2 in the heart, CM-specific transgenic overexpression of MEK-1, the direct upstream activator of ERK1/2, induces physiologic hypertrophy (271) and attenuates ischemic injury (272, 273), whereas ERK1$^{-/-}$ and ERK2$^{+/-}$ mice are more susceptible to ischemic injury (271). Here, the reduced activation of ERK1/2 in hearts from the GC-A$^{8E/8E}$ mice is mechanistically consistent with decreased hypertrophic growth observed in these mice with development. Moreover, physiologic cardiac hypertrophy associated with lactation was exaggerated in GC-A$^{-/-}$ mice and correlated with increased cardiac ERK1/2 phosphorylation and activity (260). Conversely, in GC-A$^{-/-}$ mice, exaggeration of pathologic hypertrophy post-TAC was not dependent on ERK1/2 activity (179, 233). Finally, the ability of ANP to block phenylephrine-dependent increases in neonatal rat CM CSA was shown to require increased, not decreased, ERK1/2 activity, which differs from our model (274). Regardless, the majority of data indicate that GC-A-dependent CM ERK1/2 inhibition is context dependent, such that reduced activation of ERK1/2 in GC-A$^{8E/8E}$ mice attenuates developmental hypertrophy but is not required for pathologic hypertrophy in the GC-A$^{-/-}$ mice post-TAC. Hence, the mechanism that GC-A uses to regulate cardiac hypertrophy in development as demonstrated by the GC-A$^{8E/8E}$ mice is distinct from the mechanism associated with pathologic cardiac hypertrophy as originally suggested by Scott et al. (234).

Surprisingly, we observed much greater GC-A activity in ventricular membranes from both female GC-A$^{8E/8E}$ and GC-A$^{WT/WT}$ mice compared to membranes from male mice of each genotype. To our knowledge, this is the first demonstration of a sex difference in cardiac GC-A activity. One explanation for why only male GC-A$^{8E/8E}$ mice have smaller hearts is that the ANP-dependent GC-A activity in the female GC-A$^{WT/WT}$ ventricles is elevated above the threshold level required to inhibit the CM ERK1/2 pathway. In contrast, GC activity in the male WT mice is below this threshold. Thus, the increased activity observed in the male GC-A$^{8E/8E}$ mice is now high enough to inhibit the CM ERK1/2 pathway. In contrast, GC-A activity in the female GC-A$^{WT/WT}$ mice is already sufficiently elevated to inhibit the CM ERK1/2 pathway, and therefore, the additional GC-A activity observed in the female GC-A$^{8E/8E}$ mice provides no additional benefit. Interestingly, the increased GC-A activity in female ventricles may explain the cardioprotective effects of estrogen on CMs mediated by GC-A (275, 276). These studies determined that estrogen increases ANP concentrations, while our data

demonstrates that GC-A activity is much higher in ventricles from female mice. The increases in both ANP and GC-A activity in murine female ventricles would increase cGMP concentrations in CMs, which is a known inhibitor of cardiac hypertrophy (178, 179, 253).

In conclusion, we developed a novel mouse model to study the physiologic consequences of NP-dependent, but phosphorylation-independent, activation of GC-A *in vivo*. Using this model and subcutaneous injections of a long-lived ANP analog, we determined that preventing dephosphorylation-dependent inactivation of GC-A has measurable, physiological consequences. The male GC-A$^{8E/8E}$ mice have smaller hearts due to reduced CM hypertrophy, despite exhibiting elevated plasma aldosterone and testosterone concentrations. Activation of GC-A with fsANP produced greater and more sustained plasma cGMP elevations, which correlated with larger and longer reductions of cardiac ERK1/2 phosphorylation in male GC-A$^{8E/8E}$ mice. Thus, increased cardiac GC-A activity reduces CM size in male GC-A$^{8E/8E}$ mice by decreasing ventricular ERK1/2 activity, a well-known regulator of cardiac hypertrophy. Finally, we note that GC-A$^{8E/8E}$ mice not only have less cardiac phospho-ERK1/2 protein, but they also have elevated plasma aldosterone levels compared to the WT mice. Importantly, these two differences are most apparent at longer time periods after injection with fsANP, which is consistent with the disparities being mediated by the prolonged GC activity of the GC-A-8E protein endogenously expressed in the GC-A$^{8E/8E}$ mice.

FIGURES

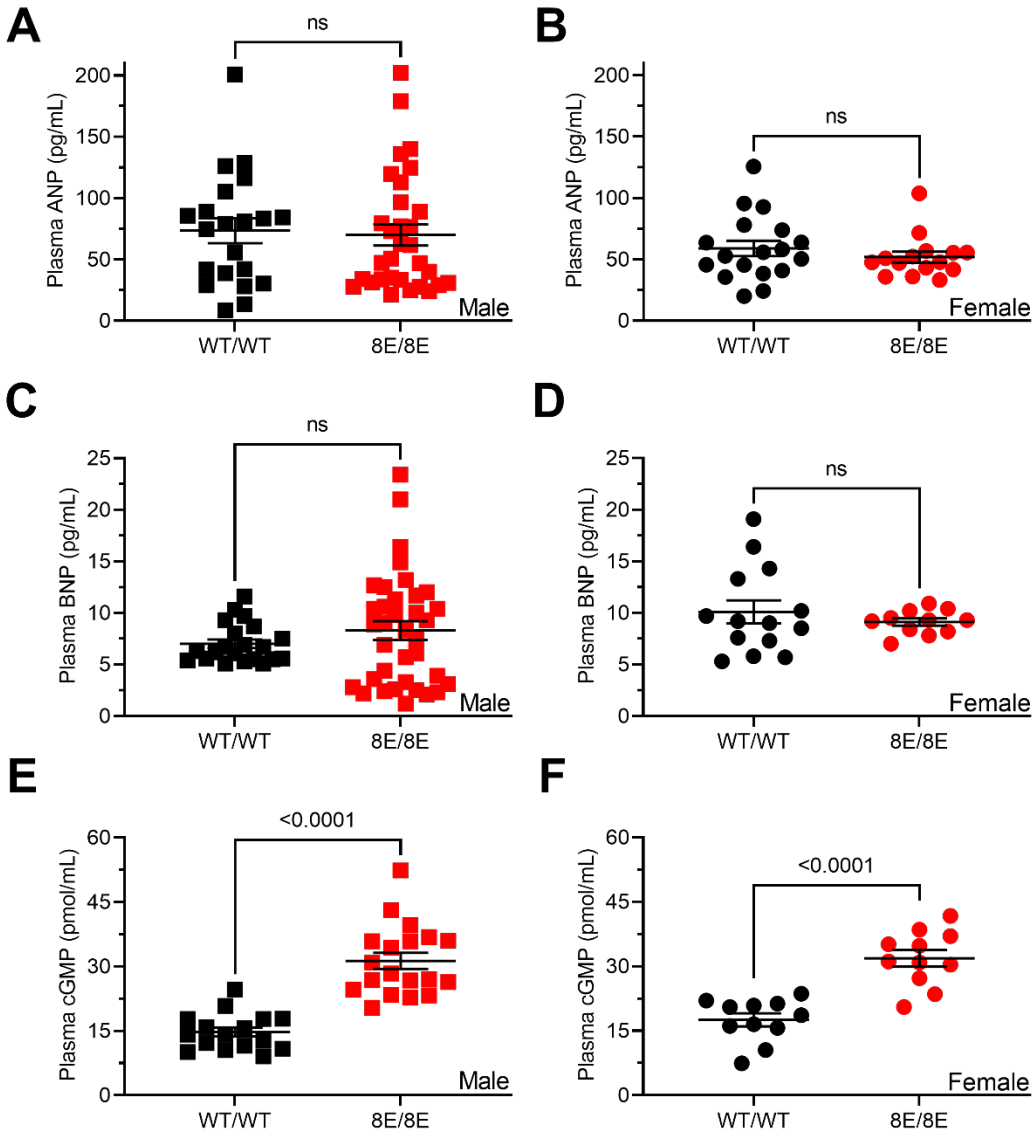

Figure 1. GC-A$^{8E/8E}$ mice of both sexes have elevated plasma cGMP, but not NP concentrations.

Plasma ANP, BNP and cGMP concentrations from GC-A$^{WT/WT}$ (black) or GC-A$^{8E/8E}$ (red) (A, C, E) male (squares) and (B, D, F) female (circles) mice. n = 11-36 mice per group. Statistical differences were determined using a two-tailed student's t-test with significant associated p values shown in each panel.

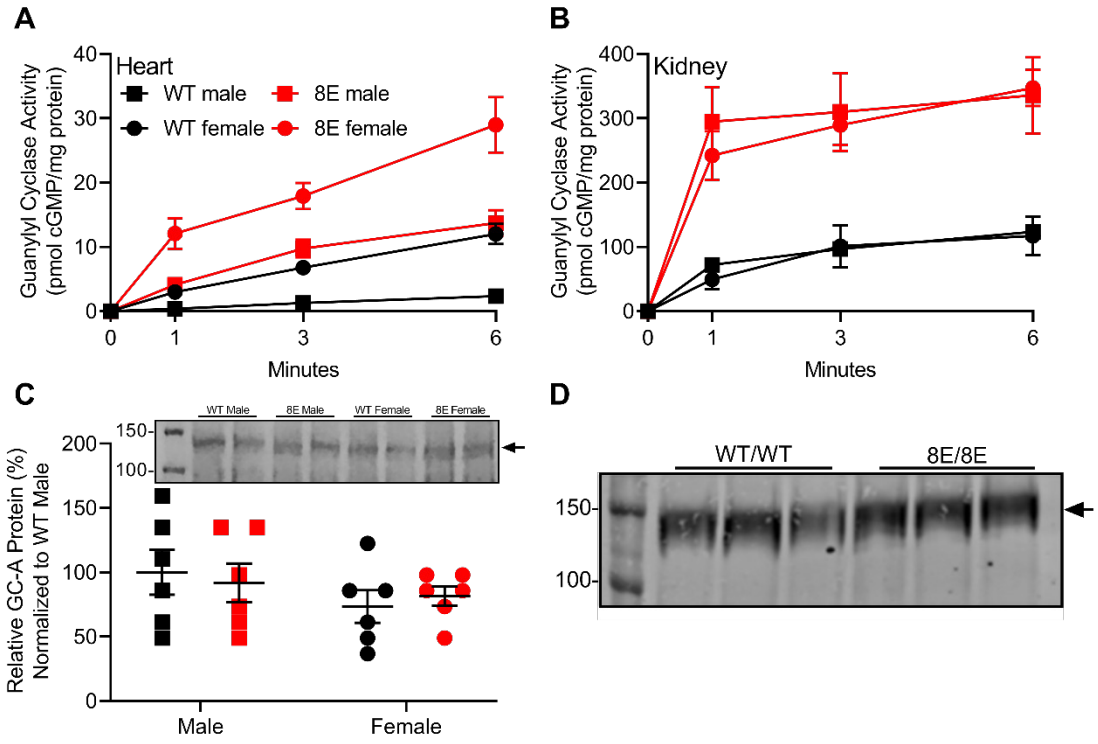

Figure 2. GC-A$^{8E/8E}$ mice of both sexes have greater ANP-dependent guanylyl cyclase activity, but not GC-A protein levels, than GC-A$^{WT/WT}$ mice.

Guanylyl cyclase activity determined in the presence of 1 μM ANP, 1 mM GTP, and 1 mM ATP in membranes from (A) cardiac ventricle or (B) whole kidney of male or female GC-A$^{WT/WT}$ and GC-A$^{8E/8E}$ mice. (C) Sequential immunoprecipitation-western blot analysis and quantitation of GC-A from individual GC-A$^{WT/WT}$ and GC-A$^{8E/8E}$ mouse hearts. (D) Sequential immunoprecipitation-western blot analysis of GC-A from male GC-A$^{WT/WT}$ and GC-A$^{8E/8E}$ mouse kidney membranes. Right arrows in panels C and D indicate GC-A. Numbers on the left side of panels C and D indicate 100 and 150 kDa MW markers. Each lane in panel D represents the isolation of GC-A from one kidney from an individual mouse. For panels A-C, n = 6 per group. The symbols indicate the mean and the vertical bars within symbols indicate SEM. For panel C, no significant differences were observed between the groups.

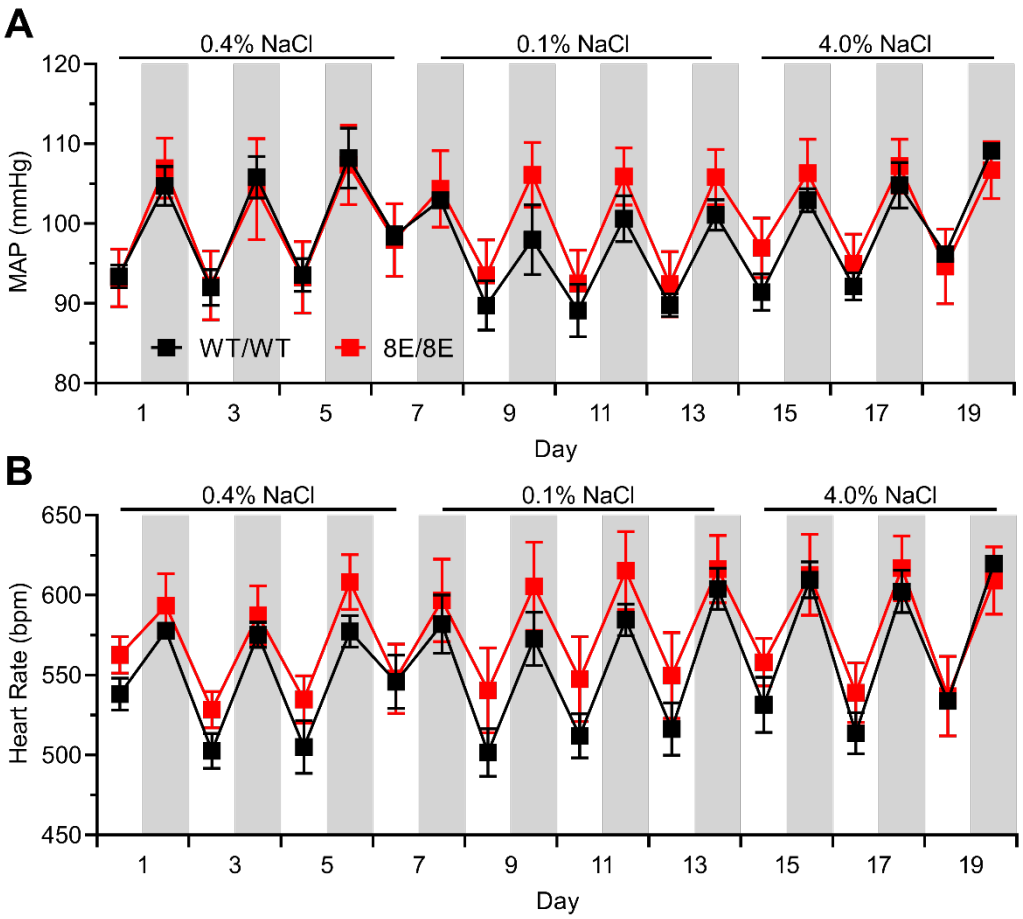

Figure 2. Mean arterial pressure and heart rate do not differ between male GC-A$^{WT/WT}$ and GC-A$^{8E/8E}$ mice regardless of salt intake.

(A) Mean arterial pressure (MAP) and (B) heart rate measured in beats per minute (bpm) for GC-A$^{WT/WT}$ and GC-A$^{8E/8E}$ in 16-week-old male mice fed the indicated dietary NaCl concentrations. n = 6 per group. White columns are “lights on” and gray columns are “lights off” measurements. The symbols indicate the mean and the vertical bars within symbols indicate SEM. Two-way repeated-measures ANOVA demonstrated no significant differences between GC-A$^{WT/WT}$ and GC-A$^{8E/8E}$ mice for either MAP or heart rate.

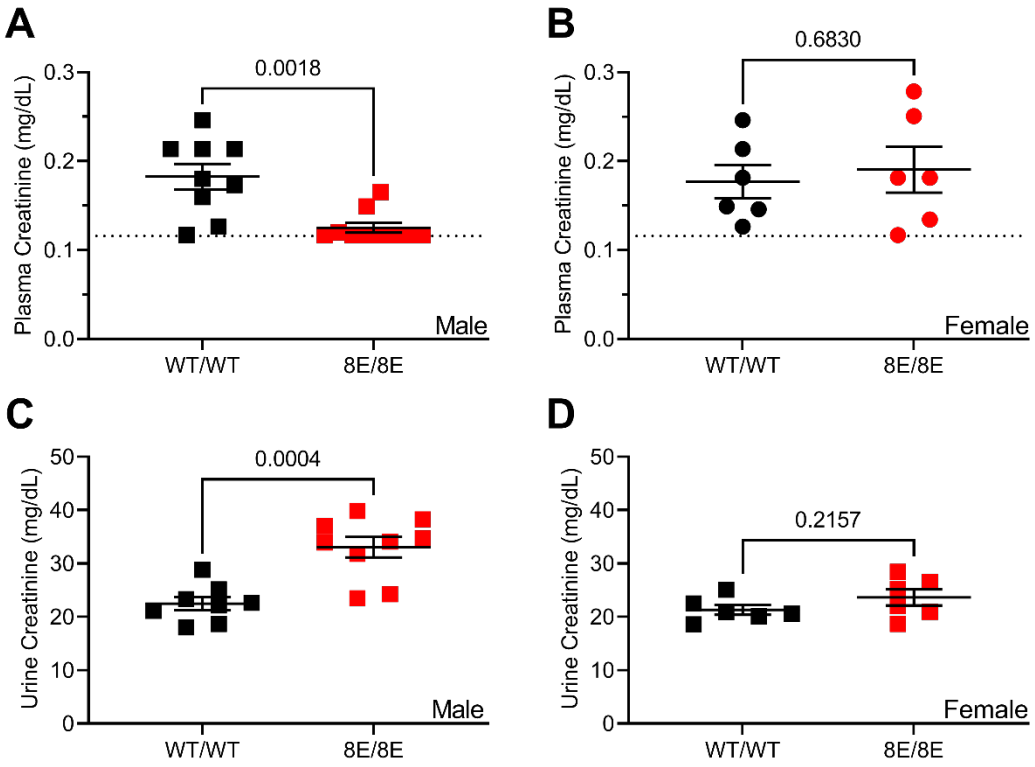

Figure 3. GC-A$^{8E/8E}$ male mice have decreased plasma and increased urinary creatinine concentrations, respectively.

Plasma and urine were collected from 12-week-old male and female mice. (A) Male and (B) female plasma creatinine concentrations. (C) Male and (D) female urine creatinine concentrations. Dotted line in panels A and B indicate the creatinine assay's limit of detection. n = 6-10 mice per group. Long horizontal bars indicate the mean, and the shorter bars indicate SEM. Statistical differences were determined using a Mann-Whitney test for panels A and B. A two-tailed student's t-test was used to determine significance for panels C and D. Associated p values are shown in each panel for each test.

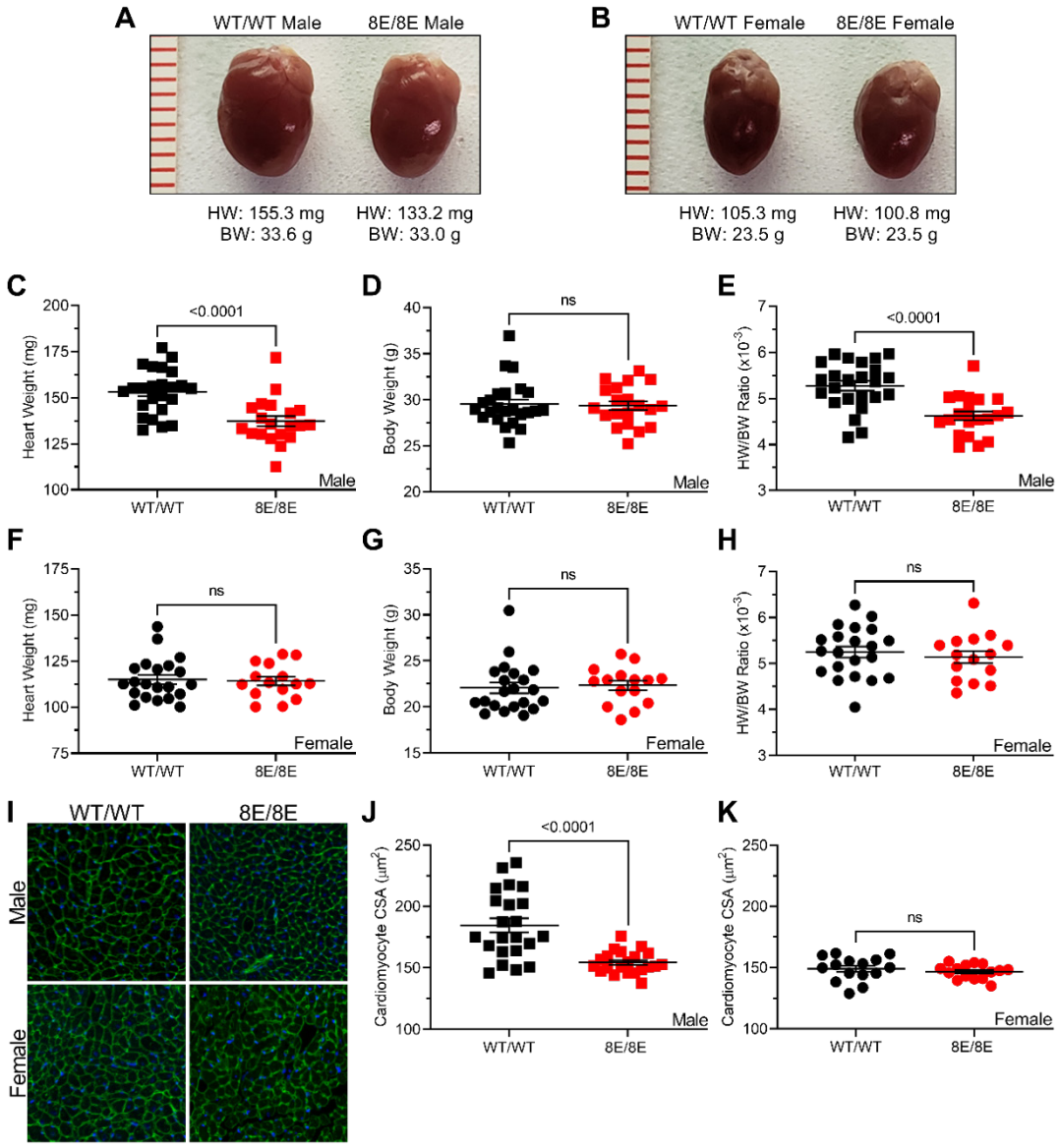

Figure 4. Hearts from male GC-A$^{8E/8E}$ mice weigh less because they have smaller cardiomyocytes.

Hearts from male and female GC-A$^{WT/WT}$ and GC-A$^{8E/8E}$ mice were collected for morphological analysis. Photos of (A) male and (B) female hearts from 12-week-old mice. Male (C) heart weight, (D) body weight, and (E) heart weight-to-body weight ratio (HW/BW). Female (F) heart weight, (G) body weight, and (H) HW/BW. Representative images of male and female cardiomyocyte (CM) cross sectional area (CSA) from ventricular tissue stained with WGA and DAPI (I). Quantitative results from (J) male and (K) female CM CSA analysis, which was performed with NIH ImageJ by measuring the

CSA of 250 CM per heart and averaging the individual values for each heart. n = 15-24 mice per group. Long horizontal bars indicate the mean and vertical bars indicate SEM. Statistical differences were determined using a two-tailed student's t-test with associated p values shown in each panel.

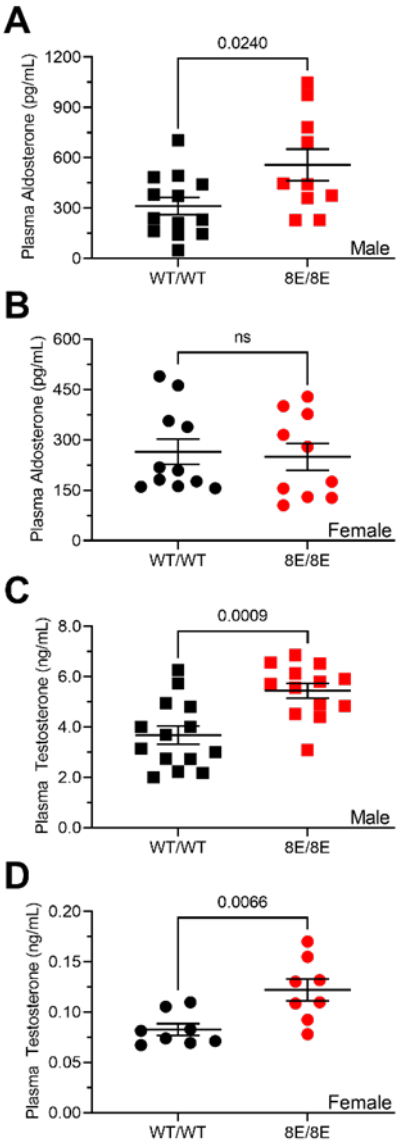

Figure 5. Male GC-A$^{8E/8E}$ mice have elevated plasma aldosterone and testosterone concentrations.

Plasma from male or female GC-A$^{WT/WT}$ and GC-A$^{8E/8E}$ mice was analyzed for aldosterone and testosterone concentrations by ELISAs. Male (A) and female (B) plasma aldosterone concentrations. Male (C) and female (D) plasma testosterone concentrations. n = 8-14 mice per group. Long horizontal bars indicate the mean and vertical bars indicate SEM. Statistical differences were determined using a two-tailed student's t-test with associated p values shown in each panel.

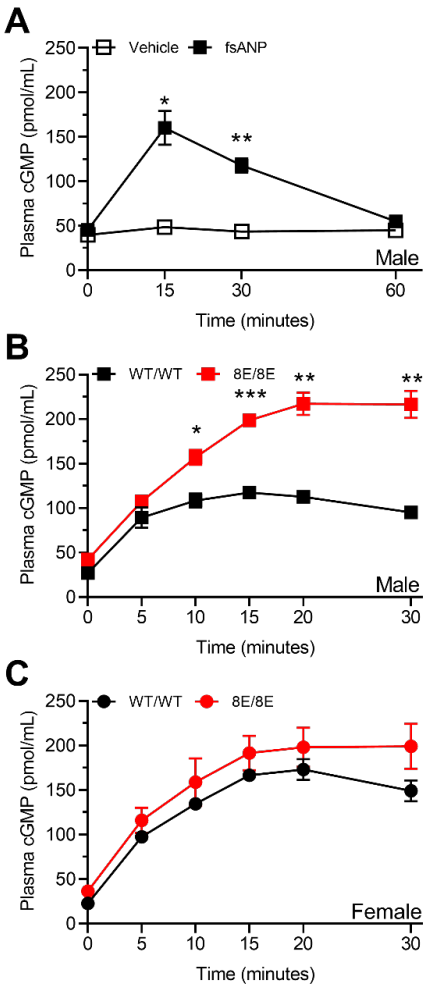

Figure 6. fsANP injections result in a greater and more sustained elevation of plasma cGMP in male GC-A8E/8E compared to male GC-AWT/WT mice.

(A) Injection of fsANP, but not saline vehicle, transiently increases plasma cGMP in male GC-A$^{WT/WT}$ mice. (B) Plasma cGMP concentrations in male GC-A$^{WT/WT}$ and GC-A$^{8E/8E}$ mice as a function of time after fsANP injection. (C) Plasma cGMP concentration in female GC-A$^{WT/WT}$ and GC-A$^{8E/8E}$ as a function of time after fsANP injection. The symbols represent the means and the vertical bars within the symbols represent the SEM. n = 3-5 mice per treatment. Statistically significant differences were determined by two-way-ANOVA with multiple comparisons where * = $p<0.05$, ** = $p<0.01$, and *** = $p<0.001$.

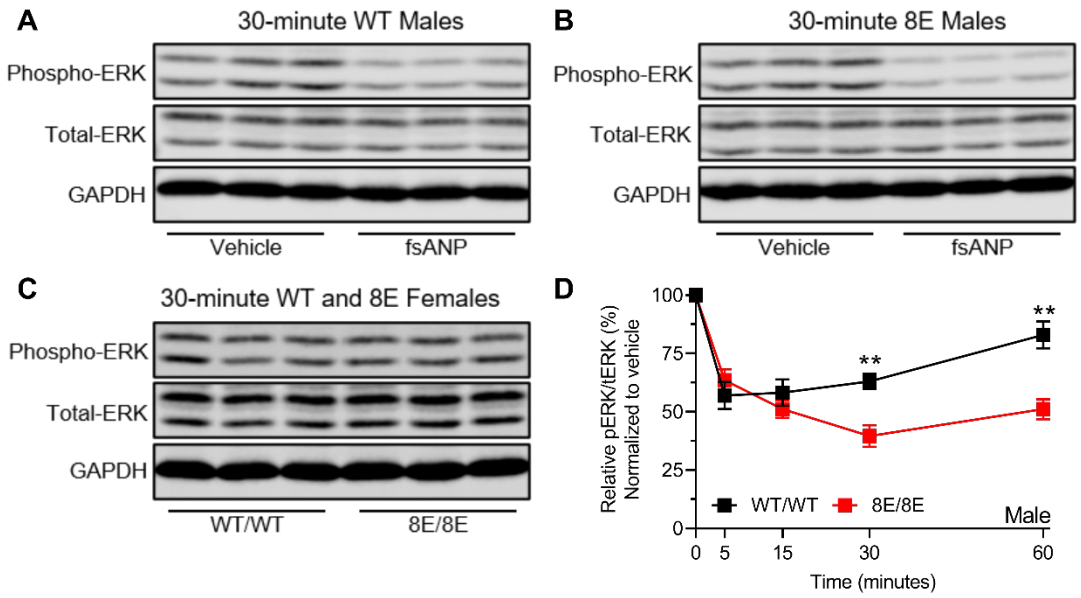

Figure 7. fsANP injection suppresses ventricular ERK1/2 activity to a greater extent and for a longer period of time in male GC-A$^{8E/8E}$ compared to male GC-A$^{WT/WT}$ mice.

Western blots of ventricular extracts probed for phospho-ERK1/2, total-ERK1/2, and GAPDH after injection with vehicle or fsANP in male GC-A$^{WT/WT}$ or GC-A$^{8E/8E}$ mice for (A and B) 30-minutes. (C) Western blot from female GC-A$^{WT/WT}$ and GC-A$^{8E/8E}$ mice 30 minutes after fsANP injection. (D) Relative ventricular ERK1/2 activities of male GC-A$^{WT/WT}$ and GC-A$^{8E/8E}$ mice normalized to vehicle control values as a function of time after fsANP injection. n = 4-7 mice per treatment. The symbols represent the means and the vertical bars within the symbols represent the SEM. Statistically significant differences were determined by two-way-ANOVA with multiple comparisons where ** = $p<0.01$.

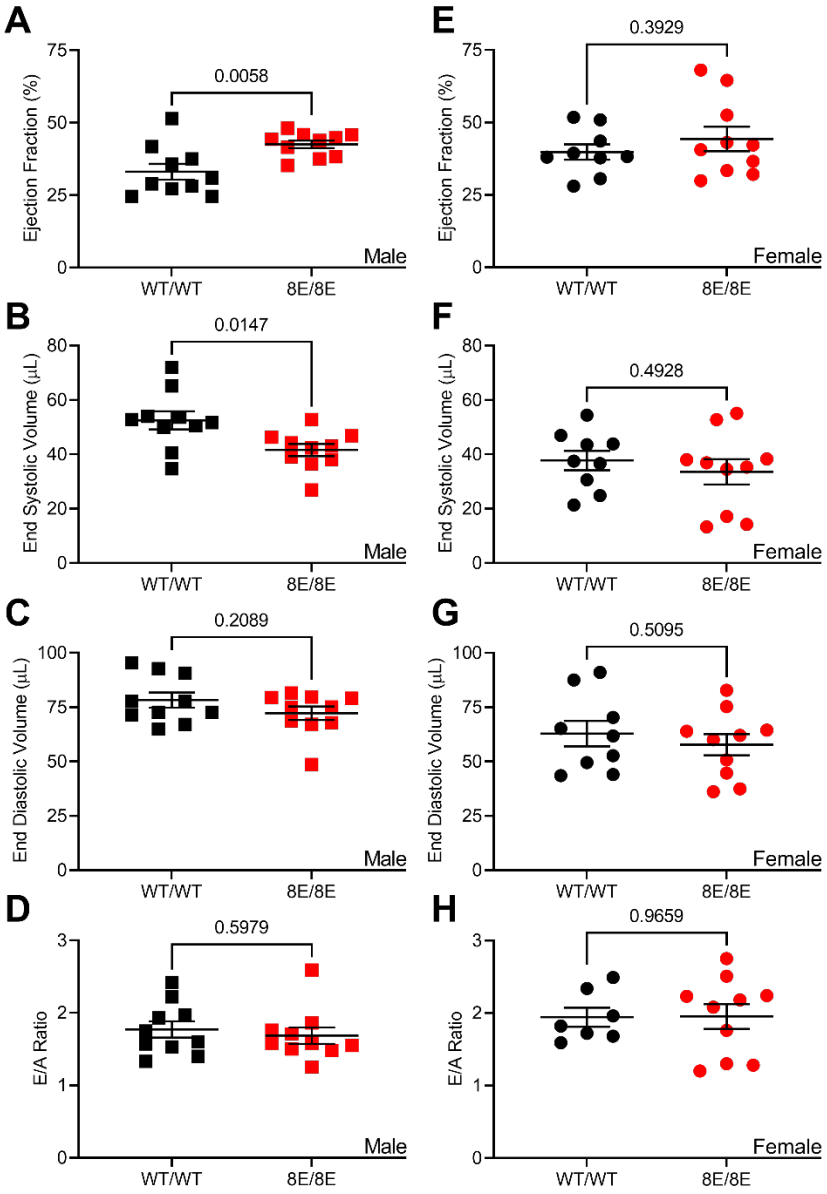

Figure 8. Male, but not female, GC-A$^{8E/8E}$ hearts have improved systolic function. 12-13-week-old male (left panels) and female (right panels) GC-A$^{WT/WT}$ (black symbols) and GC-A$^{8E/8E}$ (red symbols) mice were assessed by echocardiography for (A, E) ejection fraction; (B, F) end systolic volume; (C, G) end diastolic volume; (D, H) E/A Ratio. n = 7-10 mice per group. Long horizontal bars indicate the mean and vertical bars indicate SEM. Statistical differences were determined using a two-tailed student's t-test with associated p values shown in each panel.

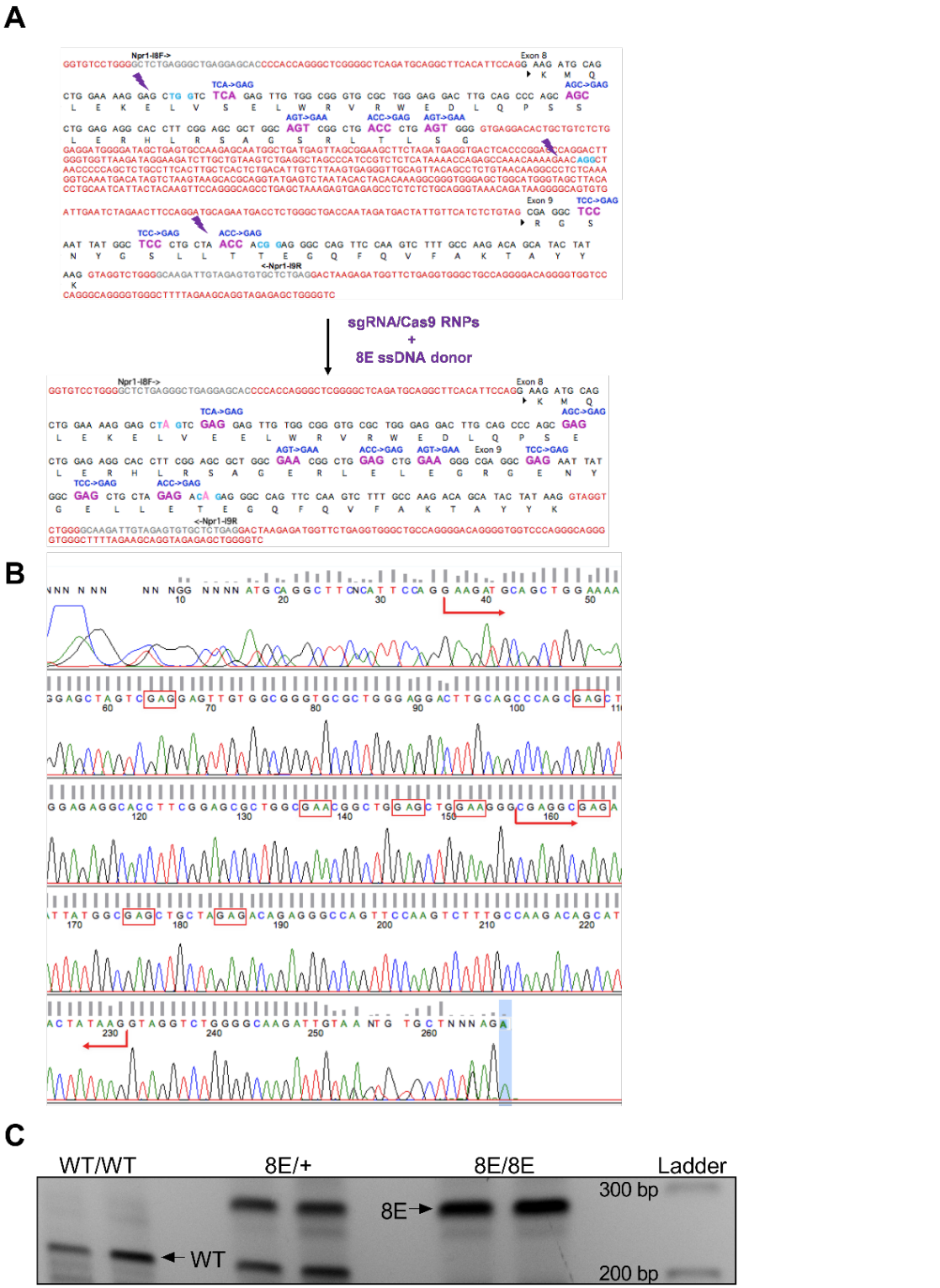

Supplemental Figure 1. GC-A$^{8E/8E}$ mice were generated by CRISPR/Cas9 mediated gene editing.

(A) Schematic depiction of CRISPR/Cas9 targeting sites with the protospacer adjacent motif (PAM) shown in light blue and the purple bolts indicating cleavage sites. 8E ssDNA donor serves as the template for homology-directed repair after DNA cleavage leading to knock-in of GC-A-8E and fusion of exons 8 and 9 sequence of the Npr1 allele. Pink nucleotides represent silent mutations to prevent re-cleavage of the Npr1 8E knock-in allele and genotyping primer sequence (Npr1-I8F + Npr1-I9R) is shown in grey. (B) Sequencing of GC-A confirms that all 8 previously identified phosphorylated serines and threonines (19, 30) were mutated to glutamates. (C) DNA amplified by PCR from each line that was separated on an agarose gel indicates successful generation of WT (GC-$A^{WT/WT}$), heterozygous (GC-$A^{8E/+}$), and homozygous knock-in (GC-$A^{8E/8E}$) mice. Lanes represent PCR amplified fragments from DNA extracted from tail snips of individual mice.

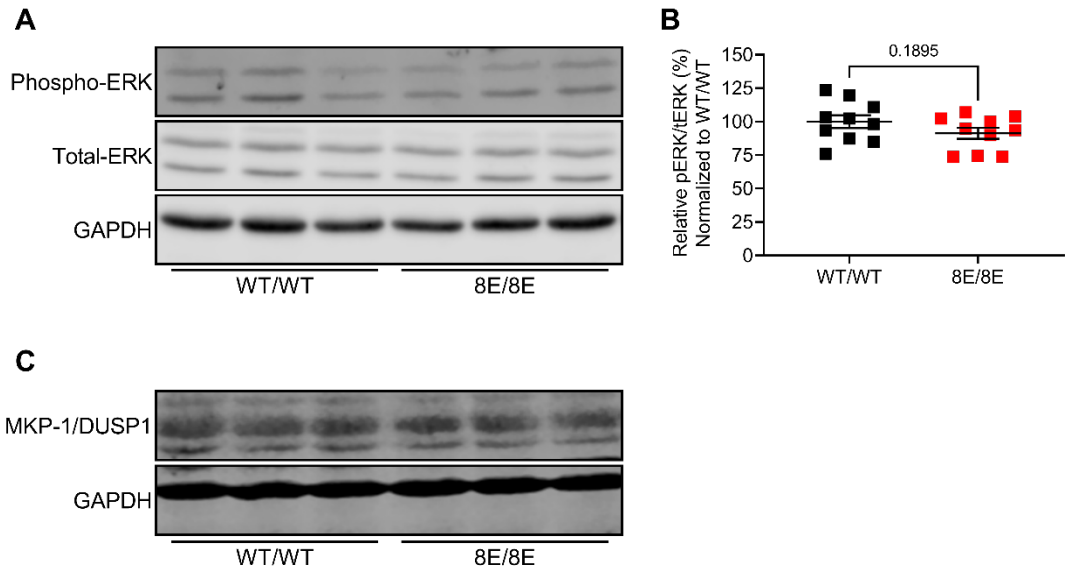

Supplemental Figure 2. Non-statistically significant decrease in ventricular ERK1/2 activity in 12-week-old male GC-A$^{8E/8E}$ mice.

Cardiac ERK1/2 activity from 12-week-old male GC-A$^{WT/WT}$ and GC-A$^{8E/8E}$ mice. (A) Representative western blot probed for phospho-ERK1/2, total-ERK1/2 and GAPDH. (B) Relative ventricular ERK1/2 activities of male GC-A$^{WT/WT}$ and GC-A$^{8E/8E}$ mice. (C) Representative western blot probed for MKP-1/DUSP1 and GAPDH. Long horizontal bars indicate the mean and vertical bars indicate SEM. Statistical differences were determined using a two-tailed student's t-test with the associated p value shown in panel B.

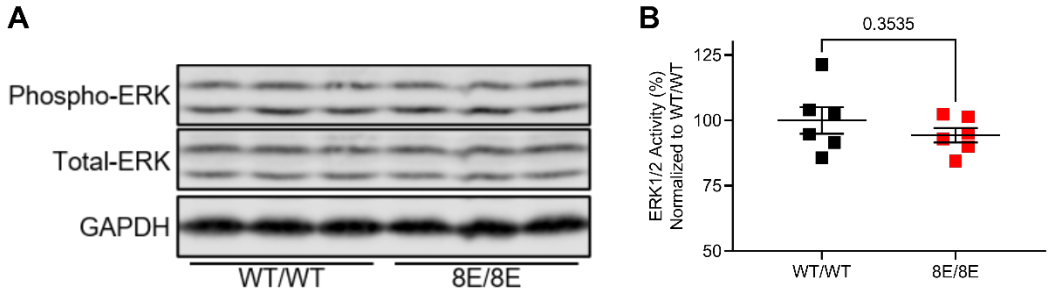

Supplemental Figure 3. No difference in cardiac ERK1/2 activity in 4-week-old GC-A$^{WT/WT}$ and GC-A$^{8E/8E}$ males.

Cardiac ERK1/2 activity from 4-week-old male GC-A$^{WT/WT}$ and GC-A$^{8E/8E}$ mice. (A) Representative western blot probed for phospho-ERK1/2, total-ERK1/2 and GAPDH. (B) Relative ventricular ERK1/2 activities of male GC-A$^{WT/WT}$ and GC-A$^{8E/8E}$ mice. n = 6 mice per group. Long horizontal bars indicate the mean and vertical bars indicate SEM. Statistical differences were determined using a two-tailed student's t-test with the associated p value shown in panel B.

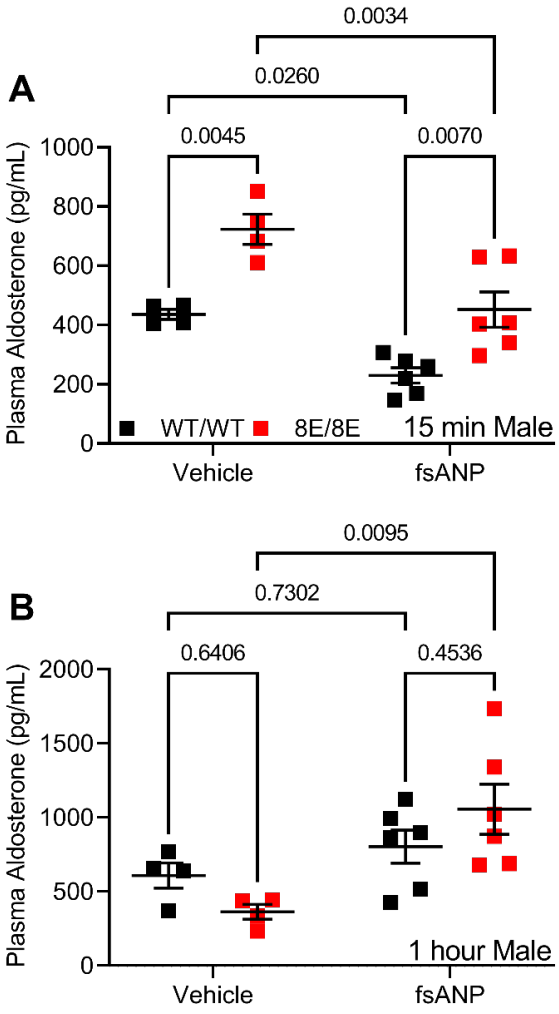

Supplemental Figure 4. Acute activation of GC-A with fsANP decreases plasma aldosterone similarly in male GC-A$^{WT/WT}$ and GC-A$^{8E/8E}$ in the short term, but not in the long term.

(A) Plasma aldosterone concentrations from male GC-A$^{WT/WT}$ and GC-A$^{8E/8E}$ mice 15 minutes after subcutaneous injection with saline or fsANP. (B) Plasma aldosterone concentrations from male GC-A$^{WT/WT}$ and GC-A$^{8E/8E}$ mice 60 minutes after subcutaneous injection with saline or fsANP. n = 4-6 mice per treatment. The symbols represent the means and the vertical bars within the symbols represent the SEM. Statistically significant differences were determined by two-way-ANOVA with multiple comparisons where p-values for each comparison are shown.

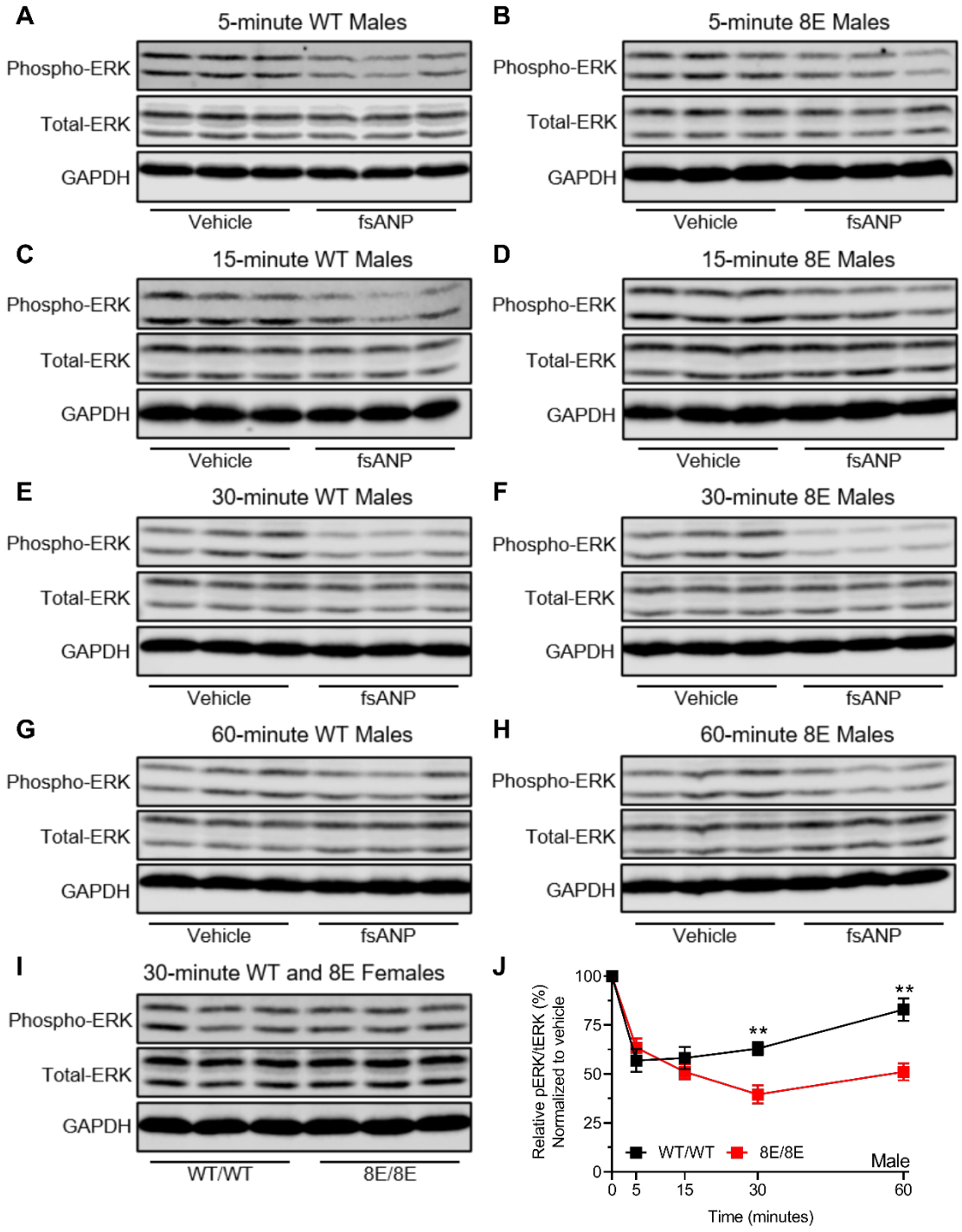

Supplemental Figure 5. fsANP injection suppresses ventricular ERK1/2 activity to a greater extent and for a longer period of time in male GC-A$^{8E/8E}$ compared to male GC-A$^{WT/WT}$ mice.

Western blots of ventricular extracts probed for phospho-ERK1/2, total-ERK1/2, and GAPDH after injection with vehicle or fsANP in male GC-$A^{WT/WT}$ or GC-$A^{8E/8E}$ mice for (A and B) 5-, (C and D) 15-, (E and F) 30-, or (G and H) 60- minutes. (I) Western blot from female GC-$A^{WT/WT}$ and GC-$A^{8E/8E}$ mice 30 minutes after fsANP injection. (J) Relative ventricular ERK1/2 activities of male GC-$A^{WT/WT}$ and GC-$A^{8E/8E}$ mice normalized to vehicle control values as a function of time after fsANP injection. n = 4-7 mice per treatment. The symbols represent the means and the vertical bars within the symbols represent the SEM. Statistically significant differences were determined by two-way-ANOVA with multiple comparisons where ** = $p<0.01$.

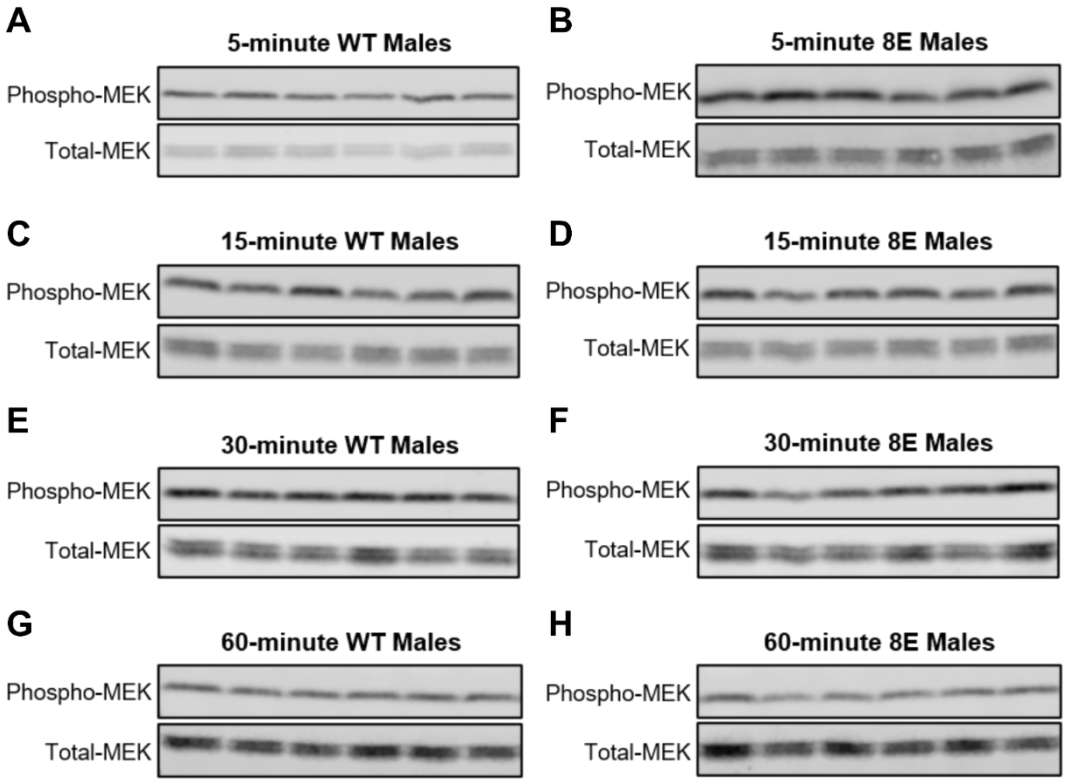

Supplemental Figure 6. No change in ventricular MEK activity in male GC-AWT/WT and GC-A8E/8E mice after fsANP injection.

Cardiac MEK activity from 12-week-old male GC-A$^{WT/WT}$ and GC-A$^{8E/8E}$ mice 5-, 15-, 30- and 60- minutes after fsANP injection. Ventricular lysates were prepared from GC-A$^{WT/WT}$ and GC-A$^{8E/8E}$ mice. Thirty micrograms of ventricular lysates were fractionated on a 10% gel by SDS-PAGE and transferred for 1 h at 100 Volts to a polyvinylidene difluoride membrane. The membrane was blocked with blocking buffer for 1 h at room temperature and then incubated overnight at 4°C with 1:1000 phospho-MEK antibody. The membrane was washed 3 x 5 min with TBST and then incubated with IRDye 680 goat anti-rabbit antibody with a dilution of 1:15,000 for 1 h at room temperature. The membrane was washed 3 × 5 min with TBST and then once with TBS and then visualized and quantified on a Li-Cor infrared imaging device. The membrane was then stripped and reprobed for total-MEK using the same procedure described above.

Supplemental Table 1A. Morphological parameters at 12 weeks of age.

PARAMETER	WT MALE (24)	8E MALE (20)	WT FEMALE (21)	8E FEMALE (15)
HW (mg)	153.2 ± 12.2	1 37.3 ± 12.3****	115.1 ± 11.4	114.1 ± 9.3
BW (g)	29.6 ± 2.5	29.4 ± 2.2	22.1 ± 2.7	22.3 ± 2.0
HW/BW (mg/g)	5.3 ± 0.5	4.6 ± 0.4****	5.3 ± 0.5	5.1 ± 0.5
CM CSA (μm^2)	184.5 ± 27.2	154.3 ± 9.0****	149.0 ± 9.9	146.7 ± 5.8
LW (mg)	231.5 ± 39.8	221.0 ± 42.5	212.6 ± 25.8	219.7 ± 34.8
LvW (mg)	1356 ± 173.3	1318 ± 206.0	1112 ± 238.5	1015 ± 136.5
KW (mg)	360.0 ± 44.9	340.1 ± 38.1	243.0 ± 34.2	257.9 ± 17.8

Data are presented as Mean ± standard deviation for the number of mice indicated in parenthesis

HW, heart weight; BW, body weight; CM CSA, cardiomyocyte cross-sectional area; LW, lung weight; LvW, liver weight; KW, kidney weight * Indicates $P<0.05$; ** $P<0.01$; *** $P<0.001$; **** $P<0.0001$ vs WT/WT of the same sex.

Supplemental Table 1B. Echocardiography at 12 weeks of age

CARDIAC FUNCTION	WT MALE (10)	8E MALE (10)	WT FEMALE (9)	8E FEMALE (10)
HR (bpm)	438 ± 40	434 ± 52	435 ± 53	436 ± 56
SV (μL)	25.8 ± 7.6	30.6 ± 4.7	25.1 ± 9.8	24.2 ± 4.3
EF (%)	33.1 ± 8.6	42.5 ± 4.2**	39.8 ± 8.0	44.3 ± 13.3
FS (%)	15.7 ± 4.7	20.6 ± 2.4**	19.1 ± 4.5	21.9 ± 8.0
EDV (μL)	78.3 ± 10.9	72.2 ± 9.8	62.9 ± 17.6	57.8 ± 15.4
ESV (μL)	52.5 ± 10.6	41.6 ± 7.1*	37.7 ± 10.7	33.6 ± 14.7
CO (ml/min)	11.2 ± 2.6	13.3 ± 2.5	10.7 ± 3.4	10.4 ± 1.7
IVS;s (mm)	0.88 ± 0.14	0.97 ± 0.15	0.88 ± 0.06	0.99 ± 0.18
IVS;d (mm)	0.73 ± 0.07	0.74 ± 0.08	0.68 ± 0.06	0.75 ± 0.09
LVID;s (mm)	3.5 ± 0.3	3.2 ± 0.3*	3.1 ± 0.4	2.9 ± 0.6
LVID;d (mm)	4.2 ± 0.2	4.1 ± 0.2	3.8 ± 0.4	3.7 ± 0.4
LVPW;s (mm)	0.93 ± 0.1	0.97 ± 0.1	0.90 ± 0.1	0.95 ± 0.1
LVPW;d (mm)	0.72 ± 0.1	0.74 ± 0.1	0.69 ± 0.1	0.68 ± 0.1
E/A	1.8 ± 0.4	1.7 ± 0.4	1.9 ± 0.3	2.0 ± 0.5
E (mm/s)	458 ± 78	494 ± 67	458 ± 126	534 ± 119
AOV (mm/s)	752 ± 104	817 ± 189	694 ± 153	608 ± 90 (9)

Data are presented as Mean ± standard deviation for the number of mice indicated in parentheses. HR, heart rate; SV, stroke volume; EF, ejection fraction; FS, fractional shortening; EDV, end diastolic volume; ESV, end systolic volume; CO, cardiac output; IVS;s, interventricular septal thickness at systole; IVS;d, interventricular septal thickness at diastole; LVID;s, left ventricular internal diameter systole; LVID;d, left ventricular internal diameter diastole; LVPW;s, left ventricular posterior wall systole; LVPW;d, left ventricular posterior wall diastole; E/A, early mitral valve filling velocity/ late mitral valve filling velocity; E, early mitral valve filling velocity ; AoV, peak aortic velocity. Statistical differences were determined using a two-tailed student's t-test. * Indicates $P<0.05$; ** $P<0.01$; *** $P<0.001$; **** $P<0.0001$ vs WT/WT of the same sex.

CHAPTER 3: PREVENTION OF GUANYLYL CYCLASE–B DEPHOSPHORYLATION RESCUES ACHONDROPLASTIC DWARFISM

Brandon M. Wagner[1], Jerid W. Robinson[2], Yun-Wen Lin[3], Yi-Ching Lee[3], Nabil Kaci[4], Laurence Legeai-Mallet[4], and Lincoln R. Potter[1,2]

[1]Departments of Integrative Biology and Physiology, [2]Biochemistry, Molecular Biology, and Biophysics, and Surgery at the University of Minnesota, Medical School, Minneapolis, MN 55455 USA. [3]Institute for Cellular and Organismic Biology, Academia Sinica, Taipei, Taiwan. [4]Université de Paris, Imagine Institute, Laboratory of Molecular and Physiopathological Bases of OsteochonDrodysplasia, INSERM UMR 1163, F-75015, Paris, France.

Published in:

Journal of Clinical Investigation Insight. 2021, 6(9):e147832.

SUMMARY

Activating mutations in the fibroblast growth factor receptor 3 (FGFR3) or inactivating mutations in guanylyl cyclase B (GC-B), also known as NPR-B or Npr2, cause short-limbed dwarfism. FGFR3 activation causes dephosphorylation and inactivation of GC-B, but the contribution of GC-B dephosphorylation to achondroplasia (ACH) is unknown. GC-$B^{7E/7E}$ mice that express a glutamate-substituted version of GC-B that cannot be inactivated by dephosphorylation were bred with mice expressing FGFR3-G380R, the most common human ACH mutation, to determine if GC-B dephosphorylation is required for ACH. Crossing GC-$B^{7E/7E}$ mice with $FGFR3^{G380R/G380R}$ mice increased naso-anal and long (tibia and femur), but not cranial, bone length twice as much as crossing GC-$B^{7E/7E}$ mice with $FGFR3^{WT/WT}$ mice from 4 to 16 weeks of age. Consistent with increased GC-B activity rescuing ACH, long bones from the GC-$B^{7E/7E}$/$FGFR3^{G380R/G380R}$ mice were not shorter than those from GC-$B^{WT/WT}$/$FGFR3^{WT/WT}$ mice. At two weeks of age, male but not female $FGFR3^{G380R/G380R}$ mice had shorter long bones and smaller growth plate hypertrophic zones, whereas female but not male GC-$B^{7E/7E}$ mice had longer bones and larger hypertrophic zones. In 2-week-old males, crossing $FGFR3^{G380R/G380R}$ mice with GC-$B^{7E/7E}$ mice increased long bone length and hypertrophic zone area to levels observed in mice expressing WT versions of both receptors. We conclude that preventing GC-B dephosphorylation rescues reduced axial and appendicular skeleton growth in a mouse model of achondroplasia.

INTRODUCTION

Achondroplasia (ACH) is the most common form of human skeletal dwarfism, which affects about 1 in 20,000 live births world-wide (201-203). ACH is disproportionate dwarfism. Both the appendicular and axial skeleton are affected. Skeletal defects include rhizomelic bowing of long bones, macrocephaly, midface hypoplasia, maxillary hypoplasia, depressed nasal bridges and spinal foramen magnum stenosis. Adults with ACH have an average height of just over four feet and more than 80% of ACH cases spontaneously occur through mutations in sperm associated with increased paternal age (277). The vast majority of achondroplasia cases result from a single amino acid substitution in fibroblast growth factor receptor 3 (FGFR3) that increases the tyrosine kinase activity of the receptor (202, 203). The most common missense mutation in humans is p.Gly380Arg. Cell culture studies determined that mutations that cause more deleterious ACH phenotypes result in greater increases in phosphorylation and activation of FGFR3 (278). Murine transgenic studies demonstrated that expression of Fgfr3 gain of function mutations (p.Gly380Arg) in chondrocytes and osteoblasts results in ACH (205, 206).

FGFR3 is a tyrosine kinase receptor that signals through multiple downstream pathways including: ERK1/2/MAPK, p38/MAPK, PI3K/AKT, STATs, and PLC□ (201). In the growth plate, FGFR3 activates both STATs and the ERK1/2 kinases (279). Although disruption of the Stat1 gene rescued the chondrocyte proliferation deficiency in *Fgfr3*$^{G374R/+}$ mice, these mice still developed an achondroplasia-like phenotype (280). In contrast, activated MEK1 expression in chondrocytes of mice lacking active Stat1 yielded an achondroplasia-like phenotype with a decreased hypertrophic chondrocyte zone but no decrease in chondrocyte proliferation (280). Numerous ACH mouse models have been generated with bone and growth plate cartilage anomalies associated with small proliferative and hypertrophic chondrocyte area and less matrix secretion (205, 206). Recently, the mouse *Fgfr3* gene was replaced with the human FGFR3-G380R cDNA to generate a humanized drug discovery model (207). These mice recapitulate the disproportionate shortening of the limbs, kyphosis, and midface hypoplasia observed in ACH patients, but unlike humans and other ACH murine models, expression of two FGFR3-G380R alleles (FGFR3$^{G380R/G380R}$) is required for maximum skeletal reductions in these animals (207).

Guanylyl cyclase (GC-B) is a membrane enzyme that produces cGMP when activated by C-type natriuretic peptide (CNP) (9, 85, 230, 281). Under basal conditions, the pseudokinase domain of GC-B is phosphorylated on multiple serines and threonines, which is required to transmit the CNP activation signal to the catalytic domain (135, 148, 200). However, prolonged CNP exposure or brief exposure to antagonistic hormones or growth factors results in GC-B dephosphorylation and inactivation (135, 140, 141, 184-186). Phosphorylation is absolutely required for CNP-dependent activation of GC-B and alanine substitutions for the known phosphorylation sites yields an enzyme that is not activated by CNP (135, 148, 200). In contrast, conversion of the phosphorylated serines and threonines to glutamate to constitutively mimic the negative charge of the phosphorylated residues produces an enzyme that is activated by CNP but not inactivated by dephosphorylation (154, 184-186, 217). GC-B knock out mice or GC-B mice with alanine substitutions for the phosphorylated serines and threonines are dwarfed and have smaller growth plates that are similar to those of ACH mice (60, 98, 200). In humans, inactivating mutations in both alleles of GC-B cause acromesomelic dysplasia Maroteaux (AMDM) type dwarfism (98, 99, 190), whereas CNP overexpression or constitutively activating mutations in GC-B cause skeletal overgrowth (64, 196-198, 209). Natriuretic peptide clearance receptor (NPR-C) also binds CNP and degrades it (229). Inactivation of NPR-C (66, 71, 72) or elevated blood osteocrin concentrations (226), a natural decoy peptide for NPR-C (282-284), increase both plasma CNP levels and long bone growth (226).

Plasma CNP is elevated in human ACH and AMDM patients (192, 193, 285). Importantly, ACH mice overexpressing a CNP transgene (209) or subcutaneously injected with CNP (210) or the proteolytically resistant CNP analog, BMN-111 (211), display increased hypertrophic chondrocytes and matrix production that is correlated with ERK1/2 but not STAT3 inhibition (209, 211). However, activation of p38 MAP kinase is also associated with CNP/GC-B-dependent increases endochondral bone growth (286, 287).

Both FGFR3 and GC-B are highly expressed in proliferating chondrocytes and reciprocal antagonism between the FGF-FGFR3 and CNP-GC-B pathways has been reported by multiple investigators (209, 210, 214, 215). Specifically, CNP-GC-B signaling was shown to inhibit FGFR3-dependent MAP kinase activation via protein kinase G regulation of Raf-1 (215, 288). Conversely, FGF inhibits CNP-dependent cGMP

elevations by increasing GC-B dephosphorylation (216, 217). Importantly, FGF failed to inactivate GC-B-7E in cell culture and in live tibial tissue, consistent with FGF-dependent inactivation of GC-B requiring decreased receptor phosphorylation (216, 217). Since inactivation of GC-B causes a similar phenotype to that observed with FGFR3 gain of function mutations, and FGFR3 activation causes GC-B dephosphorylation and inactivation, we hypothesized that GC-B dephosphorylation is required for the FGFR3-dependent ACH. If this hypothesis is correct, then preventing GC-B dephosphorylation by substituting glutamates for known phosphorylation sites should prevent or reduce the severity of FGFR3-dependent ACH.

To test this hypothesis, we crossed mice where one allele of the FGFR3 gene was replaced with the human FGFR3-G380R gain of function gene (207) with mice expressing one GC-B-7E allele (186) to generate mouse lines of all possible genetic combinations. We observed that both naso-anal and long bone length of the $FGFR3^{G380R/G380R}$; $GC\text{-}B^{7E/7E}$ mice was greater than that for $FGFR3^{G380R/G380R}$; $GC\text{-}B^{WT/WT}$ mice. Importantly, we also observed that the hypertrophic zones of two-week old growth plates of the $FGFR3^{G380R/G380R}$; $GC\text{-}B^{7E/7E}$ male mice were the same size as those in WT male mice. Thus, prevention of GC-B dephosphorylation at an early age improved defective chondrocyte differentiation sufficiently to allow normal long bone growth.

METHODS

Animals. Male and female WT and GC-B$^{7E/7E}$ mice (originally described as *Npr2*$^{7E/7E}$) were genotyped and maintained as previously described on a C57BL6/J background (186). The FGFR3$^{G380R/G380R}$ mice were genotyped and maintained on a mixed C57BL6/129 Sv line (207). Crosses between the GC-B$^{7E/+}$ C57BL6/J mice and the FGFR$^{ACH/+}$ C57BL6/129 Sv mice produced all the genotypes shown in figures 1 and 2. Mice were fed standard chow under specific-pathogen-free conditions. Animal care was compliant with the University of Minnesota Institutional Animal Care and Use Committee approved protocol number 1806A-35995.

Naso-anal, cranial, tibial, and femoral measurements. Naso-anal measurements were conducted on conscious male and female mice once weekly from 4 to 16 weeks of age for the duration of the study using a digital caliper. Mice were euthanized at 16 weeks and their tibias, femurs, and craniums were isolated and measured using a digital caliper. In a separate study, tibia and femur length from two-week-old mice were determined as described above.

Growth plate histology. 2-week-old male and female mice were euthanized, and femurs were harvested and fixed in 4% paraformaldehyde for 24h and then stored in fresh 4% paraformaldehyde until they were embedded in paraffin and sectioned. The bone sections were then stained with hematoxylin and eosin and imaged with a 5X or 10X objective lenses. The upper and lower bounds of the cross-sectional area of the hypertrophic zones were identified by a morphology of columnar, stacked cells that were measured in millimeters in an unbiased manner using ImageJ software. The freehand selection tool in ImageJ determined the number of square millimeters of the identified hypertrophic region from each section of bone as indicated by the blue outline in the images shown in figures 6 and 7. In a blinded manner, the square millimeter value from each femoral section was determined and plotted as a single value in figures 6B and 7B.

Statistics. Statistics and graphs were generated with Prism 8 software (GraphPad Software, La Jolla, CA). For the naso-anal growth curves, a mixed-model two-way ANOVA with repeated measures was applied using Geisser-Greenhouse correction for sphericity and Tukey's correction for multiple comparisons. Hence, the naso-anal length values described under results were derived from repetitive measurements on the same animal at multiple ages. The remaining analyses including the growth plate

measurements were performed using a standard, one-way ANOVA assuming Gaussian distribution and equal SD with Tukey's correction for multiple comparisons. Except for the naso-anal growth curves, each symbol in a figure represents a measurement from an individual mouse. The longer horizontal bar within each group of symbols represents the mean and the shorter bars above and below the mean represent the standard error of the mean. For the naso-anal growth curves, each point represents the mean length measurement at the indicated age, and bars above and below the mean indicate standard error of the mean. Differences were considered significantly different when the p value was less than 0.05.

RESULTS

Generation of the mouse lines. To evaluate the contribution of GC-B dephosphorylation to ACH, we crossed the GC-B$^{7E/+}$ mice as originally described as Npr$^{7E/+}$ by Shuhaibar et al. (186) or as GC-B$^{7E/+}$ by Robinson et al. (228) with the FGFR3$^{G380R/+}$ mice originally described as FGFR3$^{ACH/+}$ by Lee et al. (207) to generate all the murine lines shown in figures 1 and 2. The F1 cross generated F2 littermates of every possible combination of the FGFR3 and GC-B genes in a mixed C57BL6/129 Sv background. The F2 pups were weaned and genotyped 21 days after birth. Naso-anal measurements were performed once weekly from 4 to 16 weeks of age. Initial visual characterization of 16-week-old male mice indicated that expression of two GC-B-7E alleles rescued the majority of the naso-anal length defect but failed to rescue the midface hypoplasia defect in mice expressing two FGFR3^{G380R} alleles that was obvious to the naked eye (Fig. 1). Quantitation of the skeletal growth characteristics of the various mouse lines is described in detail below.

FGFR3-G380R and GC-B-7E exhibit sex-specific gene-dosage effects. Although the effects of FGFR3-G380R and GC-B-7E expression on naso-anal length of mixed male and female populations have been described (207, 217), the effects of sex have not been reported for either murine receptor. Using repeated measures analysis from 4 weeks to 16 weeks of age, we observed that expression of one allele of FGFR3-G380R decreased skeletal length in male mice by 4.7% but only decreased skeletal length by 1.3% in female mice compared to WT controls (Fig. 2A and B). Expression of two FGFR3-G380R alleles further decreased skeletal length in both sexes, but bone length was decreased to a greater extent (11.4%) in males, than in females (8.6%) (Fig. 2A and B). In contrast, expression of a single allele of GC-B-7E increased skeletal length 3.7% in females but only increased skeletal length 1.8% in males (Fig. 2C and D). Expression of two alleles of GC-B-7E increased skeletal length 4.1% in males but increased skeletal length 5.3% in females (Fig. 2C and D).

When comparing naso-anal length differences at a single age of 16 weeks, single and double FGFR3-G380R alleles decreased naso-anal length of male mice 5.7% and 11.0%, but females were reduced by 1.7% and 10.3% (Fig. 2E). In contrast, single and double alleles of GC-B-7E increased naso-anal length 1.7% and 5.4%, and 3.3% and 5.0% in males and females, respectively (Fig. 2F). Thus, a single allele of FGFR3-

G380R produces a significant decrease in long bone length in adult male but not female mice. Conversely, a single allele of GC-B-7E significantly increased long bone growth in females but not males.

GC-B$^{7E/7E}$ expression increases naso-anal length more in ACH mice than in WT mice. To evaluate the contribution of GC-B dephosphorylation to ACH, we generated the mouse lines shown in panels A and B of Fig. 3. These data indicate that expressing two alleles of GC-B-7E in mice with two alleles of FGFR3-G380R increases naso-anal length to a greater extent than expressing two alleles of GC-B-7E in mice with two WT FGFR3 alleles. Specifically, GC-B$^{7E/7E}$ expression in an ACH background increased naso-anal length 8.4% and 6.7% in male and female mice, respectively, compared to 4.1% and 5.3% increases in FGFR3$^{WT/WT}$ mice. When examining naso-anal growth at a single time period of sixteen weeks, expression of two GC-B-7E alleles increased growth by 5.3% in males and 4.7% in females in FGFR3$^{WT/WT}$ mice, but by 8.4% and 8.0%, respectively, in FGFR3$^{G380R/G380R}$ mice (Fig. 3C and D). The fact that GC-B-7E expression increases naso-anal length more in FGFR3$^{G380R/G380R}$ mice than in FGFR3$^{WT/WT}$ mice is consistent with GC-B dephosphorylation contributing to the reductions in naso-anal growth associated with ACH. In other words, GC-B-7E prevents FGFR3$^{G380R/G380R}$ – dependent reductions in the axial skeleton.

GC-B-7E increases individual long bone length more in ACH mice than in WT mice. Femurs and tibias from male and female GC-B$^{WT/WT}$; FGFR3$^{WT/WT}$, GC-B$^{7E/7E}$; FGFR3$^{WT/WT}$, GC-B$^{WT/WT}$; FGFR3$^{G380R/G380R}$, and GC-B$^{7E/7E}$; FGFR3$^{G380R/G380R}$ mice were excised and measured at 16-weeks of age. Homozygous GC-B-7E expression in either the ACH (FGFR3$^{G380R/G380R}$) or WT (FGFR3$^{WT/WT}$) background resulted in greater long bone growth (Fig. 4). However, the 12.6% and 7.9% increase in femur length observed for male and female GC-B$^{7E/7E}$ mice expressing two FGFR3-G380R alleles was significantly greater than the 4.3% and 5.0% increase in femur length observed in male and female GC-B$^{7E/7E}$ mice expressing two WT FGFR3 alleles (Fig. 4D and E). In fact, expression of two GC-B-7E alleles restored femoral and tibial lengths in both male and female FGFR3$^{G380R/G380R}$ mice to lengths that were not significantly different from values observed for mice expressing two WT alleles for both receptors (Fig. 4B and C). These data indicate that GC-B-7E expression prevents FGFR3$^{G380R/G380R}$ – dependent reductions in long bone length and improves the appendicular skeleton.

Cranial length and midface hypoplasia are not rescued by GC-B-7E expression. Although cranial length was slightly longer in mixed populations of male and female GC-B$^{7E/7E}$ mice compared to mixed populations of GC-B$^{WT/WT}$ mice, and the cranial length of the FGFR3$^{G380R/G380R}$ mice with two GC-B-7E alleles (24.15mm) was slightly greater than that for mice with two GC-B-WT alleles (23.00mm)($p = 0.15$)(Fig. 4F), post-hoc power calculations indicated that our study was significantly underpowered for this analysis (power = 36%). Based on the differences observed in our initial study, we would need 50 mice per group to reach 80% power, which is prohibitive. Consistent with the lack of differences in cranial length data, GC-B$^{7E/7E}$ expression failed to rescue the midface hypoplasia and macrocephaly exhibited by the FGFR3$^{G380R/G380R}$ mice in Fig. 1.

FGFR3-G380R and GC-B-7E expression affect long bone growth in 2-week-old mice in sex specific manners. To better define the earliest time at which the effects of the FGFR3-G380R and GC-B-7E alleles affect long bone growth, we measured tibia and femur length from two-week old male and female FGFR3$^{WT/WT}$/GC-B$^{WT/WT}$, FGFR3$^{WT/WT}$/GC-B$^{7E/7E}$, FGFR3$^{G380R/G380R}$/GC-B$^{WT/WT}$ and FGFR3$^{G380R/G380R}$/GC-B$^{7E/7E}$ mice (Fig. 5). Interestingly, we observed that tibias and femurs from two-week-old mice expressing two FGFR3-G380R alleles were only shorter in male mice. Conversely, tibias and femurs were only longer in female two-week-old mice expressing two GC-B-7E alleles. As with the older mice, GC-B-7E expression rescued tibia and femur reductions observed in the FGFR3$^{G380R/G380R}$ two-week-old male mice. Hence, the single gene effects of FGFR3-G380R and GC-B-7E on tibia and femur length occur as early as two weeks of age but only in sex-specific manners. Importantly, GC-B-7E expression rescued the long bone reductions observed for the two-week-old FGFR3$^{G380R/G380R}$ male mice as it did for sixteen-week-old male and female mice.

Prevention of GC-B dephosphorylation rescues reduced hypertrophic zone area in two-week-old FGFR3$^{G380R/G380R}$ male mice. Growth plates from 2-week old femurs were sectioned, stained and analyzed as previously described (207). The growth plates from the FGFR3$^{WT/WT}$/GC-B$^{WT/WT}$ mice were compared with growth plates from FGFR3$^{WT/WT}$/GC-B$^{7E/7E}$, FGFR3$^{G380R/G380R}$/GC-B$^{WT/WT}$ and FGFR3$^{G380R/G380R}$/GC-B$^{7E/7E}$ mice to determine how increased GC-B activity affects hypertrophic zone area in mice expressing mutant and WT FGFR3. Specifically, we examined if the expression of GC-B-7E increased hypertrophic zone area to a greater extent in FGFR3$^{G380R/G380R}$ growth plates compared to FGFR3$^{WT/WT}$ growth plates. Previous murine studies indicated that

CNP primarily increases chondrocyte hypertrophy (differentiation) as opposed to proliferation (289).

Analysis of growth plates from male mice of each genotype indicated that GC-$B^{7E/7E}$ expression increased the hypertrophic zone area in animals expressing either $FGFR3^{WT/WT}$ or $FGFR3^{G380R/G380}$ (Fig. 6). However, the GC-$B^{7E/7E}$ - dependent increase in hypertrophic zone area was greater in the $FGFR3^{G380R/G380R}$ mice (70.2% increase, p value = 0.003) compared to the $FGFR3^{WT/WT}$ mice (29.6% increase, p value = 0.11). In fact, the hypertrophic zones were not significantly different between the $FGFR3^{G380R/G380R}$/GC-$B^{7E/7E}$ mice and the $FGFR3^{WT/WT}$/GC-$B^{WT/WT}$ mice (p value = 0.80), which is consistent with GC-$B^{7E/7E}$ expression rescuing the hypertrophic zone defect in the $FGFR3^{G380R/G380R}$ mice.

In female mice, hypertrophic zone decreases were not observed in $FGFR3^{G380R/G380R}$ compared to $FGFR3^{WT/WT}$ mice at 2 weeks (p value = 0.87). However, GC-B-7E expression increased hypertrophic zones in both $FGFR3^{WT/WT}$ (27.7% increase, p value = 0.007) and $FGFR3^{G380R/G380R}$ (18.2% increase, p value = 0.032) female mice (Fig. 7A and B). In contrast to the males, hypertrophic zone area in $FGFR3^{G380R/G380R}$/GC-$B^{7E/7E}$ female mice was significantly larger than that observed in $FGFR3^{WT/WT}$/GC-$B^{WT/WT}$ female mice (p value = 0.0099), possibly because the FGFR3-G380R mutations failed to decrease long bone growth in the female mice at this early age. Together, these data indicate that the inhibitory effects of the FGFR3-G380R mutations occur earlier in male than female mice, whereas the positive effects of GC-B-7E expression on growth plate area occur earlier in females than males.

DISCUSSION

In this report, skeletal phenotypes of mice expressing GC-B-7E alleles and FGFR3-G380R alleles were analyzed and described as a function of age. Our results demonstrate that blocking dephosphorylation-dependent inactivation of GC-B rescues the disproportionate dwarfism of the $FGFR3^{G380R/G380R}$ mice by preventing the FGFR3-G380R-dependent decreases in growth plate hypertrophic zone area as graphically summarized in Fig. 8. The rescue was observed at multiple biological levels including naso-anal length, individual femur and tibia length, as well as growth plate hypertrophic zone area. Specific interactions between GC-B and FGFR3 on long bone growth were also identified. For example, crossing the $GC\text{-}B^{7E/7E}$ mice with the $FGFR3^{G380R/G380R}$ mice had a greater effect on naso-anal and long bone length than crossing the $GC\text{-}B^{7E/7E}$ mice with $FGFR3^{WT/WT}$ mice.

Sex-specific, single allele differences for both genes on long bone growth were also described for the first time. For single FGFR3-G380R alleles in adult mice, greater skeletal length effects were observed in males, whereas for GC-B-7E, greater effects were observed in females. Increased CNP-GC-B dependent bone growth in females is consistent with studies showing that CNP expression is more sensitive to exogenous CNP infusion in female compared to male rats (290). Unexpectedly, analysis of two-week old femurs and tibias indicated that only males had FGFR3-G380R-dependent reductions in long bone growth, whereas only females exhibited GC-B-7E-dependent increases in bone growth at two-weeks of age. Histological examination of two-week old growth plates confirmed that FGFR3-G380R expression decreased hypertrophic zone area of male but not female growth plates. In contrast, GC-B-7E expression increased the hypertrophic zone area in female but not male growth plates. Importantly, GC-B-7E expression rescued the hypertrophic zone defects in the male $FGFR3^{G380R/G380R}$ mice. In fact, there was no difference in the size of the growth plates from the $FGFR3^{G380R/G380R}/GC\text{-}B^{7E/7E}$ mice compared to mice expressing WT versions of both receptors, which is consistent with a rescue of the reduced hypertrophic zone by GC-B-7E expression. Sex specific effects of ACH on limb lengthening and bone age delay in children have been described but whether these effects are related to our results in mice is currently unknown (291, 292).

The differences in naso-anal growth between the various genetic lines changed very little over the 4 to 16-week measurement period, which indicates that the primary effects of GC-B on long bone growth occurs before 4 weeks of age. Large differences in both two-week old bones and growth plate hypertrophic zones between mice expressing GC-B-7E and FGFR3-G380R alleles support the idea that the major skeletal effects resulting from the activation of these receptors occurs long before closure of the epiphyseal growth plate. Previously reported increases in murine CNP mRNA at three weeks compared to six weeks supports the notion that early GC-B activity facilitates endochondral bone growth (226). Identifying when GC-B activation exerts its greatest effect on the growth plate may be important for determining optimal timing of BMN-111 treatment of children with ACH. Please see below.

While the FGFR3$^{G380R/G380R}$ mice with two alleles of GC-B-7E are not dwarfed, they retain the midface hypoplasia that is a hallmark of ACH. This finding suggests that although GC-B dephosphorylation is a primary mechanism by which the appendicular and axial skeleton is regulated, the majority of the cranial abnormality is not rescued by increased GC-B activity. However, treatment with BMN-111 and the phosphatase inhibitor LB-100 rescued skull base abnormalities in an *ex vivo* embryonic skull culture assay from Fgfr3$^{Y367C/+}$ mice (293). Thus, a reasonable interpretation of our cranial length data is that since only a small portion of the skull is stimulated by GC-B, differences in cranial length between GC-B$^{WT/WT}$ and GC-B$^{7E/7E}$ mice is difficult to demonstrate when measuring the total length of the skull. Hence, the majority of the skull growth occurs by membranous ossification, but a small portion at the base of the skull grows by endochondral ossification, which is stimulated by GC-B.

We suggest that GC-B dephosphorylation is both necessary and sufficient for ACH-dependent reductions in long bone growth. Regarding the “sufficiency” claim, a plethora of reports have shown that inactivating mutations in only GC-B result in dwarfism in mice, rats, and humans (98, 99, 190, 194, 200, 294, 295). Hence, it is clear that inactivation of GC-B as occurs with dephosphorylation (135, 148), is sufficient to cause ACH-like dwarfism. The data supporting the “necessary” claim are that mice expressing alanine substitutions for the phosphorylated serines and threonines in GC-B are dwarfed (200) and the GC-B$^{7E/7E}$ mice that express a version of GC-B that cannot be inactivated by dephosphorylation are immune to the long bone and growth plate reductions seen in the FGFR3 $^{G380R/G380R}$ mice. Thus, if GC-B is never phosphorylated,

the mice are dwarfed. Conversely, if GC-B cannot be inactivated by dephosphorylation, as is the case in the GC-B$^{7E/7E}$ mice, then they are resistant to ACH.

Finally, multiple investigators have reported that CNP or BMN-111 (vosoritide) injections increase long bone growth in animal models of ACH (61, 199, 209-212, 296, 297). Recent clinical phase III studies also indicate that vosoritide increases growth curves in achondroplastic children (213, 298, 299). The fact that BMN-111 is effective in these various ACH models means that a significant fraction of GC-B is phosphorylated, since dephosphorylated GC-B is not activated by CNP, or presumably, CNP analogs (135, 148). According to our hypothesis, GC-B dephosphorylation resulting from constitutive activation of FGFR3, is a significant part of the molecular explanation for ACH, although we cannot rule out that other FGFR3 activated signaling pathways also participate in this process. Importantly, if preventing GC-B dephosphorylation recues ACH as we suggest, then therapies that preserve or increase the phosphorylation state of GC-B, should increase long bone growth in ACH models. Consistent with this hypothesis, the phosphatase inhibitor LB-100 was recently shown to synergistically work with BMN-111 to improve long bone growth in mice (293). Future experiments are required to determine if this combination therapy will be safe and effective in other mammalian species including humans.

FIGURES

Figure 1. Expression of two GC-B$^{7E/7E}$ alleles rescues the naso-anal length but not the mid-face hypoplasia defect in FGFR3$^{G380R/G380R}$ mice.

Male 16-week-old mice of the indicated genotype are shown for visual comparison. The WT or mutant versions of the FGFR3 or GC-B genes that are expressed in each line are shown at the bottom of the figure. The red arrows indicate midface hypoplasia.

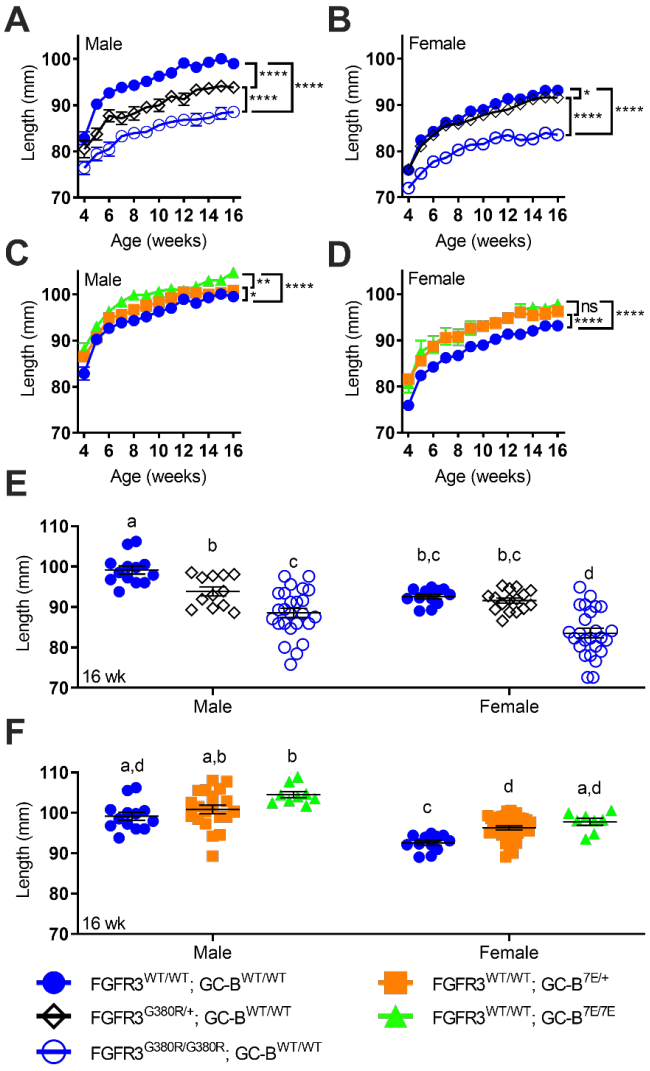

Figure 2. Naso-anal lengths of FGFR3$^{WT/WT}$, FGFR3$^{G380R/+}$, FGFR3$^{G380R/G380R}$, GC-B$^{WT/WT}$, GC-B$^{7E/+}$, or GC-B$^{7E/7E}$ mice according to sex.

(A and B) Comparison of naso-anal lengths with zero, 1, or 2 alleles of FGFR3-G380R in a WT-GC-B background in male (A) or female (B) mice. (C and D) Comparison of zero, 1, or 2 alleles of GC-B-7E in a WT-FGFR3 background in male (C) or female (D) mice. (E) Comparison of naso-anal lengths with zero, 1, or 2 alleles of FGFR3-G380R in a WT-GC-B background in male and female mice at 16 weeks of age. (F) Comparison of zero, 1, or 2 alleles of GC-B-7E in a WT-FGFR3 background in male and female mice at 16 weeks of age. *, **, ***, and **** indicate statistical significance at $p<0.05$, 0.01, 0.001 and 0.0001, respectively. For E and F, treatments with different letters are significantly different from one another where $p<0.05$

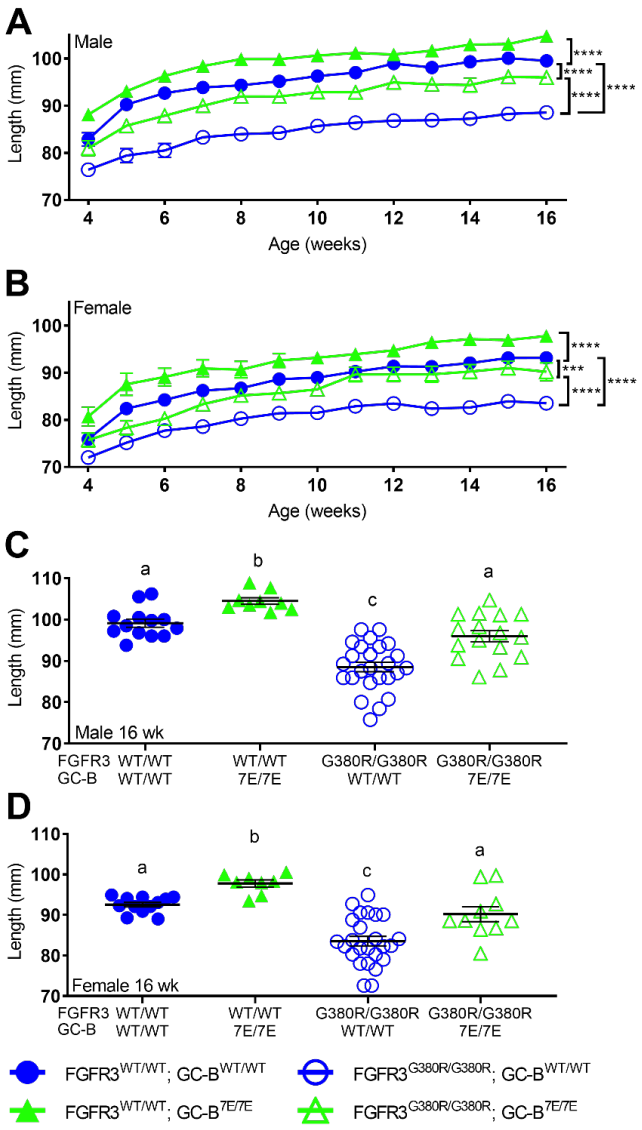

Figure 3. Expression of two GC-B-7E alleles rescues FGFR3-G380R-dependent naso-anal length reductions.

(A and B) Comparison of naso-anal lengths in male (A) or female (B) mice with 2 alleles of GC-B-7E in a homozygous WT-FGFR3 or FGFR3-G380R background from 4 to 16 weeks of age. (C and D) Comparison of 16-week-old naso-anal lengths in male (C) or female (D) mice expressing 2 alleles of GC-B-7E in a WT-FGFR3 or homozygous FGFR3-G380R background. *** and **** indicate statistical significance at $p<0.001$ and 0.0001, respectively, where n = 7-35 for male and 4-46 female mice for each data point for A and B. For C and D, treatments with different letters are significantly different from one another where $p<0.05$ and n = 8-25.

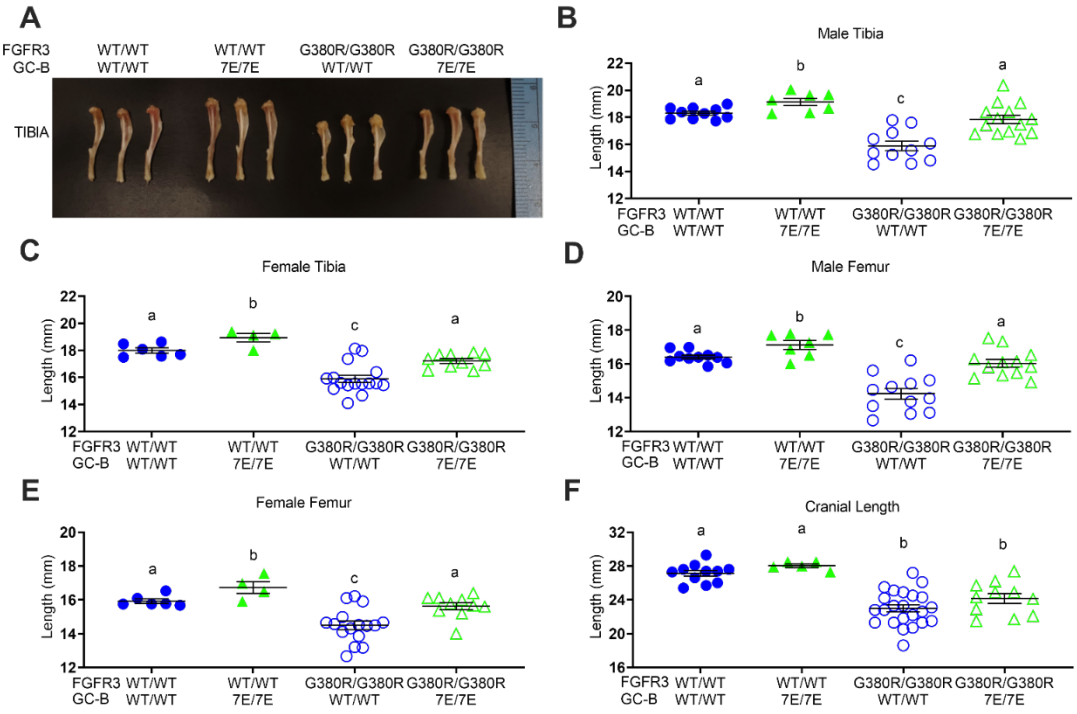

Figure 4. GC-B$^{7E/7E}$ expression rescues long bone but not cranial length abnormalities of ACH in 16-week-old mice.

Femurs, tibias, and craniums from 16-week-old male and female GC-B$^{WT/WT}$; FGFR3$^{WT/WT}$, GC-B$^{7E/7E}$; FGFR3$^{WT/WT}$, GC-B$^{WT/WT}$; FGFR3$^{G380R/G380R}$, and GC-B$^{7E/7E}$; FGFR3$^{G380R/G380R}$ mice were excised and measured. (A) Representative tibias from 16-week-old male mice of the indicated genotypes. (B-F) Lengths of male tibias (B), female tibias (C), male femurs (D), female femurs (E), and mixed male and female craniums (F). n = 4-23 mice per genotype. Treatments with different letters are significantly different from one another, where $p<0.05$.

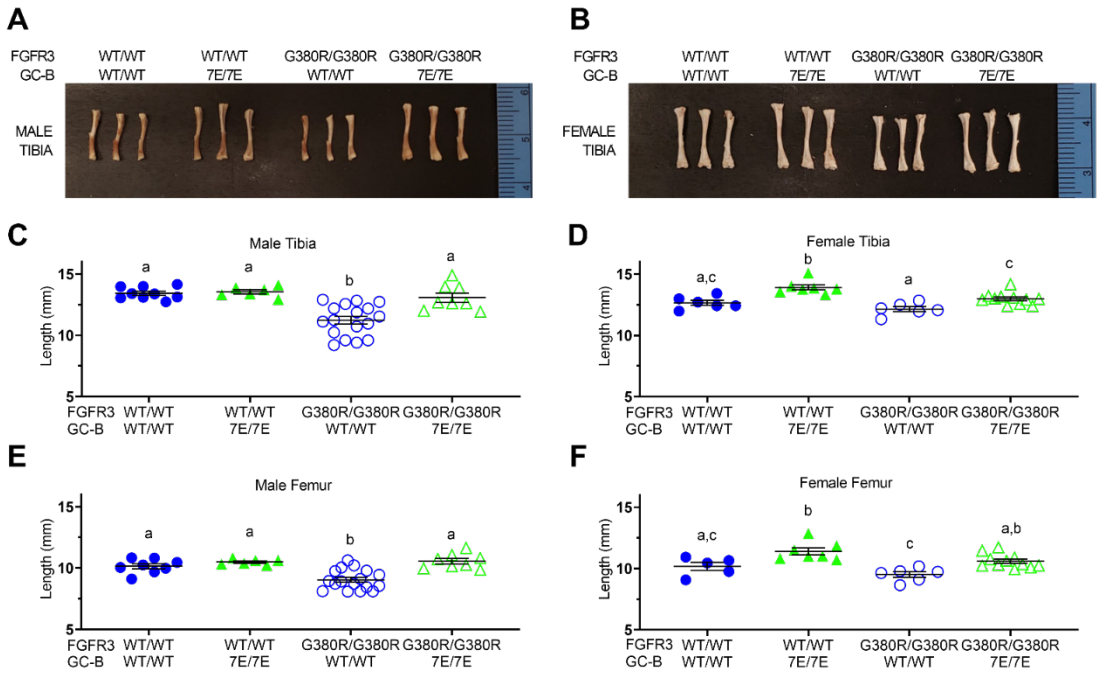

Figure 5. GC-B$^{7E/7E}$ expression rescues FGFR3$^{G380R/G380R}$ - dependent shortening of 2-week-old male tibias and femurs.

Femurs and tibias from 2-week-old male and female GC-B$^{WT/WT}$; FGFR3$^{WT/WT}$, GC-B$^{7E/7E}$; FGFR3$^{WT/WT}$, GC-B$^{WT/WT}$; FGFR3$^{G380R/G380R}$, and GC-B$^{7E/7E}$; FGFR3$^{G380R/G380R}$ mice were excised and measured. (A and B) Photographs of representative tibias from 2-week-old male (A) or female (B) mice of the indicated genotypes. (C-F) Lengths of male tibias (C), female tibias (D), male femurs (E), female femurs (F). n = 5-13 mice per genotype. Treatments with different letters are significantly different from one another, where $p<0.05$.

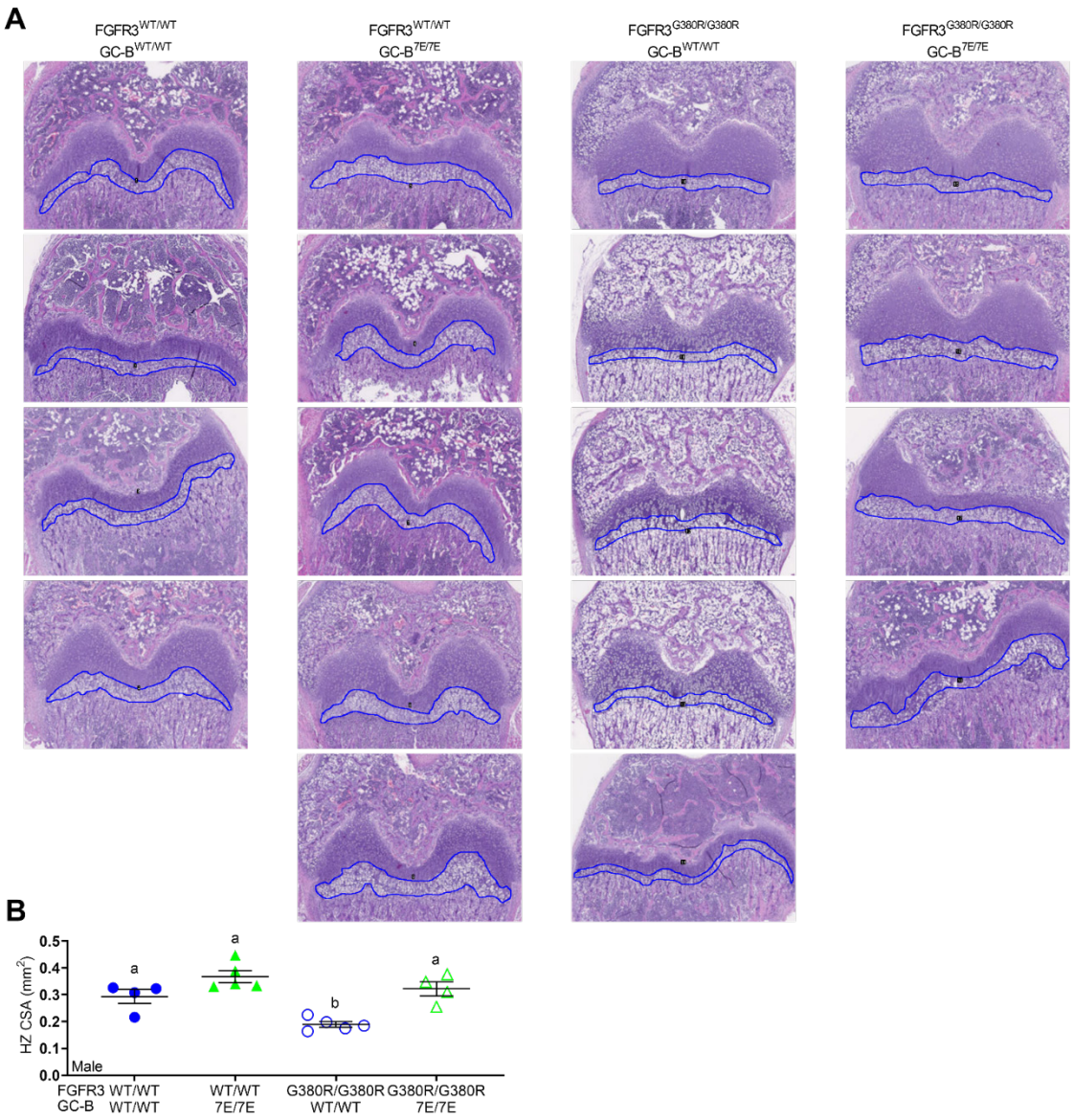

Figure 6. GC-B$^{7E/7E}$ expression rescues growth plate hypertrophic zone reductions in FGFR3$^{G380R/G380R}$ male mice.

Femoral growth plates from 2-week-old male mice were sectioned, stained with H&E, and the hypertrophic zone (HZ) cross-sectional area (CSA) was measured. (A) Images at 5X magnification were used for HZ CSA. Blue outlines indicate HZ CSA measured. (B) Quantitative graph of HZ CSA from A. n = 4-5 mice per genotype. Treatments with different letters are significantly different from one another, where $p<0.05$.

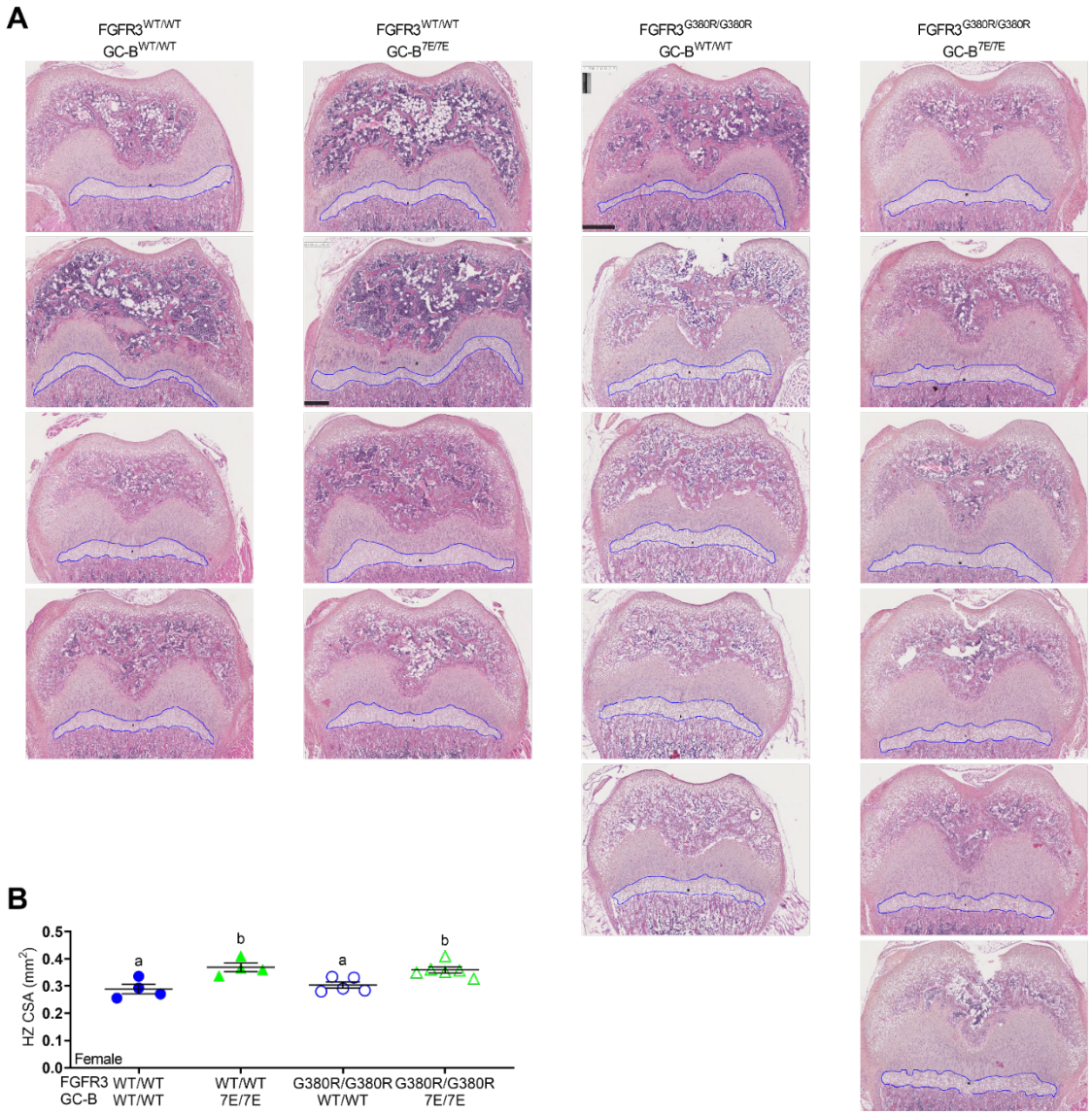

Figure 7. GC-B$^{7E/7E}$ expression expands the hypertrophic zone in FGFR3$^{WT/WT}$ and FGFR3$^{G380R/G380R}$ female mice.

Femoral growth plates from 2-week-old female mice were sectioned, stained with H&E, and the hypertrophic (HZ) cross-sectional area (CSA) was measured. (A) Images at 5X magnification used for HZ CSA. Blue outlines indicate HZ CSA measured. (B) Quantitative graph of HZ CSA from A. n = 4-6 mice per genotype. Treatments with different letters are significantly different from one another, where $p<0.05$.

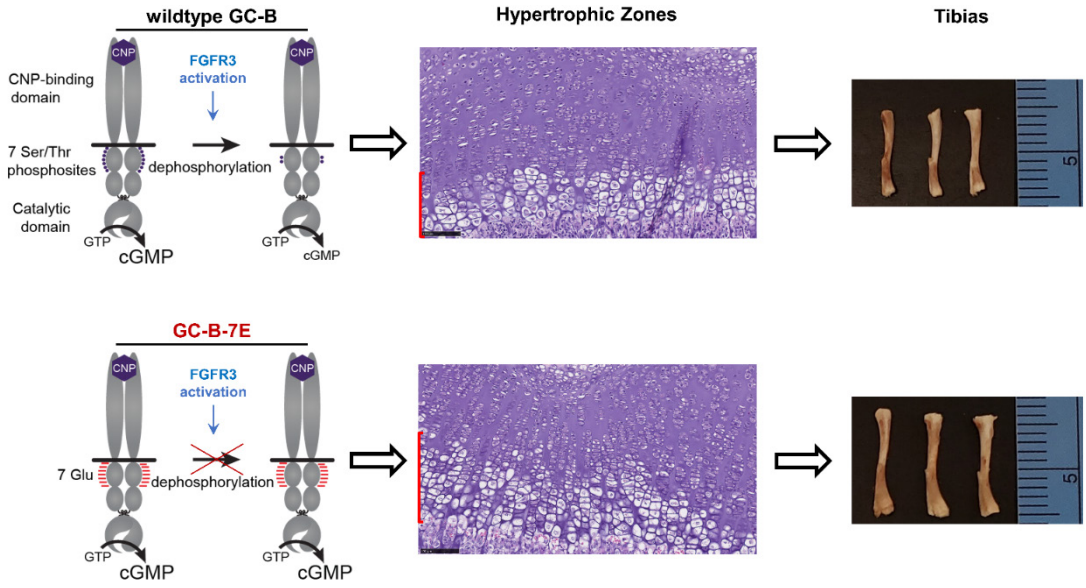

Figure 8. A model depicting how FGFR3-dependent dephosphorylation of GC-B results in achondroplasia.

Upper panel: FGFR3 activation increases the dephosphorylation of WT GC-B, which results in reduced chondrocyte cGMP concentrations and smaller growth plate hypertrophic zone area as depicted by the red bar on the left side of the “Hypertrophic Zones” panel. The reduced hypertrophic zone area ultimately leads to impaired long bone growth that results in shorter tibias. Bottom panel: GC-B-7E cannot be inactivated by dephosphorylation in response to FGFR3 activation, which results in elevated cGMP concentrations, larger hypertrophic zone area, and longer tibias.

CHAPTER 4: GUANYLYL CYCLASE-B DEPENDENT BONE FORMATION IN MICE IS ASSOCIATED WITH YOUTH, INCREASED OSTEOBLASTS, AND DECREASED OSTEOCLASTS

Brandon M. Wagner[a], Jerid W. Robinson[b], Andrew M. Benton[c], Gordon L. Warren[c], Timothy C. R. Prickett[d], Eric A. Espiner[d], Sundeep Khosla[e], Dana Gaddy[f], Larry J. Suva[g], Lincoln R. Potter[a,b]

[a]Departments of Integrative Biology and Physiology and [b]Department of Biochemistry, Molecular Biology, and Biophysics at the University of Minnesota, Minneapolis, MN, USA, [c]Department of Physical Therapy, Georgia State University, Atlanta, GA, USA; [d]Department of Medicine, University of Otago, Christchurch, New Zealand; [e]Robert and Arlene Kogod Center on Aging and Division of Endocrinology, Mayo Clinic College of Medicine, Rochester, MN, USA; [f]Departments of Veterinary Integrative Biosciences and [g]Physiology and Pharmacology, Texas A&M University, College Station, TX, USA

Submitted to:
Bone, February 2022

SUMMARY

C-type natriuretic peptide (CNP) activation of guanylyl cyclase-B (GC-B) catalyzes the synthesis of cGMP in chondrocytes and osteoblasts. Elevated cGMP stimulates long bone growth, whereas inactivating mutations in CNP or GC-B reduce cGMP, which causes dwarfism. GC-B$^{7E/7E}$ mice that express a GC-B mutant that cannot be inactivated by dephosphorylation exhibit increased CNP-dependent GC-B activity, which increases bone length, as well as bone mass and strength. Importantly, how GC-B increases bone mass is not known. Here, we injected 12-week-old, wild type mice once daily for 28 days with or without BMN-111 (Vosoritide), a proteolytically resistant CNP analog. We found that BMN-111 treated mice not only had elevated osteocalcin, a serum marker for osteoblasts, they also had elevated levels of collagen 1 C-terminal telopeptide, a marker for osteoclasts. Consistent with the serum markers, tibias from these mice had more osteoblasts and osteoid as well as more osteoclasts. Importantly, mineral apposition rates and trabecular bone mass were not elevated in response to BMN-111. Because 9-week-old male GC-B$^{7E/7E}$ mice have increased bone mass and strength but do not exhibit increased mineral apposition rates, we examined 4-week-old male GC-B$^{7E/7E}$ mice and found that the younger mice had increased serum osteocalcin, but not collagen 1 C-terminal telopeptide. Furthermore, tibias from these mice had 37% more osteoblasts, 26% fewer osteoclasts, and 36% and 40% higher mineral apposition and bone formation rates, respectively. Finally, we observed that tibias from 16-week-old GC-B$^{7E/7E}$ mice had lost some of the gains in bone mass and strength that were observed at 9-weeks of age. We conclude that GC-B-dependent bone formation is coupled to an early developmental stage where osteoblasts are not only increased but osteoclasts are also decreased.

INTRODUCTION

C-type natriuretic peptide (CNP) activation of guanylyl cyclase-B (GC-B) elevates cGMP in chondrocytes and osteoblasts, which increases long bone length, volume, and strength (85, 228-230). CNP activation requires phosphorylation of multiple intracellular serines and threonines in GC-B (135, 148, 153), and dephosphorylation of these residues in response to fibroblast growth factor (FGF) or luteinizing hormone signaling inactivates the enzyme (184-186, 216). In humans, gain-of-function mutations in FGF receptor 3 (FGFR3) cause achondroplasia (202, 203), and loss-of-function mutations in GC-B cause acromesomelic dysplasia Maroteaux-type (AMDM-type) dwarfism (98, 99, 190). Conversely, CNP overexpression or mutations that result in constitutive activation of GC-B cause skeletal overgrowth, bone deformity, and in some cases, reductions in bone mineral density (BMD) (64, 65, 196-198).

Activation of GC-B promotes chondrocyte proliferation and hypertrophy in the growth plate of long bones (300, 301). Mice lacking either CNP or GC-B are dwarfed and exhibit similar growth plate reductions to those of mice with FGFR3 gain-of-function mutations that cause achondroplasia (60, 98). Mice expressing a mutant form of GC-B containing alanine substitutions for the phosphorylated serines and threonines (148) are also dwarfed due to smaller growth plates (200). In contrast, mice expressing GC-B-7E ($GC\text{-}B^{7E/7E}$ mice), a glutamate-substituted enzyme that is activated by CNP, but cannot be inactivated by dephosphorylation (186, 216), have enlarged growth plates, longer bones and are resistant to FGFR3-dependent growth plate reductions (217, 236). Treatment with CNP or BMN-111, a proteolytically resistant CNP analog currently in clinical development for the treatment of pediatric achondroplasia (213), increases bone growth in rodent models of achondroplasia (199, 209, 211). Furthermore, BMN-111 in combination with LB-100, a PPP family phosphatase inhibitor, stimulated bone growth in cultured fetal mouse femurs to a greater extent than BMN-111 alone (293).

Although GC-B regulation of chondrocyte proliferation and hypertrophy is well established, much less is known about GC-B regulation of osteoblasts, bone mass, and bone strength. Previous work shows that increased CNP/GC-B activity is strongly linked to increases in osteoid and bone markers of formation and resorption (228). Further, in adult humans these same markers associate with dynamic changes in endogenous CNP production (302), yet the precise role of CNP in maintaining bone health remains

unclear. Studies on cultured osteoblasts demonstrated that CNP increases the mRNA expression of osteocalcin, type-I collagen, and alkaline phosphatase, in addition to stimulating alkaline phosphatase activity and mineralization (218, 219). CNP also increases the proliferation of osteoblasts (218, 223). Soluble GC (sGC) activators are osteoanabolic in adult mice as well. Daily activation of sGC increased osteoblast numbers and bone formation, which resulted in increased trabecular bone volume fraction and BMD in both intact adult female and ovariectomized mice (303, 304). Male 9-week-old GC-B$^{7E/7E}$ mice have increased osteoblasts and osteoid but similar number of osteoclasts compared to wild type mice. Importantly, tibias from these GC-B$^{7E/7E}$ mice have greater trabecular and cortical bone mass that results in stiffer and stronger bones (228). In contrast, chronic activation of GC-B in transgenic mice overexpressing CNP was associated with decreased trabecular bone volume and cortical cross-sectional area when examined at 8-weeks of age (62). Thus, the current literature suggests that chronic, unregulated GC-B activity results in decreased bone content and strength, whereas intermittent elevations of cGMP, either by sGC activators or increased CNP-dependent GC-B activity observed in GC-B$^{7E/7E}$ mice, result in increased bone mass and strength.

In the current study, to investigate whether GC-B activation has beneficial effects in the adult skeleton, we have examined tibias for changes in bone content and formation from 16-week-old male and female mice that were treated with BMN-111 or saline as a control for 28 days. Hypothesizing that daily injection of BMN-111 for 4 weeks would stimulate bone formation and increase bone content compared to mice injected without BMN-111, we find that BMN-111 increases serum osteocalcin and collagen 1 C-terminal telopeptide (CTX) formation as well as surface osteoblasts, osteoid, and osteoclasts, but bone content, bone formation and bone mineralization were unaffected. These findings contrast with earlier studies [3] on 9-week-old male GC-B$^{7E/7E}$ mice where bone content and strength as well as turnover markers were all increased, yet no significant change in mineral apposition or bone formation rates were observed when compared to 9-week-old GC-B$^{WT/WT}$ mice (228), suggesting that the osteoanabolic effect resulting from the increased CNP-dependent GC-B activity may occur prior to 9 weeks of age. Accordingly, we have now examined tibias from 4- and 16-week-old male GC-B$^{WT/WT}$ and GC-B$^{7E/7E}$ mice. Our data indicate that the role of GC-B in bone formation changes with age and that GC-B dependent increases in

osteoblasts, without concomitant decreases in osteoclasts, is not sufficient to increase bone mass in adult mice.

METHODS

Reagents. BMN-111 [Cyc(23,39)]H2N-PGQEHPNARKYKGANKKGLSKGCFGLKLDRIGSMSGLGC-OH was synthesized by New England Peptide (Gardner, MA) and distributed in lyophilized vials of 1 mg each at >95% purity by HPLC. Each vial was reconstituted in sterile saline to a final concentration of 17.5 μM for female mice or 21 μM for male mice and frozen in aliquots. Each aliquot was thawed prior to injection and not reused.

Animals. Male and female GC-B$^{WT/WT}$ and GC-B$^{7E/7E}$ mice (originally described as *Npr2*$^{7E/7E}$) were genotyped and maintained on a C57BL/6 background as previously described (186). Male GC-B$^{WT/WT}$ and GC-B$^{7E/7E}$ mice were studied initially to avoid complications of fluctuating estrogen levels. The effects of BMN-111 were studied on 12-week-old male and female mice. Mice were subcutaneously injected once daily with or without 70 nmol/kg BMN-111 as previously described (212). Mice were fed standard chow under specific-pathogen-free conditions. Animal care was compliant with the University of Minnesota Institutional Animal Care and Use Committee.

Micro-computed tomography. Tibias were wrapped in saline-soaked gauze and scanned using the XT H 225 μCT (Nikon Metrology Inc., Brighton, MI, USA) at an isotropic voxel size of 6.7 μm. The scan settings were 90 kV, 90 μA, 720 projections, 2 frames per projection, and an integration time of 708 milliseconds. 3D reconstructions used the software CT Pro 3D (Nikon metrology, Inc., Brighton, MI, USA). Bitmap datasets for each scan were made using VGStudio MAX 2.1 (Volume Graphics GmbH, Heidelberg, Germany). Morphometric analysis was completed with the SkyScan CT-Analyser (CTAn) software (Bruker micro-CT, Belgium). The parameters measured are those recommended by Bouxsein and colleagues (305). For trabecular measurements, the proximal tibial metaphysis was analyzed. The region started 0.5 mm distal from the proximal epiphyseal growth plate and extended 1.7 mm further distally. The cortical site analyzed was a 0.5 mm region located in the middle of the diaphysis. For cortical thickness, measurements from the entire region were averaged and compared between treatments. All 3D models were created with the CT-Volume (CTVol) software (Bruker micro-CT, Belgium). Three-dimensional reconstructions were created by stacking the regions of interest from each two-dimensional slice and then applying a gray-scale

threshold and Gaussian noise filter specifically optimized for murine trabecular bone as described (305).

Three-point bending mechanical tests. Tibias used for μCT were also analyzed by 3-point bending as previously described (228). Tibial length was measured with digital calipers and the mid-diaphysis of the tibia was identified. Tibial bone mechanical properties were then determined by performing three-point bending at mid-diaphysis on a Mecmesin MultiTest 1-D test machine using a Mecmesin AFG-25 load cell (Mecmesin, West Sussex, UK) with a 25-N capacity and 5-mN resolution. Bones were placed onto a set of supports separated by 10 mm such that the lateral side of the bone was placed downward. Load was applied with a loading rate of 2 mm/min until bone fracture. The maximum force before fracture was recorded as the ultimate load. The stiffness was calculated by measuring the slope of the elastic region of the force-displacement curve. Energy absorbed to ultimate load and to failure were calculated by integrating the force-displacement curve until the ultimate load was reached and the bone fractured, respectively.

Serum Bone Marker Measurements. Serum samples were collected between 12:00 and 4:00 pm from mice fed *ad libitum*. For the BMN-111 studies, serum was collected approximately 24 hours after the final injection. Osteocalcin was measured in serum from mice using a mouse osteocalcin EIA kit from Alfa Aesar. CTX was measured using mouse RatLaps (CTX-1) EIA kit from Immunodiagnostic Systems (Boldon, UK). All ELISAs were conducted according to the manufacturer's instructions.

Static and Dynamic Bone Histomorphometry. Left tibiae from 4-week-old male GC-$B^{WT/WT}$ and GC-$B^{7E/7E}$ mice were fixed, embedded, sectioned, and stained for static histomorphometry as previously reported (306). Analysis was performed blinded using the OsteoMeasure image analysis system (OsteoMetrics, Inc., Decatur, GA). Dynamic histomorphometry experiments performed on tibias were double labeled with calcein (30mg/kg). 16-week-old saline and BMN-111 treated mice were injected with calcein 19 and 26 days after the initial saline or BMN-111 injection for a 7-day inter-label period and then euthanized 2 days later. Dynamic histomorphometry experiments were performed on 4-week-old mice injected with calcein at 28 and 31 days of age for a 3-day inter-label period and then euthanized 2 days later.

NT-proCNP measurements. To examine the possibility that endogenous CNP production is affected by increased GC-B activity [42], NT-proCNP was measured in

plasma from GC-B$^{WT/WT}$ and GC-B$^{7E/7E}$ 9-week-old male mice. Blood was collected from by cardiac puncture and allowed to clot at room temperature for 30 minutes. The clotted blood was centrifuged at 6000 x g for 5 minutes at 4°C, and the supernatant serum was transferred to a separate tube and stored at -80°C until analyzed for NT-proCNP concentrations. Serum NT-proCNP concentrations were determined by ELISA as previously described (307).

Statistics. Statistics and graphs were generated with Prism 9 software (GraphPad Software, La Jolla, CA). Groups were analyzed for normality and equality of variance using both the D'Agaostino & Pearson and Shapiro-Wilk normality tests and the F test. If either group failed one of the normality tests or the equality of variance test, p-values were obtained by a Mann-Whitney test where $p \leq 0.05$ was considered significant. If both groups passed both normality tests and equality of variance test, p-values were obtained using an unpaired, two-tailed student's t-test, where $p \leq 0.05$ was considered significant. Each symbol in a figure represents a single value from the left or right tibia of an individual mouse. Long horizontal bars represent the mean and the shorter bars above and below the mean represent SEM.

RESULTS

BMN-111 treatment increases serum biomarkers of bone formation and turnover in adult mice. To determine if BMN-111 has beneficial actions on the adult skeleton, we subcutaneously injected 12-week-old male and female WT C57BL/6 mice with 70 nmol/kg BMN-111 or saline only once daily for 4 weeks. On the 28th day after the first injection, serum was collected from each mouse and examined for osteocalcin and CTX concentrations by ELISA as markers for osteoblasts and osteoclasts, respectively. Male and female mice treated with BMN-111 exhibited 50% and 33% greater serum osteocalcin concentrations, respectively, than saline injected control mice (Figure 1A and B). Serum CTX was also elevated 61% in the female mice (Figure 1C). CTX was also elevated in male mice, but the increase was not statistically significant different from that measured in saline treated control mice (Figure 1D). These data suggest that daily injection of BMN-111 stimulates osteoblast activity in adult mice of both sexes and increases osteoclast activity in females to a greater extent than in males.

BMN-111 treatment increases osteoblasts as well as osteoclasts but does not increase bone content in adult mice. To determine if BMN-111 increases bone content in adult mice, tibias were collected from the same BMN-111 and saline-control treated mice described above and analyzed by micro-computed tomography (μCT). Trabecular bone volume fraction (BV/TV) was not significantly different in tibias from either male or female mice treated with or without BMN-111 (Figure 2A and B). Trabecular number trended towards an increase in both sexes of the BMN-111 treated mice, but the differences were not statistically significant (Figure 2C and D). Static histomorphometry revealed significant increases of 33% and 58% in osteoid width in tibias from both male and female mice treated with BMN-111, respectively (Figure 2E and F). BMN-111 injections also increased the number of osteoblasts per bone perimeter by 180% in tibias from adult male mice (Figure 2G). Osteoblasts were elevated in the tibias from female mice treated with BMN-111, but differences were not significantly different from the control mice (Figure 2H). Importantly, osteoclasts per bone perimeter were significantly increased by 43% and 52% in tibias from BMN-111 treated male and female mice, respectively (Figure 2I and J).

Injection of BMN-111 does not increase the bone formation rate in adult mice. To examine changes in mineral apposition rate (MAR) and bone formation rate to bone

surface (BFR/BS) in BMN-111 treated mice, dynamic histomorphometry was performed on tibias from the male and female mice described above. Consistent with the μCT data, there were no significant differences in MAR (Figure 3A and B) or BFR/BS (Figure 3C and D) in male or female mice treated with BMN-111.

Osteocalcin, but not CTX, levels are elevated in 4-week-old male GC-B$^{7E/7E}$ mice. Based on our recent study demonstrating that GC-B$^{7E/7E}$ mice rescue the growth plate hypertrophic zone reductions in a mouse model of achondroplasia by 2-weeks of age (236), we hypothesized that the ability of GC-B$^{7E/7E}$ to stimulate osteoblast activity and ultimately produce more bone occurs during an early developmental period. To examine this possibility, serum osteocalcin and CTX concentrations were measured in 4-week-old mice. Serum osteocalcin levels were elevated 61% in male GC-B$^{7E/7E}$ compared to male GC-B$^{WT/WT}$ mice (Figure 4A), but serum CTX values did not differ between the two genotypes (Figure 4B). These data are consistent with elevated osteoblast, but not osteoclast, activity in 4-week-old GC-B$^{7E/7E}$ mice.

Tibias from 4-week-old male GC-B$^{7E/7E}$ mice have more osteoblasts and fewer osteoclasts. To determine if the elevated serum osteocalcin levels in the 4-week-old male GC-B$^{7E/7E}$ mice correlate with an osteoanabolic effect, tibias from 4-week-old male GC-B$^{WT/WT}$ and GC-B$^{7E/7E}$ mice were collected and analyzed histologically. Consistent with the initial reports on GC-B$^{7E/7E}$ mice at 18-weeks (217) and 9-weeks (228), we found that tibias from 4-week-old male GC-B$^{7E/7E}$ were 5% longer than tibias from male GC-B$^{WT/WT}$ mice (Figure 5A). Static histomorphometry on the same tibias revealed that bones from 4-week-old male GC-B$^{7E/7E}$ mice had 12% greater cortical thickness compared to the GC-B$^{WT/WT}$ mice (Figure 5B). Furthermore, tibias from the GC-B$^{7E/7E}$ males had a 39% increase in osteoblasts to bone surface (Ob.S/BS) and a 33% decrease in osteoclasts (Oc.S/BS) to bone surface (Figure 5C and D), as well as a 37% increase and 26% decrease in osteoblasts and osteoclasts per bone perimeter, respectively (Figure 5E and F).

Tibias from 4-week-old male GC-B$^{7E/7E}$ mice have increased mineral apposition and bone formation rates compared to tibias from GC-B$^{WT/WT}$ mice. Initial studies on tibias from male 9-week-old GC-B$^{7E/7E}$ mice revealed no significant differences in dynamic bone indices compared to tibias from GC-B$^{WT/WT}$ mice (228). Hence, we concluded that the osteoanabolic effect of GC-B$^{7E/7E}$ must precede 9 weeks of age. To test this hypothesis, dual calcein-labeled tibias from 4-week-old male GC-B$^{WT/WT}$ and

GC-B$^{7E/7E}$ mice were analyzed by dynamic histomorphometry. While we observed no difference in labeled surface to bone surface (Figure 6A), male GC-B$^{7E/7E}$ mice had a 36% greater MAR and a 40% increase in BFR/BS compared to the GC-B$^{WT/WT}$ mice (Figures 6B and 6C). Together with the static histomorphometry results, these data strongly suggest that the reason adult GC-B$^{7E/7E}$ mice have stronger, stiffer, and tougher bones is because they mineralize bone at a greater rate during early development, which is correlated not only with an increase in osteoblasts but also with a decrease in osteoclasts as observed in tibias from 4-week-old mice.

Trabecular bone does not differ between tibias from 16-week-old male GC-B$^{7E/7E}$ and GC-B$^{WT/WT}$ mice. Since our initial studies on the GC-B$^{7E/7E}$ mice reported that 9-week-old male GC-B$^{7E/7E}$ mice had significantly greater trabecular bone mass and BMD (228) and our data above suggest that daily injection of BMN-111 is not sufficient to increase bone mass in adult mice, we investigated if the increase in bone mass observed in the 9-week-old GC-B$^{7E/7E}$ mice was maintained as the mice aged. Tibial proximal metaphyses from 16-week-old male mice were analyzed by μCT. Surprisingly, we found that the trabecular indices that were increased in the 9-week-old GC-B$^{7E/7E}$ mice were no longer significantly different between 16-week-old male GC-B$^{WT/WT}$ and GC-B$^{7E/7E}$ mice (Figure 7A-E).

Bone strength and stiffness is decreased in 16-week-old compared to 9-week-old GC-B$^{7E/7E}$ mice. To determine if the GC-B$^{7E/7E}$ mice maintained their stiffer and stronger bones with age as initially observed in bones from 9-week-old mice (228), tibias from 16-week-old male GC-B$^{WT/WT}$ and GC-B$^{7E/7E}$ mice were analyzed by 3-point bending. Consistent with the μCT data, the 3-point bending analysis indicated that tibias from 16-week-old male GC-B$^{7E/7E}$ mice lost their increases in ultimate load (Figure 8A), stiffness (Figure 8B), and energy absorbed to failure (Figure 8D). They also lost most, but not all, of their energy absorbed to ultimate load (Figure 8C). Although the tibias from 16-week-old male GC-B$^{7E/7E}$ mice had 10% ($p=0.0780$) greater ultimate load and 26% ($p=0.0502$) greater energy absorbed to ultimate load compared to tibias from 16-week-old male GC-B$^{WT/WT}$ mice, these differences were much less than the 35% ($p<0.0001$) and 42% ($p=0.0006$) increases initially observed in 9-week-old GC-B$^{7E/7E}$ mice, respectively (228). These biomechanical tests along with the μCT data indicate that by 16 weeks, the GC-B$^{7E/7E}$ mice had lost a significant amount of their increases in bone mass, strength, and stiffness that was initially observed at 9 weeks.

NT-proCNP levels do not differ between GC-B$^{WT/WT}$ and GC-B$^{7E/7E}$ mice. Serum NT-proCNP concentrations were determined from 8 GC-B$^{WT/WT}$ and 13 GC-B$^{7E/7E}$ 9-week-old male mice. Mean values for the GC-B$^{WT/WT}$ and the GC-B$^{7E/7E}$ mice were 29.85 and 25.90 pmol/L, respectively. These values were not significantly different from one another as indicated by a *p value of 0.3221* when tested by a two-tailed students t-test. Thus, similarly to GC-A$^{8E/8E}$ mice that do not have differing ANP or BNP concentrations compared to GC-A$^{WT/WT}$ mice (308), serum NP-proCNP concentrations were not significantly changed in the GC-B$^{7E/7E}$ mice.

DISCUSSION

Prior studies have determined that intermittent surges in GC-B activity increase bone length (217, 236, 293) as well as bone content and strength in rodents (199, 228). Here, we investigated whether activation of GC-B with BMN-111 in adult male and female mice once daily for 28 consecutive days is sufficient to increase bone content. Although daily injections of BMN-111 increased serum biomarkers of bone formation and bone resorption in adult mice, neither bone content nor bone formation rate were significantly different in tibias in animals injected with or without BMN-111. Similarly, Hirota et al. reported that trabecular thickness in femurs from 8-week-old female rats lacking CNP was lower than that in WT rats and was restored by subcutaneous administration of BMN-111 for 4 weeks. However, BMN-111 administration in WT rats had no effect on bone content (199), which is similar to our murine data. Together, these data suggest that bone turnover, but not bone formation, is increased in tibia from rodents treated with CNP or BMN-111.

We further investigated how increased GC-B activity regulates bone content in GC-B$^{7E/7E}$ mice, a genetic model with increased CNP-dependent GC-B activity, that have increased bone mass and strength at 9-weeks of age (228). Examination of tibias from 4-week-old GC-B$^{7E/7E}$ male mice determined that osteoblasts and osteoclasts were substantially increased and decreased, respectively, compared to tibias from GC-B$^{WT/WT}$ mice. Importantly, dynamic histomorphometric analysis revealed that 4-week-old, but not 9-week-old, GC-B$^{7E/7E}$ mice have significantly elevated mineral apposition and bone formation rates. In a study examining the other end of the age spectrum, we found that by 16-weeks of age, the GC-B$^{7E/7E}$ mice had lost much of their gains in bone mass and strength that were initially observed at 9-weeks of age (228). These data are consistent with those of Kondo et al. who found that transgenic CNP expression resulted in a greater decline in mouse femoral BV/TV when measured at 8 weeks compared to 6 weeks of age (62). Together, the data described above suggests that GC-B-dependent increases in bone formation are limited to an early developmental window in rodents when activation of GC-B is associated with decreases in osteoclasts as well as increases osteoblasts.

Although daily injection of BMN-111 for 4 weeks did not increase bone content or bone formation in adult male and female mice, significant increases in serum

osteocalcin, osteoid width, osteoblasts, and osteoclasts in the BMN-111 treated mice were observed. As described above, intravenous administration of BMN-111 in WT female rats from 4 to 8 weeks of age also failed to increase BV/TV, however, the BMN-111 infusions did modestly increase plasma osteocalcin levels (199). In contrast, tibias from 11-week-old WT female mice treated with sGC activator, cobinamide, for 5 weeks had increased MAR, BFR/BS, and trabecular BV/TV (304). Interestingly, we observed a significant increase in osteoblasts in male, but not female, mice treated with BMN-111, whereas treatment with cobinamide increased osteoblasts in female mice. Importantly, cobinamide significantly decreased osteoclasts compared to vehicle, whereas BMN-111 increased osteoclasts in male and female mice compared to control animals, which may explain why treatment with BMN-111 did not increase bone content or bone formation in adult mice.

Our new data showing that 16-week-old GC-B$^{7E/7E}$ mice have reduced bone mass and strength compared to 9-week-old GC-B$^{7E/7E}$ mice are consistent with results from transgenic mice overexpressing CNP and humans with constitutively activating GC-B mutations that also exhibit reductions in bone content (62, 197, 198). Studies on transgenic mice overexpressing osteocrin, which binds the natriuretic peptide clearance receptor, thereby increasing circulating CNP concentrations available to activate GC-B, found that 10-week-old transgenic mice had longer bones, but not increased trabecular indices or osteocalcin (226). The same study also reported that CNP mRNA expression in tibial epiphyseal cartilage declines from higher levels at 3-weeks of age to lower levels at 6-weeks of age in WT mice (226). Since GC-B-7E exhibits increased enzyme activity only in the presence of CNP, like the WT enzyme, decreases in circulating CNP may explain why MAR and BFR were elevated in tibias from 4-week-old, but not in 9-week-old, GC-B$^{7E/7E}$ mice.

The results described in the present report combined with our previous report on 9-week-old GC-B$^{7E/7E}$ mice indicate that prior CNP/GC-B dependent gains in bone mass are reversible, but the conditions necessary for this reversibility are not clear. It is possible that increased GC-B activity observed in the GC-B$^{7E/7E}$ mice increases bone formation during endochondral growth but inhibits bone formation as the mice age into adulthood, which results in less bone mass and strength similar to what has been observed in CNP transgenic mice and patients with GC-B gain of function mutations (60, 62, 196-198). One obvious explanation for why GC-B activation increases bone

formation in 4-week-old mice but not in 9- and 12-week-old mice is that osteoclasts are elevated in the older mice but are decreased in the younger mice in response to GC-B activation. To our knowledge, there is little evidence that GC-B directly regulates osteoclasts, however one report demonstrated that CNP stimulates bone resorption in mouse bone marrow cultures by activating existing osteoclasts rather than stimulating their formation (220). However, a later report found that CNP stimulated cGMP production in mixed avian bone cells but not in purified osteoclasts, suggesting that osteoclasts do not directly respond to CNP (221). Regardless, the fact that BMN-111 did not result in increased bone mass in 12-week-old WT mice and GC-B$^{7E/7E}$ mice but have increased mineral apposition and bone formation rates at 4-weeks but not at 9-weeks, suggests that GC-B-dependent increases in bone mass and strength are intrinsically connected to an early developmental process. Conceivably, contributions from CNP/GC-B-induced increases in hypertrophic chondrocytes transforming to an osteoblast lineage (309), together with the differential functions of osteoclasts affecting mineralized cartilage degradation versus bone resorption (310), determine the response of bone turnover markers and bone accretion in animals with active growth plates, as observed in our studies.

In conclusion we found that once daily injection of BMN-111 for 4 weeks increased osteoid width, osteoblasts, and osteoclasts, but not bone mass or bone formation rates in 12-week-old WT mice. In contrast, we found that tibias from 4-week-old GC-B$^{7E/7E}$ mice had more osteoblasts, fewer osteoclasts, and increased MAR and BFR/BS compared to GC-B$^{WT/WT}$ mice. Examination of tibias from 16-week-old mice revealed that GC-B$^{7E/7E}$ mice had lost some of the initial gains in bone mass and strength observed at 9 weeks (228). Hence, we suggest that GC-B-dependent regulation of bone mass and bone formation is age-dependent such that increased GC-B activity in young, developing mice increases bone formation resulting in a transient increase in bone mass and strength, whereas increased GC-B activity in older, adult mice is not sufficient to increase or maintain bone mass. Of note, the ability of GC-B activation to stimulate bone formation in young mice is correlated with decreases in osteoclasts and the inability of GC-B activation to stimulate gains in bone mass in adult mice is correlated with increases in osteoclasts. Finally, phase 3 clinical trials demonstrated that BMN-111 injections increase long bone length in children with achondroplasia (213) and additional studies are underway to determine if earlier treatment will result in greater increases.

The results described here suggest that early administration of BMN-111 may also increase bone density and strength as well as length in children treated with BMN-111.

FIGURES

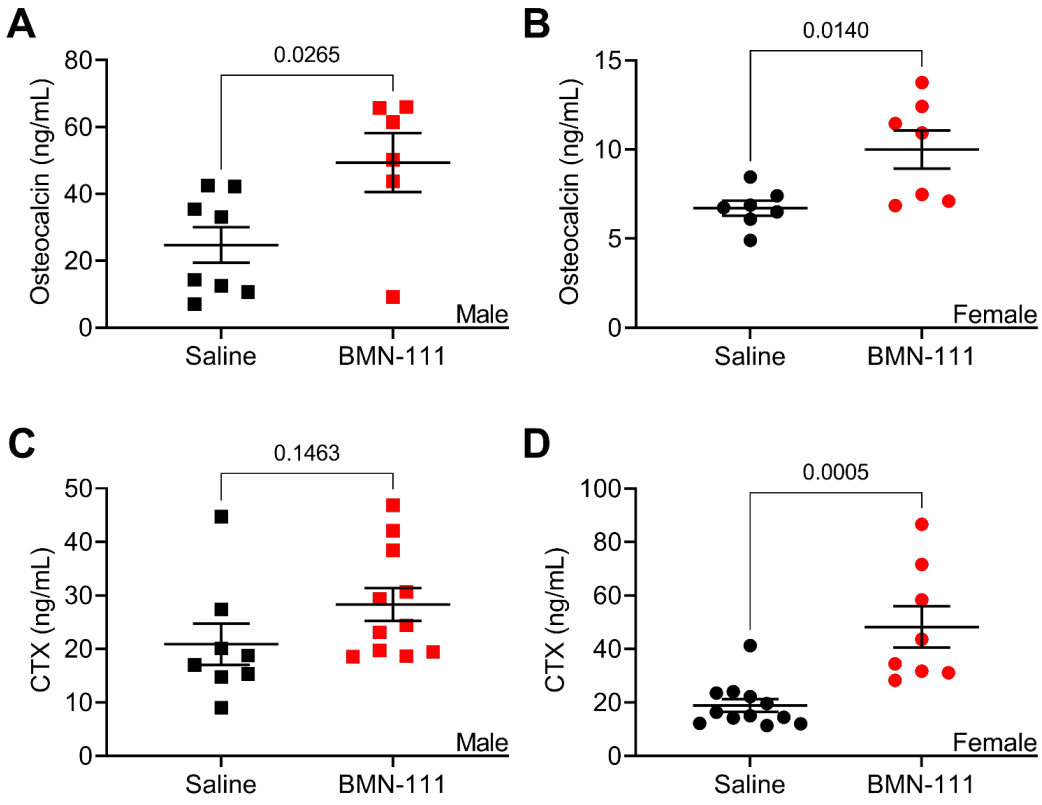

Figure 1. BMN-111 increases osteocalcin and CTX in adult male and female mice. 12-week-old male and female WT C57BL/6 mice were injected once daily with or without 70 nmol/kg/day BMN-111 for 4 weeks. Serum osteocalcin (A and B) and collagen 1 C-terminal telopeptide (CTX) (C and D) concentrations were determined at the end of the treatment period by ELISA. n=6-12 mice per group. Long horizontal bars indicate the mean and the shorter bars above and below represent SEM. p-values from a two-tailed student's t-test are shown in each panel.

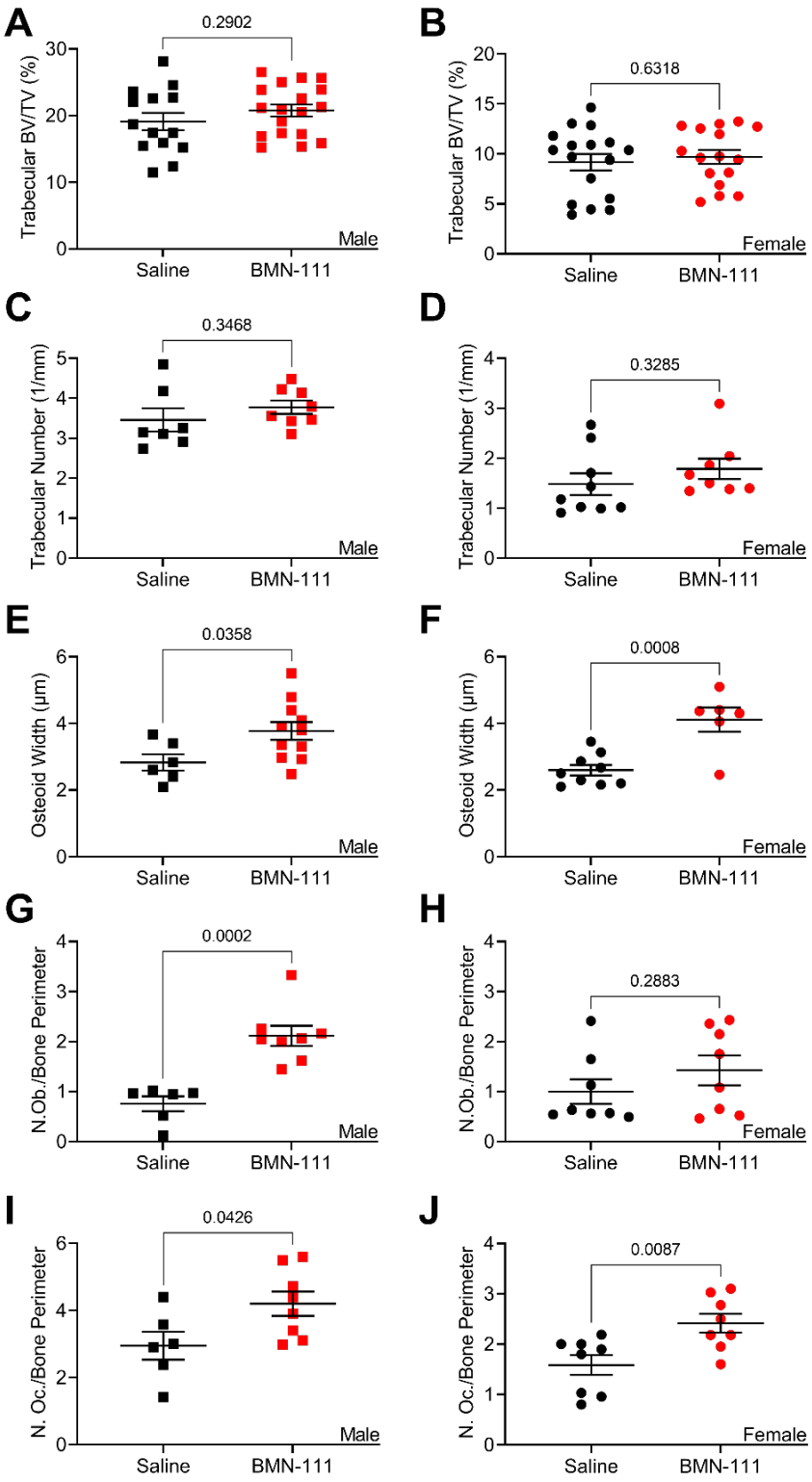

Figure 2. Injection of BMN-111 increases osteoblasts and osteoclasts, but not bone content, in adult mice.

12-week-old male (left panels) and female (right panels) WT C57BL/6 mice were injected once daily with 70 nmol/kg/day BMN-111 for 28 days. Tibias were extracted and analyzed by micro computed tomography for changes in trabecular bone volume fraction (BV/TV) (A and B) and trabecular number (C and D). Tibias were analyzed by static histomorphometry for osteoid width (E and F), number of osteoblasts per bone perimeter (G and H), and number of osteoclasts per bone perimeter (I and J). n = 6-18 mice per group. Long horizontal bars show the mean and the shorter bars above and below represent SEM. p-values from a two-tailed student's t-test are shown in each panel.

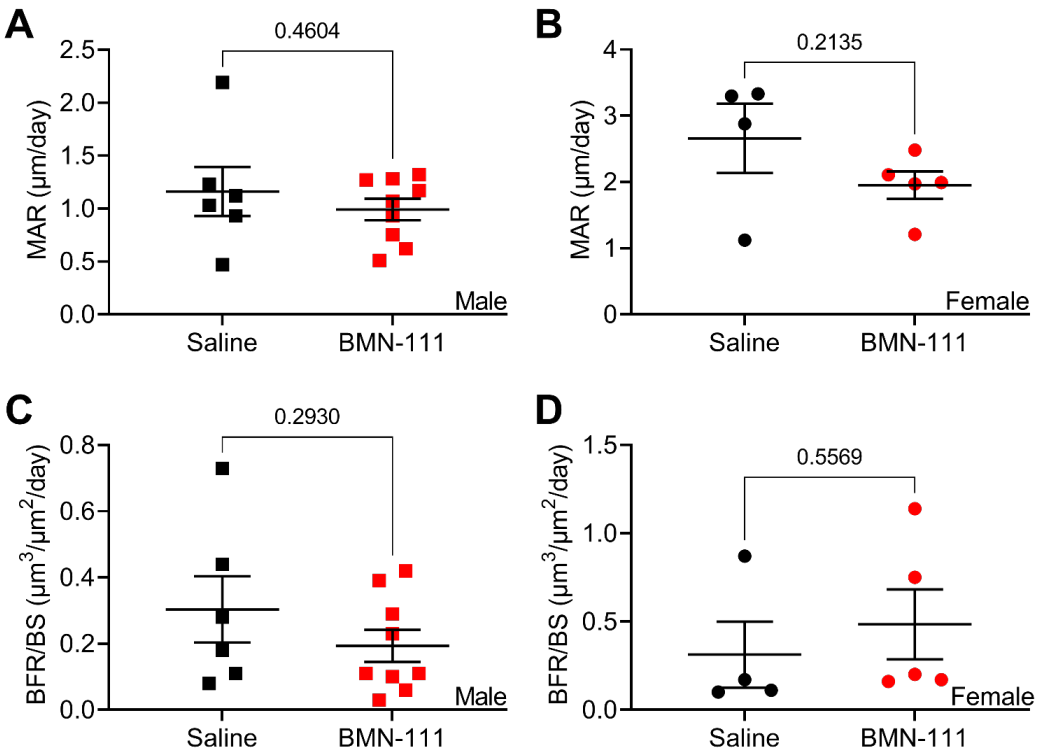

Figure 3. Injection of BMN-111 does not increase bone formation rate in adult mice.

12-week-old male and female WT C57BL/6 mice were injected once daily with 70 nmol/kg/day BMN-111 for 4 weeks. Dynamic histomorphometry was performed on tibias extracted after the treatment period to determine (A and B) the mineral apposition rate (MAR) and (C and D) the bone formation rate (BFR/BS). n=4-9 mice per group. Long horizontal bars show the mean and the shorter bars above and below represent SEM. p-values from a two-tailed student's t-test are shown in each panel.

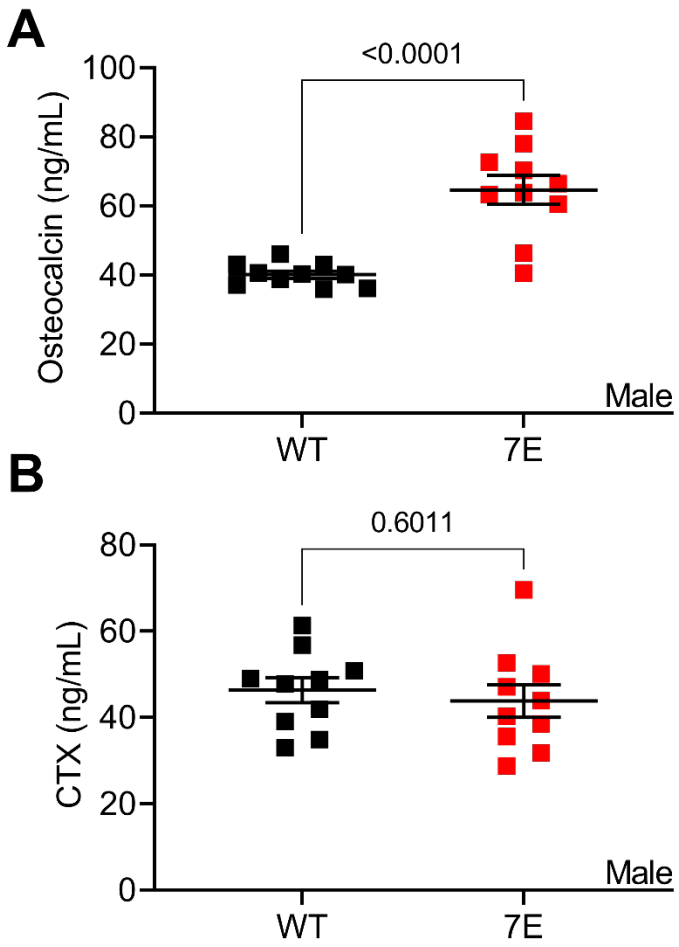

Figure 4. 4-week-old male GC-B7E/7E mice have elevated serum osteocalcin but not CTX.

Serum from 4-week-old male GC-B$^{WT/WT}$ and GC-B$^{7E/7E}$ mice was collected and assayed for (A) osteocalcin and (B) collagen 1 C-terminal telopeptide (CTX). n=10 mice per group. Long horizontal bars show the mean and the shorter bars above and below represent SEM. p-values from a two-tailed student's t-test are shown in each panel.

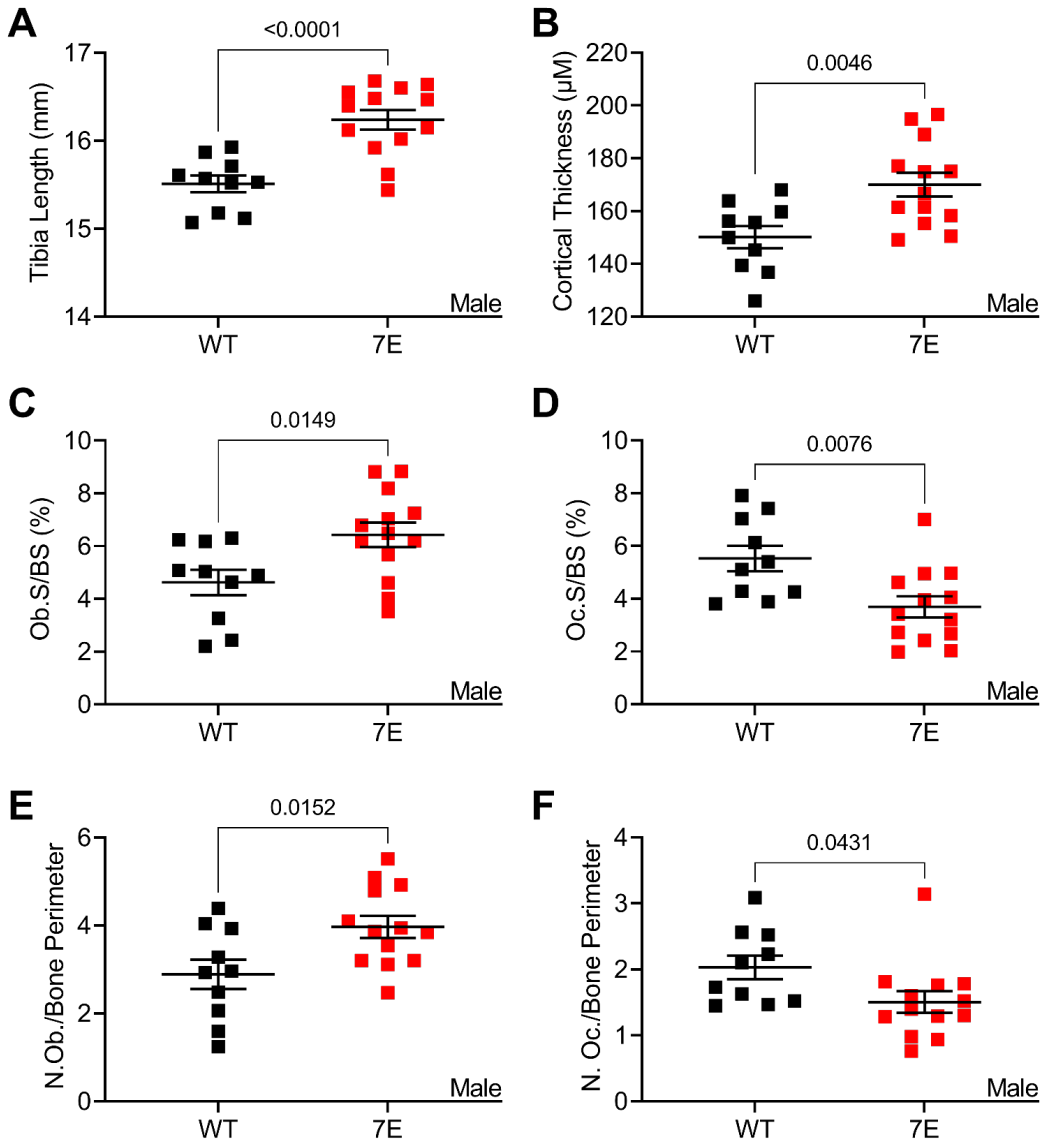

Figure 5. Tibias from 4-week-old male GC-B7E/7E mice have increased osteoblasts and cortical thickness but decreased osteoclasts.

Tibias from 4-week-old male GC-B$^{7E/7E}$ and GC-B$^{WT/WT}$ mice were collected and (A) tibia length was measured. Static histomorphometry was performed on the same tibias for (B) cortical thickness, (C) osteoblast per bone surface (Ob.S/BS), (D) osteoclast per bone surface (Oc.S/BS), (E) osteoblasts per bone perimeter and (F) osteoclasts per bone perimeter. n=10-13 mice per group. Long horizontal bars show the mean and the shorter bars above and below represent SEM. p-values from a two-tailed student's t-test are shown in each panel.

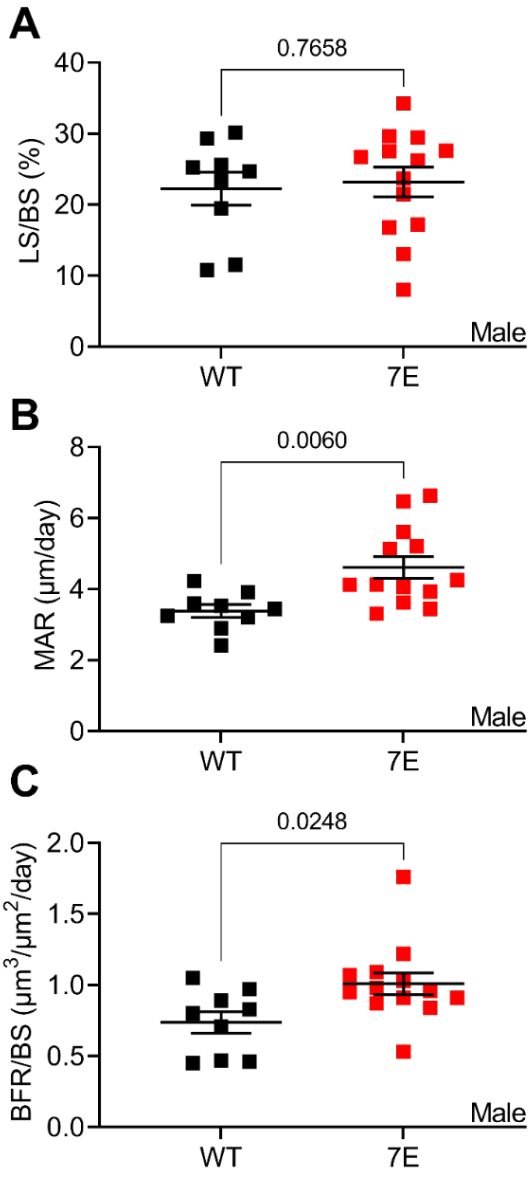

Figure 6. Tibias from 4-week-old male GC-B7E/7E mice have elevated mineral apposition and bone formation rates compared to male GC-BWT/WT mice.

Tibias from 4-week-old male GC-B$^{7E/7E}$ and GC-B$^{WT/WT}$ mice were dual calcein-labeled using a 3-day inter-label period. Dynamic histomorphometry was performed to determine (A) labeled surface/bone surface (LS/BS), (B) mineral apposition rate (MAR) and (C) bone formation rate per bone surface (BFR/BS). n=10-13 mice per group. Long horizontal bars show the mean and the shorter bars above and below represent SEM. p-values from a two-tailed student's t-test are shown in each panel.

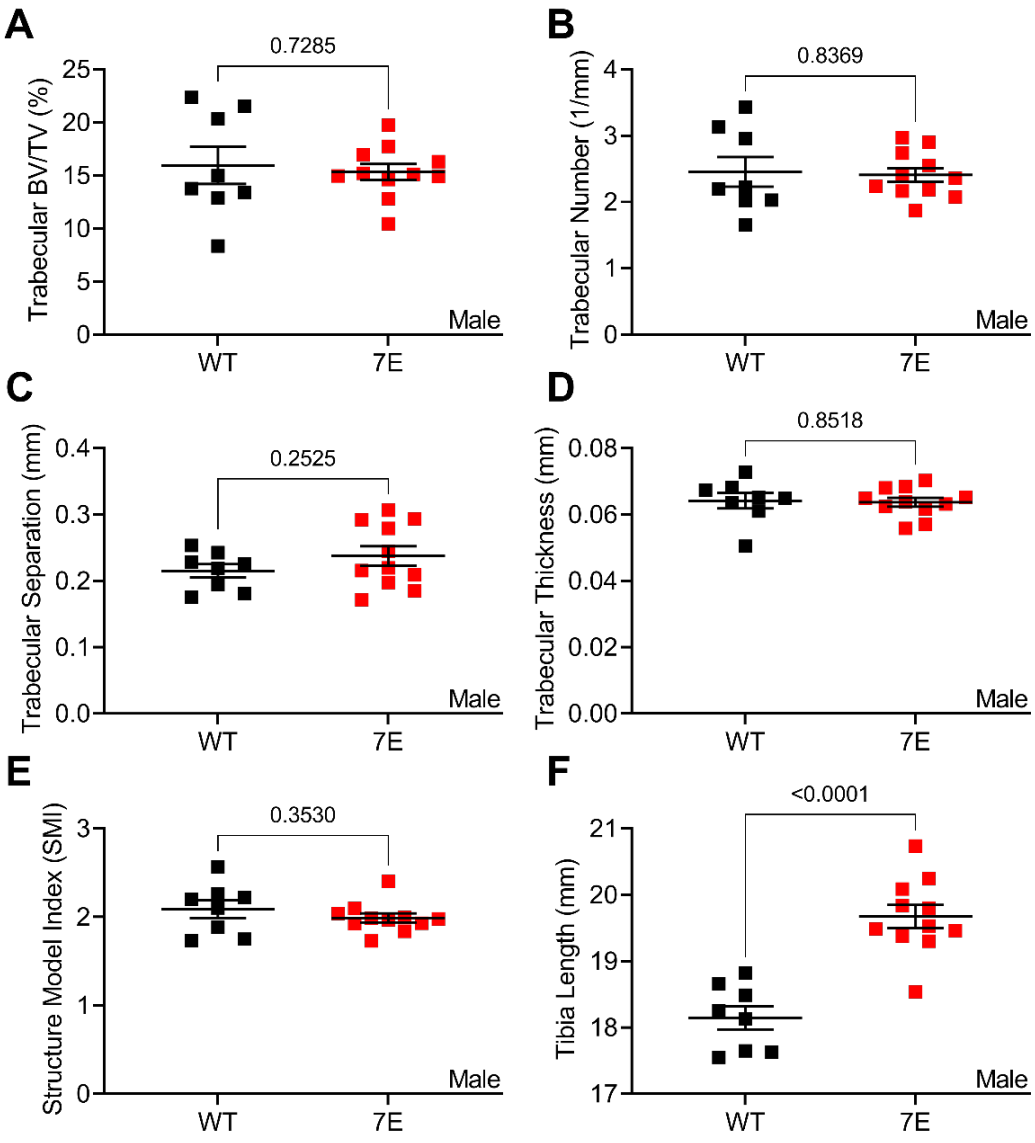

Figure 7. Trabecular bone content between 16-week-old male GC-B7E/7E and GC-BWT/WT mice does not differ.

Proximal metaphyses of tibias from 16-week-old male GC-B$^{7E/7E}$ and GC-B$^{WT/WT}$ were analyzed by μCT for (A) trabecular BV/TV, (B) trabecular number, (C) trabecular separation, (D) trabecular thickness, (E) structure model index, and (F) tibia length. n=8-11 mice per group. Long horizontal bars show the mean and the shorter bars above and below represent SEM. p-values from a two-tailed student's t-test are shown in each panel.

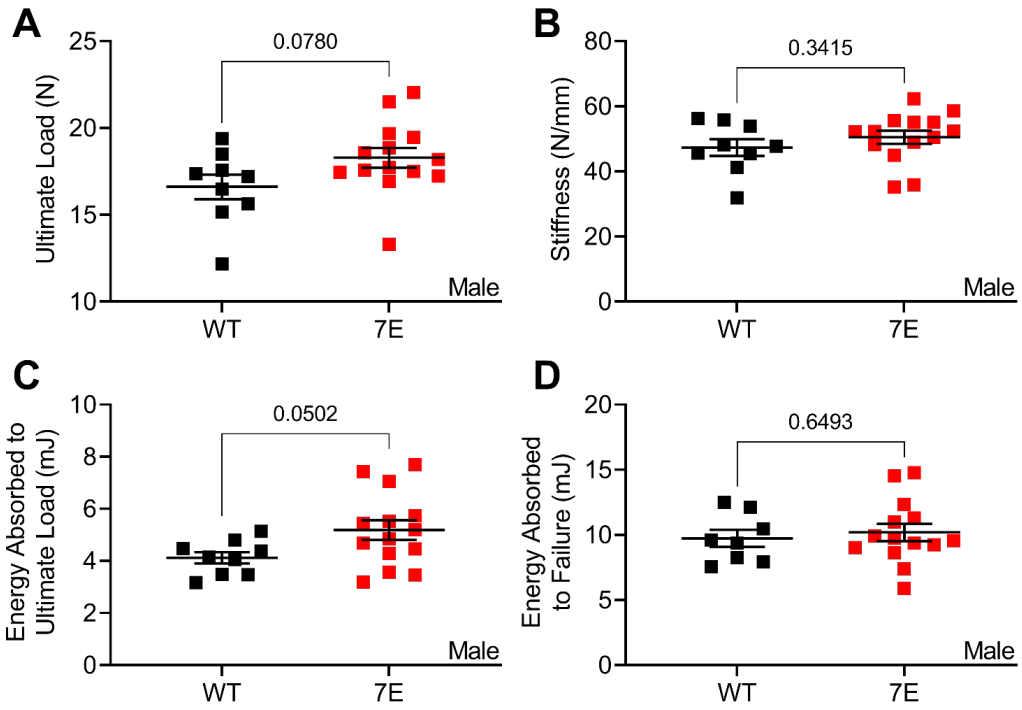

Figure 8. Initial gains in tibial strength and stiffness observed in male GC-B7E/7E mice are lost by 16 weeks of age.

Tibias from 16-week-old male mice were analyzed by 3-point bending to determine (A) ultimate load, (B) stiffness, (C) energy absorbed to ultimate load, and (D) energy absorbed to failure. n=8-14 mice per group. Long horizontal bars show the mean and the shorter bars above and below represent SEM. p-values from a two-tailed student's t-test are shown in each panel.

CHAPTER 5: CONCLUSIONS AND FUTURE DIRECTIONS

CONCLUSIONS

My thesis research has focused on determining the physiological consequences of increased phosphorylation-dependent activation of GC-A and GC-B using novel mouse models that express mutant forms of these two membrane GCs that cannot be inactivated by dephosphorylation. Since these mice express GC-A-8E or GC-B-7E at their endogenous loci and under the control of their endogenous promoters, they are excellent physiological models for the study of these receptors. Also, in contrast to receptor knockout and natriuretic peptide overexpression models, our mice, like their WT counterparts, only exhibit increased GC activity in the presence of natriuretic peptides. Hence, these mice are unique gain of function animal models that facilitate the study of natriuretic peptide-dependent cGMP functions.

My first project in the Potter Laboratory was to investigate the initial observations that 12-week-old GC-A$^{8E/8E}$ mice have reduced body and heart weights compared to WT, which was the result of a collaboration with Dr. Timothy O'Connell's Lab. Additionally, I was tasked with determining why the GC-A$^{8E/8E}$ mice had smaller hearts. The training I received as an undergraduate researcher in the O'Connell Lab involved regularly excising, weighing, and subsequent aortic cannulation, perfusion and fixation of mouse hearts, which made me particularly suited for this project. We found that male GC-A$^{8E/8E}$ heart weights and heart weight-to-body weight ratios were significantly less than the WT male hearts, whereas there was no difference in body weight. However, none of these parameters were significantly different between females. Histological examination of hundreds of slides from same hearts revealed that male GC-A$^{8E/8E}$ mice had decreased cardiomyocyte cross-sectional area (CSA), which explains the difference in heart weights between the mutant and WT male mice. Consistent with the lack of difference between female heart weights, we found that GC-A$^{8E/8E}$ female hearts had similar cardiomyocyte CSA to that of the WT females. Unexpectedly, blood pressures of the male GC-A$^{8E/8E}$ and WT mice were not different, although this is consistent with previous studies demonstrating a blood pressure-independent effect of GC-A on cardiac hypertrophy (178-180). Echocardiography studies performed by Chastity Healy in the O'Connell Lab revealed that male, but not female, GC-A$^{8E/8E}$ mice have increased ejections fractions, indicating that the mutant mice have improved systolic function despite the reductions in heart size. To determine the molecular mechanisms that

mediate the reduced heart weights in the male GC-A$^{8E/8E}$ mice, we investigated known signaling proteins involved in cardiac hypertrophy. Although ERK1/2 phosphorylation was reduced in 4- and 12-week-old GC-A$^{8E/8E}$ male ventricular, these differences were not statistically different. However, previous reports and our own unpublished observations indicate that plasma ANP exhibits diurnal variations (311). Because, like WT GC-A, the GC-A-8E enzyme only exhibits increased GC activity in the presence of ANP or BNP, we decided to use a more controlled, pharmacological approach by subcutaneously injecting the proteolytically-resistant ANP analog fsANP (240, 256, 257). We showed that activation of GC-A by fsANP injection causes a greater and prolonged increase in cGMP elevations that was correlated with greater decreases in ERK1/2 phosphorylation in male GC-A$^{8E/8E}$ cardiac ventricles compared to WT, whereas no difference between the two genotypes in females was observed. These two pieces of data are consistent with the smaller hearts observed in GC-A$^{8E/8E}$ males, but not females. Lastly, membrane preparations from both female GC-A$^{8E/8E}$ and WT cardiac ventricles exhibited much greater ANP-dependent GC-A activity compared to membranes from males of the same genotype, which to our knowledge is the first demonstration of a sex-difference in cardiac GC-A activity. Hence, we suggest that the reason male GC-A$^{8E/8E}$ mice have reduced heart weights and cardiomyocyte CSA is because the prevention of dephosphorylation-dependent inactivation of GC-A results in a greater and more prolonged synthesis of cardiomyocyte cGMP, which in turn leads to greater and more sustained reductions in ERK1/2 phosphorylation and reduced physiological hypertrophy. Furthermore, we hypothesize that cardiac GC-A activity in WT females is elevated above a threshold level required to inhibit the cardiomyocyte ERK1/2 pathway, therefore the additional activity afforded by the GC-A-8E enzyme has no observable effect on cardiac hypertrophy in female mice. In contrast, cardiac GC-A activity in WT males is below this threshold, whereas expression of GC-A-8E in males increases cardiac GC-A activity above this threshold, leading to suppression of ERK1/2 activity, which results in reduced cardiac hypertrophy in the male, but not female, GC-A$^{8E/8E}$ mice.

The second project I worked on in the lab involved determining the contribution of dephosphorylation-dependent inactivation of GC-B in ACH. To do this, we used the well-studied mouse model of ACH that expresses the human FGFR3-G380R gain of function gene (207). Mice expressing two FGFR3-G380R alleles (FGFR3$^{G380R/G380R}$ mice) are

dwarfed and recapitulate the human ACH phenotype. In 2017, Robinson et al. demonstrated that dephosphorylation of GC-B was required for FGFR3-dependent inactivation of GC-B, which suggested that dephosphorylation-dependent inactivation of GC-B was essential for ACH (216). Therefore, we hypothesized that expression of two alleles of GC-B-7E would rescue the dwarfism observed in FGFR3$^{G380R/G380R}$ mice, since the mutant GC-B-7E could not be inactivated by dephosphorylation. Indeed, gross visual examination of FGFR3$^{G380R/G380R}$ GC-B$^{7E/7E}$ mice indicated that homozygous expression of GC-B-7E completely rescued the decreased naso-anal lengths of FGFR3$^{G380R/G380R}$ GC-B$^{WT/WT}$ mice. Further analysis revealed that naso-anal, femur, and tibia lengths were not different between the 16-week-old FGFR3$^{G380R/G380R}$ GC-B$^{7E/7E}$ and FGFR3$^{WT/WT}$ GC-B$^{WT/WT}$ mice. In fact, we show that GC-B-7E expression increases naso-anal and long bone length more in FGFR3$^{G380R/G380R}$ mice than FGFR3$^{WT/WT}$ mice, indicating that GC-B-7E prevents FGFR3-G380R-dependent reductions in the axial and appendicular skeleton. However, cranial length and midface hyperplasia were still apparent in FGFR3$^{G380R/G380R}$ GC-B$^{7E/7E}$ mice, which was anticipated since the majority of the skull growth occurs by membranous ossification, which is not regulated by GC-B. As expected, histological analysis of femoral growth plates from 2-week-old male FGFR3$^{G380R/G380R}$ GC-B$^{WT/WT}$ mice showed reductions in the hypertrophic zone compared to FGFR3$^{WT/WT}$ GC-B$^{WT/WT}$ growth plates, whereas the hypertrophic zones of FGFR3$^{G380R/G380R}$ GC-B$^{7E/7E}$ growth plates did not differ. Surprisingly, the hypertrophic zones in 2-week-old female FGFR3$^{G380R/G380R}$ GC-B$^{WT/WT}$ growth plates were not smaller than the growth plate hypertrophic zones from FGFR3$^{WT/WT}$ GC-B$^{WT/WT}$ mice. In contrast, we observed that GC-B-7E expands the hypertrophic zone in both FGFR3$^{WT/WT}$ and FGFR3$^{G380R/G380R}$ female mice at two-weeks of age. We concluded that dephosphorylation of GC-B is required for ACH-dependent reductions in long bone growth. Furthermore, this is the first demonstration showing that dephosphorylation of a membrane GC is the primary mechanism for a genetic disorder.

Finally, I investigated whether activation of GC-B may be useful for the treatment of osteoporosis. In 2020, Robinson et al. demonstrated that 9-week-old GC-B$^{7E/7E}$ mice have increased bone mass and bone strength (228), therefore we hypothesized that activation of GC-B would increase bone formation and bone mass in adult WT mice. We found that treatment with the long-lived CNP analog BMN-111 increased osteoblasts and osteoclasts in adult WT mice, but ultimately did not increase bone mass. To further

investigate why 9-week-old GC-B$^{7E/7E}$ mice had increased bone mass but BMN-111 treated mice did not, we examined tibias from 4- and 16-week-old GC-B$^{7E/7E}$ mice. Compared to WT, we found that tibias from 4-week-old GC-B$^{7E/7E}$ mice had increased and decreased osteoblasts and osteoclasts, respectively. Furthermore, 4-week-old GC-B$^{7E/7E}$ tibias had increased mineral apposition and bone formation rates compared to WT controls, which explains why GC-B$^{7E/7E}$ mice exhibit increased bone mass and strength at 9 weeks. Additionally, when we examined tibias from 16-week-old GC-B$^{7E/7E}$ mice, we found that neither bone mass nor strength were significantly different compared to age-matched WT mice, which suggests that the GC-B$^{7E/7E}$ mice did not maintain their initial increases in bone mass and strength that were observed at 9 weeks. Hence, we concluded that GC-B-dependent increases in bone mass are age-dependent and that the ability of increased GC-B activity to stimulate bone formation in young mice is not only correlated increases in osteoblasts, but also with decreases in osteoclasts, whereas the inability of GC-B activation to stimulate increases in bone mass is correlated with increases in osteoclasts.

FUTURE DIRECTIONS

Although I have made significant contributions to the field, there are many unanswered questions about how and when the increased natriuretic peptide-dependent GC activity of the GC-A-8E and GC-B-7E enzymes exert their physiological effects. My work described above suggest that the effects of both GC-A-8E and GC-B-7E occur during development. The findings that support this notion include: 1) unpublished results that demonstrate that the reduction in heart weights observed in 12-week-old male GC-$A^{8E/8E}$ mice is apparent by 4 weeks of age, 2) GC-B-7E rescues the ACH-dependent reductions in the growth plate hypertrophic zones and long bone lengths in 2-week-old male mice, and 3) increased GC-B activity in young mice results in greater bone mass but not in adult mice.

Since we found that the reduced cardiac hypertrophy in the 12-week-old male GC-$A^{8E/8E}$ mice was explained by a decrease in cardiomyocyte CSA compared to WT controls, the fact that a similar reduction in cardiac hypertrophy was also observed in 4-week-old GC-$A^{8E/8E}$ is presumably due to decreased cardiomyocyte hypertrophy. This is consistent with a report show that mice with global deletion of GC-A have increased heart weights at birth (179). Similarly, Scott et al. reported that embryonic and neonatal GC-A KO mice exhibit significant cardiac enlargement with either no change or a decrease in cardiomyocyte number compared to WT, which suggests that the increase in heart size is due to hypertrophy rather that hyperplasia (234). In contrast, one report indicated that neonatal GC-A KO mice have increased heart weights due to increases in cardiomyocyte number (312). While we did not measure cardiomyocyte number our GC-$A^{8E/8E}$ mouse model, the decrease in cardiomyocyte CSA we observed in the male GC-$A^{8E/8E}$ appears to completely explain the reduced cardiac hypertrophy. However, it is possible that a reduction in cardiomyocyte number contributes to the decrease in heart weight in the male GC-$A^{8E/8E}$ mice. Further experiments to test this would include measuring cardiomyocyte numbers and CSA of GC-$A^{8E/8E}$ mice at different ages to determine 1) when the effects of GC-A-8E occur and 2) if hypoplasia contributes to the decreased cardiac hypertrophy in the male GC-$A^{8E/8E}$ mice.

We also found that the growth plate reductions in male $FGFR3^{G380R/G380R}$ GC-$B^{WT/WT}$ mice occur at 2 weeks of age and that these reductions in the growth plate hypertrophic zones are prevented in 2-week-old male $FGFR3^{G380R/G380R}$ GC-$B^{7E/7E}$ mice.

Surprisingly, when we examined the growth plates of female FGFR3$^{G380R/G380R}$ GC-B$^{WT/WT}$ mice we observed no reductions in the hypertrophic zone, whereas the hypertrophic zones of female FGFR3$^{WT/WT}$ GC-B$^{7E/7E}$ mice were significantly expanded. Additionally, homozygous expression of GC-B-7E increased naso-anal lengths of both FGFR3$^{WT/WT}$ and FGFR3$^{G380R/G380R}$ mice by 4 weeks of age. Moreover, weekly naso-anal measurements indicated that the magnitude of increased naso-anal length did not change much between the ages of 4- and 16-weeks-old. These results suggest to us that a large majority of the effects of GC-B-7E on long bone growth happen early in development before 2 weeks of age. The current understanding is that GC-B counteracts FGFR3-dependent reductions in long bone growth by inhibiting the MAP kinase pathway (209, 214, 215, 288). In particular, it is thought that FGFR3 increases phosphorylation and activation of ERK1/2 to decrease hypertrophic chondrocyte differentiation (211, 280). The combination of BMN-111 and LB-100 was recently shown to enhance growth and hypertrophic chondrocyte differentiation, as well as decrease phosphorylation of ERK1/2 in growth plates of ACH mice (293). Thus, we hypothesize that because GC-B-7E is resistant to FGFR3-dependent inactivation, growth plate cGMP remains sufficiently elevated to prevent the FGFR3-induced activation of ERK1/2 in FGFR3$^{G380R/G380R}$ mice that causes the reduced hypertrophic zone chondrocytes in developing growth plates. Similarly in FGFR3$^{WT/WT}$ mice, the increased CNP-dependent cGMP production by GC-B-7E further inhibits the activation of ERK1/2 and leads to an expansion of the hypertrophic zone, thus resulting in longer bones.

My work also suggests a developmental link between GC-B and the regulation of bone mass and bone formation. The increased mineral apposition and bone formation rates in 4-week-old GC$^{7E/7E}$ mice explains the greater bone mass and bone strength these mice exhibit at 9 weeks. Furthermore, by comparing the lack of increased in bone mass in adult WT mice injected with BMN-111 for 4 weeks and the significant increases in bone mass observed in GC$^{7E/7E}$ mice, we found that there was a correlation between increased GC-B-dependent stimulation of bone formation and decreases in osteoclasts. Although both BMN-111 treated adult WT and 4-week-old GC$^{7E/7E}$ mice had increased serum biomarkers of bone formation and more osteoblasts compared to control mice, bone formation was greater only in the 4-week-old GC$^{7E/7E}$ mice. However, the number of osteoclasts and serum biomarkers of bone resorption were increased in adult WT mice treated with BMN-111 compared to saline injected mice, whereas osteoclasts were

decreased in 4-week-old $GC^{7E/7E}$ mice and serum biomarkers of bone resorption were not different compared to age-matched WT mice. Combined with our findings that the gains in bone mass and bone strength observed in 9-week-old $GC^{7E/7E}$ mice are lost by 16-weeks-age, suggests that activation of GC-B stimulates bone turnover in adult mice, whereas increased GC-B activity leads to increased bone formation in young mice. One explanation for the different outcomes in bone mass is that the increased activity of GC-B that results from GC-B-7E is not exactly the same as pharmacological activation of the WT enzyme with BMN-111. If this is the case, then future experiments comparing young, vehicle and BMN-111 injected with untreated, age-matched GC-$B^{7E/7E}$ mice would result in different outcomes in bone mass, bone strength, and bone formation.

BIBLIOGRAPHY

1. Ashman, D. F., Lipton, R., Melicow, M. M., and Price, T. D. (1963) Isolation of adenosine 3', 5'-monophosphate and guanosine 3', 5'-monophosphate from rat urine. *Biochem Biophys Res Commun* **11**, 330-334
2. Hardman, J. G., and Sutherland, E. W. (1969) Guanyl cyclase, an enzyme catalyzing the formation of guanosine 3',5'-monophosphate from guanosine trihosphate. *J Biol Chem* **244**, 6363-6370
3. Schultz, G., Bohme, E., and Munske, K. (1969) Guanyl cyclase. Determination of enzyme activity. *Life Sci* **8**, 1323-1332
4. White, A. A., and Aurbach, G. D. (1969) Detection of guanyl cyclase in mammalian tissues. *Biochim Biophys Acta* **191**, 686-697
5. Ishikawa, E., Ishikawa, S., Davis, J. W., and Sutherland, E. W. (1969) Determination of guanosine 3',5'-monophosphate in tissues and of guanyl cyclase in rat intestine. *J Biol Chem* **244**, 6371-6376
6. Schulz, S., Yuen, P. S., and Garbers, D. L. (1991) The expanding family of guanylyl cyclases. *Trends Pharmacol Sci* **12**, 116-120
7. Chrisman, T. D., Garbers, D. L., Parks, M. A., and Hardman, J. G. (1975) Characterization of particulate and soluble guanylate cyclases from rat lung. *J Biol Chem* **250**, 374-381
8. Garbers, D. L., Chrisman, T. D., Suddath, J. L., and Hardman, J. G. (1975) Formation of pyrophosphate by soluble guanylate cyclase from rat lung. *Arch Biochem Biophys* **166**, 135-138
9. Potter, L. R. (2011) Regulation and therapeutic targeting of peptide-activated receptor guanylyl cyclases. *Pharmacology & Therapeutics* **130**, 71-82
10. de Bold, A. J., Borenstein, H. B., Veress, A. T., and Sonnenberg, H. (1981) A rapid and potent natriuretic response to intravenous injection of atrial myocardial extract in rats. *Life Sci* **28**, 89-94
11. Misono, K. S., Grammer, R. T., Fukumi, H., and Inagami, T. (1984) Rat atrial natriuretic factor: isolation, structure and biological activities of four major peptides. *Biochem Biophys Res Commun* **123**, 444-451
12. Flynn, T. G., de Bold, M. L., and de Bold, A. J. (1983) The amino acid sequence of an atrial peptide with potent diuretic and natriuretic properties. *Biochem Biophys Res Commun* **117**, 859-865
13. Currie, M. G., Geller, D. M., Cole, B. R., Siegel, N. R., Fok, K. F., Adams, S. P., Eubanks, S. R., Galluppi, G. R., and Needleman, P. (1984) Purification and sequence analysis of bioactive atrial peptides (atriopeptins). *Science* **223**, 67-69
14. Kangawa, K., Tawaragi, Y., Oikawa, S., Mizuno, A., Sakuragawa, Y., Nakazato, H., Fukuda, A., Minamino, N., and Matsuo, H. (1984) Identification of rat gamma atrial natriuretic polypeptide and characterization of the cDNA encoding its precursor. *Nature* **312**, 152-155
15. Sudoh, T., Kangawa, K., Minamino, N., and Matsuo, H. (1988) A new natriuretic peptide in porcine brain. *Nature* **332**, 78-81
16. Sudoh, T., Minamino, N., Kangawa, K., and Matsuo, H. (1990) C-type natriuretic peptide (CNP): a new member of natriuretic peptide family identified in porcine brain. *Biochem Biophys Res Commun* **168**, 863-870
17. Hamet, P., Tremblay, J., Pang, S. C., Garcia, R., Thibault, G., Gutkowska, J., Cantin, M., and Genest, J. (1984) Effect of native and synthetic atrial natriuretic factor on cyclic GMP. *Biochem Biophys Res Commun* **123**, 515-527

18. Waldman, S. A., Rapoport, R. M., and Murad, F. (1984) Atrial natriuretic factor selectively activates particulate guanylate cyclase and elevates cyclic GMP in rat tissues. *J Biol Chem* **259**, 14332-14334
19. Winquist, R. J., Faison, E. P., Waldman, S. A., Schwartz, K., Murad, F., and Rapoport, R. M. (1984) Atrial natriuretic factor elicits an endothelium-independent relaxation and activates particulate guanylate cyclase in vascular smooth muscle. *Proc Natl Acad Sci U S A* **81**, 7661-7664
20. Misono, K. S., Grammer, R. T., Rigby, J. W., and Inagami, T. (1985) Photoaffinity labeling of atrial natriuretic factor receptor in bovine and rat adrenal cortical membranes. *Biochem Biophys Res Commun* **130**, 994-1001
21. Vandlen, R. L., Arcuri, K. E., and Napier, M. A. (1985) Identification of a receptor for atrial natriuretic factor in rabbit aorta membranes by affinity cross-linking. *J Biol Chem* **260**, 10889-10892
22. Yip, C. C., Laing, L. P., and Flynn, T. G. (1985) Photoaffinity labeling of atrial natriuretic factor receptors of rat kidney cortex plasma membranes. *J Biol Chem* **260**, 8229-8232
23. Hirose, S., Akiyama, F., Shinjo, M., Ohno, H., and Murakami, K. (1985) Solubilization and molecular weight estimation of atrial natriuretic factor receptor from bovine adrenal cortex. *Biochem Biophys Res Commun* **130**, 574-579
24. Schenk, D. B., Phelps, M. N., Porter, J. G., Fuller, F., Cordell, B., and Lewicki, J. A. (1987) Purification and subunit composition of atrial natriuretic peptide receptor. *Proc Natl Acad Sci U S A* **84**, 1521-1525
25. Fuller, F., Porter, J. G., Arfsten, A. E., Miller, J., Schilling, J. W., Scarborough, R. M., Lewicki, J. A., and Schenk, D. B. (1988) Atrial natriuretic peptide clearance receptor. Complete sequence and functional expression of cDNA clones. *J Biol Chem* **263**, 9395-9401
26. Kuno, T., Andresen, J. W., Kamisaki, Y., Waldman, S. A., Chang, L. Y., Saheki, S., Leitman, D. C., Nakane, M., and Murad, F. (1986) Co-purification of an atrial natriuretic factor receptor and particulate guanylate cyclase from rat lung. *J Biol Chem* **261**, 5817-5823
27. Meloche, S., McNicoll, N., Liu, B., Ong, H., and De Lean, A. (1988) Atrial natriuretic factor R1 receptor from bovine adrenal zona glomerulosa: purification, characterization, and modulation by amiloride. *Biochemistry* **27**, 8151-8158
28. Paul, A. K., Marala, R. B., Jaiswal, R. K., and Sharma, R. K. (1987) Coexistence of guanylate cyclase and atrial natriuretic factor receptor in a 180-kD protein. *Science* **235**, 1224-1226
29. Takayanagi, R., Snajdar, R. M., Imada, T., Tamura, M., Pandey, K. N., Misono, K. S., and Inagami, T. (1987) Purification and characterization of two types of atrial natriuretic factor receptors from bovine adrenal cortex: guanylate cyclase-linked and cyclase-free receptors. *Biochem Biophys Res Commun* **144**, 244-250
30. Chinkers, M., Garbers, D. L., Chang, M. S., Lowe, D. G., Chin, H. M., Goeddel, D. V., and Schulz, S. (1989) A membrane form of guanylate cyclase is an atrial natriuretic peptide receptor. *Nature* **338**, 78-83
31. Lowe, D. G., Chang, M. S., Hellmiss, R., Chen, E., Singh, S., Garbers, D. L., and Goeddel, D. V. (1989) Human atrial natriuretic peptide receptor defines a new paradigm for second messenger signal transduction. *Embo J* **8**, 1377-1384
32. Chang, M. S., Lowe, D. G., Lewis, M., Hellmiss, R., Chen, E., and Goeddel, D. V. (1989) Differential activation by atrial and brain natriuretic peptides of two different receptor guanylate cyclases. *Nature* **341**, 68-72

33. Schulz, S., Singh, S., Bellet, R. A., Singh, G., Tubb, D. J., Chin, H., and Garbers, D. L. (1989) The primary structure of a plasma membrane guanylate cyclase demonstrates diversity within this new receptor family. *Cell* **58**, 1155-1162
34. Koller, K. J., Lowe, D. G., Bennett, G. L., Minamino, N., Kangawa, K., Matsuo, H., and Goeddel, D. V. (1991) Selective activation of the B natriuretic peptide receptor by C-type natriuretic peptide (CNP). *Science* **252**, 120-123
35. Suga, S., Nakao, K., Hosoda, K., Mukoyama, M., Ogawa, Y., Shirakami, G., Arai, H., Saito, Y., Kambayashi, Y., Inouye, K., and Imura, H. (1992) Receptor selectivity of natriuretic peptide family, atrial natriuretic peptide, brain natriuretic peptide, and C-type natriuretic peptide. *Endocrinology* **130**, 229-239
36. Yan, W., Wu, F., Morser, J., and Wu, Q. (2000) Corin, a transmembrane cardiac serine protease, acts as a pro-atrial natriuretic peptide-converting enzyme. *Proc Natl Acad Sci U S A* **97**, 8525-8529
37. Chan, J. C., Knudson, O., Wu, F., Morser, J., Dole, W. P., and Wu, Q. (2005) Hypertension in mice lacking the proatrial natriuretic peptide convertase corin. *Proc Natl Acad Sci U S A* **102**, 785-790
38. de Bold, A. J., de Bold, M. L., and Sarda, I. R. (1986) Functional-morphological studies on in vitro cardionatrin release. *J Hypertens Suppl* **4**, S3-7
39. Edwards, B. S., Zimmerman, R. S., Schwab, T. R., Heublein, D. M., and Burnett, J. C., Jr. (1988) Atrial stretch, not pressure, is the principal determinant controlling the acute release of atrial natriuretic factor. *Circ Res* **62**, 191-195
40. Stasch, J. P., Hirth-Dietrich, C., Kazda, S., and Neuser, D. (1989) Endothelin stimulates release of atrial natriuretic peptides in vitro and in vivo. *Life Sci* **45**, 869-875
41. Soualmia, H., Barthelemy, C., Masson, F., Maistre, G., Eurin, J., and Carayon, A. (1997) Angiotensin II-induced phosphoinositide production and atrial natriuretic peptide release in rat atrial tissue. *J Cardiovasc Pharmacol* **29**, 605-611
42. Lachance, D., Garcia, R., Gutkowska, J., Cantin, M., and Thibault, G. (1986) Mechanisms of release of atrial natriuretic factor. I. Effect of several agonists and steroids on its release by atrial minces. *Biochem Biophys Res Commun* **135**, 1090-1098
43. Cody, R. J., Atlas, S. A., Laragh, J. H., Kubo, S. H., Covit, A. B., Ryman, K. S., Shaknovich, A., Pondolfino, K., Clark, M., Camargo, M. J., Scarborough, R. M., and Lewicki, J. A. (1986) Atrial natriuretic factor in normal subjects and heart failure patients. Plasma levels and renal, hormonal, and hemodynamic responses to peptide infusion. *J Clin Invest* **78**, 1362-1374
44. John, S. W., Krege, J. H., Oliver, P. M., Hagaman, J. R., Hodgin, J. B., Pang, S. C., Flynn, T. G., and Smithies, O. (1995) Genetic decreases in atrial natriuretic peptide and salt-sensitive hypertension [published erratum appears in Science 1995 Mar 24;267(5205):1753]. *Science* **267**, 679-681
45. John, S. W., Veress, A. T., Honrath, U., Chong, C. K., Peng, L., Smithies, O., and Sonnenberg, H. (1996) Blood pressure and fluid-electrolyte balance in mice with reduced or absent ANP. *Am J Physiol* **271**, R109-114
46. Mukoyama, M., Nakao, K., Hosoda, K., Suga, S., Saito, Y., Ogawa, Y., Shirakami, G., Jougasaki, M., Obata, K., Yasue, H., Kambayashi, Y., Inouye, K., and Imura, H. (1991) Brain natriuretic peptide as a novel cardiac hormone in humans. Evidence for an exquisite dual natriuretic peptide system, atrial natriuretic peptide and brain natriuretic peptide. *J Clin Invest* **87**, 1402-1412

47. Sudoh, T., Minamino, N., Kangawa, K., and Matsuo, H. (1988) Brain natriuretic peptide-32: N-terminal six amino acid extended form of brain natriuretic peptide identified in porcine brain. *Biochem Biophys Res Commun* **155**, 726-732
48. Ogawa, Y., Itoh, H., Tamura, N., Suga, S., Yoshimasa, T., Uehira, M., Matsuda, S., Shiono, S., Nishimoto, H., and Nakao, K. (1994) Molecular cloning of the complementary DNA and gene that encode mouse brain natriuretic peptide and generation of transgenic mice that overexpress the brain natriuretic peptide gene. *J Clin Invest* **93**, 1911-1921
49. Tamura, N., Ogawa, Y., Chusho, H., Nakamura, K., Nakao, K., Suda, M., Kasahara, M., Hashimoto, R., Katsuura, G., Mukoyama, M., Itoh, H., Saito, Y., Tanaka, I., Otani, H., and Katsuki, M. (2000) Cardiac fibrosis in mice lacking brain natriuretic peptide. *Proc Natl Acad Sci U S A* **97**, 4239-4244
50. Hagiwara, H., Sakaguchi, H., Itakura, M., Yoshimoto, T., Furuya, M., Tanaka, S., and Hirose, S. (1994) Autocrine regulation of rat chondrocyte proliferation by natriuretic peptide C and its receptor, natriuretic peptide receptor-B. *J Biol Chem* **269**, 10729-10733
51. Hagiwara, H., Sakaguchi, H., Lodhi, K. M., Suda, K., and Hirose, S. (1994) Subtype switching of natriuretic peptide receptors in rat chondrocytes during in vitro culture. *J Biochem (Tokyo)* **116**, 606-609
52. Suga, S., Nakao, K., Itoh, H., Komatsu, Y., Ogawa, Y., Hama, N., and Imura, H. (1992) Endothelial production of C-type natriuretic peptide and its marked augmentation by transforming growth factor-beta. Possible existence of "vascular natriuretic peptide system". *J Clin Invest* **90**, 1145-1149
53. Yeung, V. T., Ho, S. K., Nicholls, M. G., and Cockram, C. S. (1996) Binding of CNP-22 and CNP-53 to cultured mouse astrocytes and effects on cyclic GMP. *Peptides* **17**, 101-106
54. Wu, C., Wu, F., Pan, J., Morser, J., and Wu, Q. (2003) Furin-mediated processing of Pro-C-type natriuretic peptide. *J Biol Chem* **278**, 25847-25852
55. Totsune, K., Takahashi, K., Ohneda, M., Itoi, K., Murakami, O., and Mouri, T. (1994) C-type natriuretic peptide in the human central nervous system: distribution and molecular form. *Peptides* **15**, 37-40
56. Stingo, A. J., Clavell, A. L., Heublein, D. M., Wei, C. M., Pittelkow, M. R., and Burnett, J. C., Jr. (1992) Presence of C-type natriuretic peptide in cultured human endothelial cells and plasma. *Am J Physiol* **263**, H1318-1321
57. Minamino, N., Makino, Y., Tateyama, H., Kangawa, K., and Matsuo, H. (1991) Characterization of immunoreactive human C-type natriuretic peptide in brain and heart. *Biochem Biophys Res Commun* **179**, 535-542
58. Togashi, K., Kameya, T., Kurosawa, T., Hasegawa, N., and Kawakami, M. (1992) Concentrations and molecular forms of C-type natriuretic peptide in brain and cerebrospinal fluid. *Clin Chem* **38**, 2136-2139
59. Wei, C. M., Heublein, D. M., Perrella, M. A., Lerman, A., Rodeheffer, R. J., McGregor, C. G., Edwards, W. D., Schaff, H. V., and Burnett, J. C., Jr. (1993) Natriuretic peptide system in human heart failure. *Circulation* **88**, 1004-1009
60. Chusho, H., Tamura, N., Ogawa, Y., Yasoda, A., Suda, M., Miyazawa, T., Nakamura, K., Nakao, K., Kurihara, T., Komatsu, Y., Itoh, H., Tanaka, K., Saito, Y., and Katsuki, M. (2001) Dwarfism and early death in mice lacking C-type natriuretic peptide. *Proc Natl Acad Sci U S A* **98**, 4016-4021.
61. Kake, T., Kitamura, H., Adachi, Y., Yoshioka, T., Watanabe, T., Matsushita, H., Fujii, T., Kondo, E., Tachibe, T., Kawase, Y., Jishage, K., Yasoda, A.,

Mukoyama, M., and Nakao, K. (2009) Chronically elevated plasma C-type natriuretic peptide level stimulates skeletal growth in transgenic mice. *Am J Physiol Endocrinol Metab* **297**, E1339-1348
62. Kondo, E., Yasoda, A., Fujii, T., Nakao, K., Yamashita, Y., Ueda-Sakane, Y., Kanamoto, N., Miura, M., Arai, H., Mukoyama, M., and Inagaki, N. (2015) Increased Bone Turnover and Possible Accelerated Fracture Healing in a Murine Model With an Increased Circulating C-Type Natriuretic Peptide. *Endocrinology* **156**, 2518-2529
63. Hisado-Oliva, A., Ruzafa-Martin, A., Sentchordi, L., Funari, M. F. A., Bezanilla-López, C., Alonso-Bernáldez, M., Barraza-García, J., Rodriguez-Zabala, M., Lerario, A. M., Benito-Sanz, S., Aza-Carmona, M., Campos-Barros, A., Jorge, A. A. L., and Heath, K. E. (2017) Mutations in C-natriuretic peptide (NPPC): a novel cause of autosomal dominant short stature. *Genet Med*
64. Bocciardi, R., Giorda, R., Buttgereit, J., Gimelli, S., Divizia, M. T., Beri, S., Garofalo, S., Tavella, S., Lerone, M., Zuffardi, O., Bader, M., Ravazzolo, R., and Gimelli, G. (2007) Overexpression of the C-type natriuretic peptide (CNP) is associated with overgrowth and bone anomalies in an individual with balanced t(2;7) translocation. *Hum Mutat* **28**, 724-731
65. Moncla, A., Missirian, C., Cacciagli, P., Balzamo, E., Legeai-Mallet, L., Jouve, J. L., Chabrol, B., Le Merrer, M., Plessis, G., Villard, L., and Philip, N. (2007) A cluster of translocation breakpoints in 2q37 is associated with overexpression of NPPC in patients with a similar overgrowth phenotype. *Hum Mutat* **12**, 1183-1188
66. Boudin, E., de Jong, T. R., Prickett, T. C. R., Lapauw, B., Toye, K., Van Hoof, V., Luyckx, I., Verstraeten, A., Heymans, H. S. A., Dulfer, E., Van Laer, L., Berry, I. R., Dobbie, A., Blair, E., Loeys, B., Espiner, E. A., Wit, J. M., Van Hul, W., Houpt, P., and Mortier, G. R. (2018) Bi-allelic Loss-of-Function Mutations in the NPR-C Receptor Result in Enhanced Growth and Connective Tissue Abnormalities. *Am J Hum Genet* **103**, 288-295
67. van den Akker, F. (2001) Structural insights into the ligand binding domains of membrane bound guanylyl cyclases and natriuretic peptide receptors. *J Mol Biol* **311**, 923-937
68. Malito, E., Hulse, R. E., and Tang, W. J. (2008) Amyloid beta-degrading cryptidases: insulin degrading enzyme, presequence peptidase, and neprilysin. *Cell Mol Life Sci* **65**, 2574-2585
69. Maack, T., Suzuki, M., Almeida, F. A., Nussenzveig, D., Scarborough, R. M., McEnroe, G. A., and Lewicki, J. A. (1987) Physiological role of silent receptors of atrial natriuretic factor. *Science* **238**, 675-678
70. Almeida, F. A., Suzuki, M., Scarborough, R. M., Lewicki, J. A., and Maack, T. (1989) Clearance function of type C receptors of atrial natriuretic factor in rats. *Am J Physiol* **256**, R469-475
71. Jaubert, J., Jaubert, F., Martin, N., Washburn, L. L., Lee, B. K., Eicher, E. M., and Guenet, J. L. (1999) Three new allelic mouse mutations that cause skeletal overgrowth involve the natriuretic peptide receptor C gene (Npr3). *Proc Natl Acad Sci U S A* **96**, 10278-10283
72. Matsukawa, N., Grzesik, W. J., Takahashi, N., Pandey, K. N., Pang, S., Yamauchi, M., and Smithies, O. (1999) The natriuretic peptide clearance receptor locally modulates the physiological effects of the natriuretic peptide system. *Proc Natl Acad Sci U S A* **96**, 7403-7408.

73. Hori, R., Inui, K., Saito, H., Matsukawa, Y., Okumura, K., Nakao, K., Morii, N., and Imura, H. (1985) Specific receptors for atrial natriuretic polypeptide on basolateral membranes isolated from rat renal cortex. *Biochem Biophys Res Commun* **129**, 773-779
74. Koehn, J. A., Norman, J. A., Jones, B. N., LeSueur, L., Sakane, Y., and Ghai, R. D. (1987) Degradation of atrial natriuretic factor by kidney cortex membranes. Isolation and characterization of the primary proteolytic product. *J Biol Chem* **262**, 11623-11627
75. Sonnenberg, J. L., Sakane, Y., Jeng, A. Y., Koehn, J. A., Ansell, J. A., Wennogle, L. P., and Ghai, R. D. (1988) Identification of protease 3.4.24.11 as the major atrial natriuretic factor degrading enzyme in the rat kidney. *Peptides* **9**, 173-180
76. Watanabe, Y., Nakajima, K., Shimamori, Y., and Fujimoto, Y. (1997) Comparison of the hydrolysis of the three types of natriuretic peptides by human kidney neutral endopeptidase 24.11. *Biochem Mol Med* **61**, 47-51
77. Kenny, A. J., Bourne, A., and Ingram, J. (1993) Hydrolysis of human and pig brain natriuretic peptides, urodilatin, C-type natriuretic peptide and some C-receptor ligands by endopeptidase-24.11. *Biochem J* **291 (Pt 1)**, 83-88
78. Potter, L. R., Yoder, A. R., Flora, D. R., Antos, L. K., and Dickey, D. M. (2009) Natriuretic peptides: their structures, receptors, physiologic functions and therapeutic applications. *Handbook of experimental pharmacology*, 341-366
79. Dickey, D. M., and Potter, L. R. (2010) Human B-type natriuretic peptide is not degraded by meprin A. *Biochemical pharmacology* **80**, 1007-1011
80. Brandt, R. R., Mattingly, M. T., Clavell, A. L., Barclay, P. L., and Burnett, J. C., Jr. (1997) Neutral endopeptidase regulates C-type natriuretic peptide metabolism but does not potentiate its bioactivity in vivo. *Hypertension* **30**, 184-190
81. Charles, C. J., Espiner, E. A., Nicholls, M. G., Richards, A. M., Yandle, T. G., Protter, A., and Kosoglou, T. (1996) Clearance receptors and endopeptidase 24.11: equal role in natriuretic peptide metabolism in conscious sheep. *Am J Physiol* **271**, R373-380
82. Margulies, K. B., Barclay, P. L., and Burnett, J. C., Jr. (1995) The role of neutral endopeptidase in dogs with evolving congestive heart failure. *Circulation* **91**, 2036-2042
83. Wegner, M., Stasch, J. P., Hirth-Dietrich, C., Dressel, J., Voges, K. P., and Kazda, S. (1995) Interaction of a neutral endopeptidase inhibitor with an ANP-C receptor ligand in anesthetized dogs. *Clin Exp Hypertens* **17**, 861-876
84. Lainchbury, J. G., Richards, A. M., Nicholls, M. G., Espiner, E. A., and Yandle, T. G. (1999) Brain natriuretic peptide and neutral endopeptidase inhibition in left ventricular impairment. *J Clin Endocrinol Metab* **84**, 723-729
85. Potter, L. R. (2011) Guanylyl cyclase structure, function and regulation. *Cellular signalling* **23**, 1921-1926
86. Chinkers, M., and Wilson, E. M. (1992) Ligand-independent oligomerization of natriuretic peptide receptors. Identification of heteromeric receptors and a dominant negative mutant. *The Journal of biological chemistry* **267**, 18589-18597
87. Potter, L. R., and Hunter, T. (2001) Guanylyl cyclase-linked natriuretic peptide receptors: structure and regulation. *The Journal of biological chemistry* **276**, 6057-6060
88. Langenickel, T., Buttgereit, J., Pagel, I., Dietz, R., Willenbrock, R., and Bader, M. (2004) Forced homodimerization by site-directed mutagenesis alters guanylyl cyclase activity of natriuretic peptide receptor B. *Hypertension* **43**, 460-465

89. Schulz, S., Green, C. K., Yuen, P. S., and Garbers, D. L. (1990) Guanylyl cyclase is a heat-stable enterotoxin receptor. *Cell* **63**, 941-948
90. Bryan, P. M., Smirnov, D., Smolenski, A., Feil, S., Feil, R., Hofmann, F., Lohmann, S., and Potter, L. R. (2006) A sensitive method for determining the phosphorylation status of natriuretic peptide receptors: cGK-Ialpha does not regulate NPR-A. *Biochemistry* **45**, 1295-1303
91. Nagase, M., Katafuchi, T., Hirose, S., and Fujita, T. (1997) Tissue distribution and localization of natriuretic peptide receptor subtypes in stroke-prone spontaneously hypertensive rats. *J Hypertens* **15**, 1235-1243
92. Goy, M. F., Oliver, P. M., Purdy, K. E., Knowles, J. W., Fox, J. E., Mohler, P. J., Qian, X., Smithies, O., and Maeda, N. (2001) Evidence for a novel natriuretic peptide receptor that prefers brain natriuretic peptide over atrial natriuretic peptide. *Biochem J* **358**, 379-387.
93. Muller, D., Mukhopadhyay, A. K., Speth, R. C., Guidone, G., Potthast, R., Potter, L. R., and Middendorff, R. (2004) Spatiotemporal regulation of the two atrial natriuretic peptide receptors in testis. *Endocrinology* **145**, 1392-1401
94. Dickey, D. M., Flora, D. R., Bryan, P. M., Xu, X., Chen, Y., and Potter, L. R. (2007) Differential regulation of membrane guanylyl cyclases in congestive heart failure: natriuretic peptide receptor (NPR)-B, Not NPR-A, is the predominant natriuretic peptide receptor in the failing heart. *Endocrinology* **148**, 3518-3522
95. Chrisman, T. D., Schulz, S., Potter, L. R., and Garbers, D. L. (1993) Seminal plasma factors that cause large elevations in cellular cyclic GMP are C-type natriuretic peptides. *The Journal of biological chemistry* **268**, 3698-3703
96. Lopez, M. J., Wong, S. K., Kishimoto, I., Dubois, S., Mach, V., Friesen, J., Garbers, D. L., and Beuve, A. (1995) Salt-resistant hypertension in mice lacking the guanylyl cyclase-A receptor for atrial natriuretic peptide. *Nature* **378**, 65-68
97. Oliver, P. M., Fox, J. E., Kim, R., Rockman, H. A., Kim, H. S., Reddick, R. L., Pandey, K. N., Milgram, S. L., Smithies, O., and Maeda, N. (1997) Hypertension, cardiac hypertrophy, and sudden death in mice lacking natriuretic peptide receptor A. *Proc Natl Acad Sci U S A* **94**, 14730-14735
98. Tamura, N., Doolittle, L. K., Hammer, R. E., Shelton, J. M., Richardson, J. A., and Garbers, D. L. (2004) Critical roles of the guanylyl cyclase B receptor in endochondral ossification and development of female reproductive organs. *Proc Natl Acad Sci U S A* **101**, 17300-17305
99. Tsuji, T., and Kunieda, T. (2005) A loss-of-function mutation in natriuretic peptide receptor 2 (Npr2) gene is responsible for disproportionate dwarfism in cn/cn mouse. *J Biol Chem* **280**, 14288-14292
100. Lowe, D. G., and Fendly, B. M. (1992) Human natriuretic peptide receptor-A guanylyl cyclase. Hormone cross- linking and antibody reactivity distinguish receptor glycoforms. *J Biol Chem* **267**, 21691-21697
101. Heim, J. M., Singh, S., and Gerzer, R. (1996) Effect of glycosylation on cloned ANF-sensitive guanylyl cyclase. *Life Sci* **59**, PL61-68
102. Miyagi, M., Zhang, X., and Misono, K. S. (2000) Glycosylation sites in the atrial natriuretic peptide receptor Oligosaccharide structures are not required for hormone binding. *Eur J Biochem* **267**, 5758-5768
103. Koller, K. J., Lipari, M. T., and Goeddel, D. V. (1993) Proper glycosylation and phosphorylation of the type A natriuretic peptide receptor are required for hormone-stimulated guanylyl cyclase activity. *The Journal of biological chemistry* **268**, 5997-6003

104. Muller, D., Middendorff, R., Olcese, J., and Mukhopadhyay, A. K. (2002) Central nervous system-specific glycosylation of the type A natriuretic peptide receptor. *Endocrinology* **143**, 23-29.
105. Dickey, D. M., Edmund, A. B., Otto, N. M., Chaffee, T. S., Robinson, J. W., and Potter, L. R. (2016) Catalytically Active Guanylyl Cyclase B Requires Endoplasmic Reticulum-mediated Glycosylation, and Mutations That Inhibit This Process Cause Dwarfism. *J Biol Chem* **291**, 11385-11393
106. Lowe, D. G. (1992) Human natriuretic peptide receptor-A guanylyl cyclase is self-associated prior to hormone binding. *Biochemistry* **31**, 10421-10425
107. Ogawa, H., Qiu, Y., Ogata, C. M., and Misono, K. S. (2004) Crystal structure of hormone-bound atrial natriuretic peptide receptor extracellular domain: rotation mechanism for transmembrane signal transduction. *J Biol Chem* **279**, 28625-28631
108. Edmund, A. B., Walseth, T. F., Levinson, N. M., and Potter, L. R. (2019) The pseudokinase domains of guanylyl cyclase-A and -B allosterically increase the affinity of their catalytic domains for substrate. *Sci Signal* **12**
109. Chinkers, M., and Garbers, D. L. (1989) The protein kinase domain of the ANP receptor is required for signaling. *Science* **245**, 1392-1394
110. Koller, K. J., de Sauvage, F. J., Lowe, D. G., and Goeddel, D. V. (1992) Conservation of the kinaselike regulatory domain is essential for activation of the natriuretic peptide receptor guanylyl cyclases. *Mol Cell Biol* **12**, 2581-2590
111. Thompson, D. K., and Garbers, D. L. (1995) Dominant negative mutations of the guanylyl cyclase-A receptor. Extracellular domain deletion and catalytic domain point mutations. *J Biol Chem* **270**, 425-430
112. Singh, S., Lowe, D. G., Thorpe, D. S., Rodriguez, H., Kuang, W. J., Dangott, L. J., Chinkers, M., Goeddel, D. V., and Garbers, D. L. (1988) Membrane guanylate cyclase is a cell-surface receptor with homology to protein kinases. *Nature* **334**, 708-712
113. Ward, G. E., and Vacquier, V. D. (1983) Dephosphorylation of a major sperm membrane protein is induced by egg jelly during sea urchin fertilization. *Proc Natl Acad Sci U S A* **80**, 5578-5582
114. Ramarao, C. S., and Garbers, D. L. (1985) Receptor-mediated regulation of guanylate cyclase activity in spermatozoa. *J Biol Chem* **260**, 8390-8396
115. Shimomura, H., Dangott, L. J., and Garbers, D. L. (1986) Covalent coupling of a resact analogue to guanylate cyclase. *J Biol Chem* **261**, 15778-15782
116. Bentley, J. K., Tubb, D. J., and Garbers, D. L. (1986) Receptor-mediated activation of spermatozoan guanylate cyclase. *J Biol Chem* **261**, 14859-14862
117. Stadel, J. M., Nambi, P., Shorr, R. G., Sawyer, D. F., Caron, M. G., and Lefkowitz, R. J. (1983) Phosphorylation of the beta-adrenergic receptor accompanies catecholamine-induced desensitization of turkey erythrocyte adenylate cyclase. *Trans Assoc Am Physicians* **96**, 137-145
118. Stadel, J. M., Nambi, P., Shorr, R. G., Sawyer, D. F., Caron, M. G., and Lefkowitz, R. J. (1983) Catecholamine-induced desensitization of turkey erythrocyte adenylate cyclase is associated with phosphorylation of the beta-adrenergic receptor. *Proc Natl Acad Sci U S A* **80**, 3173-3177
119. Sibley, D. R., Nambi, P., Peters, J. R., and Lefkowitz, R. J. (1984) Phorbol diesters promote beta-adrenergic receptor phosphorylation and adenylate cyclase desensitization in duck erythrocytes. *Biochem Biophys Res Commun* **121**, 973-979

120. Sibley, D. R., Strasser, R. H., Caron, M. G., and Lefkowitz, R. J. (1985) Homologous desensitization of adenylate cyclase is associated with phosphorylation of the beta-adrenergic receptor. *J Biol Chem* **260**, 3883-3886
121. Strasser, R. H., Sibley, D. R., and Lefkowitz, R. J. (1986) A novel catecholamine-activated adenosine cyclic 3',5'-phosphate independent pathway for beta-adrenergic receptor phosphorylation in wild-type and mutant S49 lymphoma cells: mechanism of homologous desensitization of adenylate cyclase. *Biochemistry* **25**, 1371-1377
122. Ramarao, C. S., and Garbers, D. L. (1988) Purification and properties of the phosphorylated form of guanylate cyclase. *J Biol Chem* **263**, 1524-1529
123. Jaiswal, R. K., Jaiswal, N., and Sharma, R. K. (1988) Negative regulation of atrial natriuretic factor receptor coupled membrane guanylate cyclase by phorbol ester. Potential protein kinase C regulation of cyclic GMP signal in isolated adrenocortical carcinoma cells of rat. *FEBS Lett* **227**, 47-50
124. Ballermann, B. J., Marala, R. B., and Sharma, R. K. (1988) Characterization and regulation by protein kinase C of renal glomerular atrial natriuretic peptide receptor-coupled guanylate cyclase. *Biochem Biophys Res Commun* **157**, 755-761
125. Duda, T., and Sharma, R. K. (1990) Regulation of guanylate cyclase activity by atrial natriuretic factor and protein kinase C. *Mol Cell Biochem* **93**, 179-184
126. Sharma, R. K., Marala, R. B., and Duda, T. M. (1989) Purification and characterization of the 180-kDa membrane guanylate cyclase containing atrial natriuretic factor receptor from rat adrenal gland and its regulation by protein kinase C. *Steroids* **53**, 437-460
127. Larose, L., Rondeau, J. J., Ong, H., and De Lean, A. (1992) Phosphorylation of atrial natriuretic factor R1 receptor by serine/threonine protein kinases: evidences for receptor regulation. *Mol Cell Biochem* **115**, 203-211
128. Sibley, D. R., Benovic, J. L., Caron, M. G., and Lefkowitz, R. J. (1987) Regulation of transmembrane signaling by receptor phosphorylation. *Cell* **48**, 913-922
129. Huganir, R. L., and Greengard, P. (1990) Regulation of neurotransmitter receptor desensitization by protein phosphorylation. *Neuron* **5**, 555-567
130. Potter, L. R., and Garbers, D. L. (1992) Dephosphorylation of the guanylyl cyclase-A receptor causes desensitization. *The Journal of biological chemistry* **267**, 14531-14534
131. Joubert, S., Labrecque, J., and De Lean, A. (2001) Reduced activity of the npr-a kinase triggers dephosphorylation and homologous desensitization of the receptor. *Biochemistry* **40**, 11096-11105.
132. Potter, L. R., and Garbers, D. L. (1994) Protein kinase C-dependent desensitization of the atrial natriuretic peptide receptor is mediated by dephosphorylation. *The Journal of biological chemistry* **269**, 14636-14642
133. Fethiere, J., Graihle, R., Larose, L., Babinski, K., Ong, H., and De Lean, A. (1993) Distribution and regulation of natriuretic factor-R1C receptor subtypes in mammalian cell lines. *Mol Cell Biochem* **124**, 11-16
134. Gilkes, A. F., Guild, S. B., and Cramb, G. (1994) Phorbol ester activation of protein kinase C inhibits CNP-stimulated cyclic GMP production in the mouse AtT-20 pituitary tumour cell line. *Biochem Biophys Res Commun* **204**, 1318-1324
135. Potter, L. R. (1998) Phosphorylation-dependent regulation of the guanylyl cyclase-linked natriuretic peptide receptor B: dephosphorylation is a mechanism of desensitization. *Biochemistry* **37**, 2422-2429

136. Smith, J. B., and Lincoln, T. M. (1987) Angiotensin decreases cyclic GMP accumulation produced by atrial natriuretic factor. *Am J Physiol* **253**, C147-150
137. Haneda, M., Kikkawa, R., Maeda, S., Togawa, M., Koya, D., Horide, N., Kajiwara, N., and Shigeta, Y. (1991) Dual mechanism of angiotensin II inhibits ANP-induced mesangial cGMP accumulation. *Kidney Int* **40**, 188-194
138. Jaiswal, R. K. (1992) Endothelin inhibits the atrial natriuretic factor stimulated cGMP production by activating the protein kinase C in rat aortic smooth muscle cells. *Biochem Biophys Res Commun* **182**, 395-402
139. Muller, D., Cortes-Dericks, L., Budnik, L. T., Brunswig-Spickenheier, B., Pancratius, M., Speth, R. C., Mukhopadhyay, A. K., and Middendorff, R. (2006) Homologous and lysophosphatidic acid-induced desensitization of the atrial natriuretic peptide receptor, guanylyl cyclase-A, in MA-10 leydig cells. *Endocrinology* **147**, 2974-2985
140. Chrisman, T. D., and Garbers, D. L. (1999) Reciprocal Antagonism Coordinates C-type Natriuretic Peptide and Mitogen-signaling Pathways in Fibroblasts. *J Biol Chem* **274**, 4293-4299
141. Chrisman, T. D., Perkins, D. T., and Garbers, D. L. (2003) Identification of a potent serum factor that causes desensitization of the receptor for C-Type natriuretic peptide. *Cell Commun Signal* **1**, 4
142. Abbey, S. E., and Potter, L. R. (2002) Vasopressin-dependent inhibition of the C-type natriuretic peptide receptor, NPR-B/GC-B, requires elevated intracellular calcium concentrations. *The Journal of biological chemistry* **277**, 42423-42430
143. Abbey, S. E., and Potter, L. R. (2003) Lysophosphatidic acid inhibits C-type natriuretic peptide activation of guanylyl cyclase-B. *Endocrinology* **144**, 240-246
144. Abbey-Hosch, S. E., Cody, A. N., and Potter, L. R. (2004) Sphingosine-1-phosphate inhibits C-type natriuretic peptide activation of guanylyl cyclase B (GC-B/NPR-B). *Hypertension* **43**, 1103-1109
145. Potthast, R., Abbey-Hosch, S. E., Antos, L. K., Marchant, J. S., Kuhn, M., and Potter, L. R. (2004) Calcium-dependent dephosphorylation mediates the hyperosmotic and lysophosphatidic acid-dependent inhibition of natriuretic peptide receptor-B/guanylyl cyclase-B. *The Journal of biological chemistry* **279**, 48513-48519
146. Abbey-Hosch, S. E., Smirnov, D., and Potter, L. R. (2005) Differential regulation of NPR-B/GC-B by protein kinase c and calcium. *Biochemical pharmacology* **70**, 686-694
147. Potter, L. R., and Hunter, T. (1998) Phosphorylation of the kinase homology domain is essential for activation of the A-type natriuretic peptide receptor. *Molecular and cellular biology* **18**, 2164-2172
148. Potter, L. R., and Hunter, T. (1998) Identification and characterization of the major phosphorylation sites of the B-type natriuretic peptide receptor. *The Journal of biological chemistry* **273**, 15533-15539
149. Thorsness, P. E., and Koshland, D. E., Jr. (1987) Inactivation of isocitrate dehydrogenase by phosphorylation is mediated by the negative charge of the phosphate. *J Biol Chem* **262**, 10422-10425
150. Yan, M., and Templeton, D. J. (1994) Identification of 2 serine residues of MEK-1 that are differentially phosphorylated during activation by raf and MEK kinase. *J Biol Chem* **269**, 19067-19073

151. Potter, L. R., and Hunter, T. (1999) A constitutively "phosphorylated" guanylyl cyclase-linked atrial natriuretic peptide receptor mutant is resistant to desensitization. *Molecular biology of the cell* **10**, 1811-1820
152. Schröter, J., Zahedi, R. P., Hartmann, M., Gassner, B., Gazinski, A., Waschke, J., Sickmann, A., and Kuhn, M. (2010) Homologous desensitization of guanylyl cyclase A, the receptor for atrial natriuretic peptide, is associated with a complex phosphorylation pattern. *FEBS J* **277**, 2440-2453
153. Yoder, A. R., Stone, M. D., Griffin, T. J., and Potter, L. R. (2010) Mass spectrometric identification of phosphorylation sites in guanylyl cyclase a and B. *Biochemistry* **49**, 10137-10145
154. Yoder, A. R., Robinson, J. W., Dickey, D. M., Andersland, J., Rose, B. A., Stone, M. D., Griffin, T. J., and Potter, L. R. (2012) A Functional Screen Provides Evidence for a Conserved, Regulatory, Juxtamembrane Phosphorylation Site in Guanylyl Cyclase A and B. *PLoS ONE* **7**, e36747
155. Otto, N. M., McDowell, W. G., Dickey, D. M., and Potter, L. R. (2017) A Glutamate-Substituted Mutant Mimics the Phosphorylated and Active Form of Guanylyl Cyclase-A. *Mol Pharmacol* **92**, 67-74
156. Pfeifer, A., Ruth, P., Dostmann, W., Sausbier, M., Klatt, P., and Hofmann, F. (1999) Structure and function of cGMP-dependent protein kinases. *Rev Physiol Biochem Pharmacol* **135**, 105-149
157. Hofmann, F., and Wegener, J. W. (2013) cGMP-dependent protein kinases (cGK). *Methods Mol Biol* **1020**, 17-50
158. Lohmann, S. M., Vaandrager, A. B., Smolenski, A., Walter, U., and De Jonge, H. R. (1997) Distinct and specific functions of cGMP-dependent protein kinases. *Trends Biochem Sci* **22**, 307-312
159. Pfeifer, A., Klatt, P., Massberg, S., Ny, L., Sausbier, M., Hirneiss, C., Wang, G. X., Korth, M., Aszodi, A., Andersson, K. E., Krombach, F., Mayerhofer, A., Ruth, P., Fassler, R., and Hofmann, F. (1998) Defective smooth muscle regulation in cGMP kinase I-deficient mice. *Embo J* **17**, 3045-3051
160. Smolenski, A., Burkhardt, A. M., Eigenthaler, M., Butt, E., Gambaryan, S., Lohmann, S. M., and Walter, U. (1998) Functional analysis of cGMP-dependent protein kinases I and II as mediators of NO/cGMP effects. *Naunyn Schmiedebergs Arch Pharmacol* **358**, 134-139
161. Pfeifer, A., Aszodi, A., Seidler, U., Ruth, P., Hofmann, F., and Fassler, R. (1996) Intestinal secretory defects and dwarfism in mice lacking cGMP- dependent protein kinase II. *Science* **274**, 2082-2086
162. Chikuda, H., Kugimiya, F., Hoshi, K., Ikeda, T., Ogasawara, T., Shimoaka, T., Kawano, H., Kamekura, S., Tsuchida, A., Yokoi, N., Nakamura, K., Komeda, K., Chung, U. I., and Kawaguchi, H. (2004) Cyclic GMP-dependent protein kinase II is a molecular switch from proliferation to hypertrophic differentiation of chondrocytes. *Genes Dev* **18**, 2418-2429
163. Conti, M., and Beavo, J. (2007) Biochemistry and physiology of cyclic nucleotide phosphodiesterases: essential components in cyclic nucleotide signaling. *Annu Rev Biochem* **76**, 481-511
164. Maurice, D. H., Palmer, D., Tilley, D. G., Dunkerley, H. A., Netherton, S. J., Raymond, D. R., Elbatarny, H. S., and Jimmo, S. L. (2003) Cyclic nucleotide phosphodiesterase activity, expression, and targeting in cells of the cardiovascular system. *Mol Pharmacol* **64**, 533-546

165. Stangherlin, A., Gesellchen, F., Zoccarato, A., Terrin, A., Fields, L. A., Berrera, M., Surdo, N. C., Craig, M. A., Smith, G., Hamilton, G., and Zaccolo, M. (2011) cGMP signals modulate cAMP levels in a compartment-specific manner to regulate catecholamine-dependent signaling in cardiac myocytes. *Circ Res* **108**, 929-939
166. Kaupp, U. B., and Seifert, R. (2002) Cyclic nucleotide-gated ion channels. *Physiol Rev* **82**, 769-824
167. Dizhoor, A. M., and Hurley, J. B. (1999) Regulation of photoreceptor membrane guanylyl cyclases by guanylyl cyclase activator proteins. *Methods* **19**, 521-531
168. Stephen, R., Bereta, G., Golczak, M., Palczewski, K., and Sousa, M. C. (2007) Stabilizing function for myristoyl group revealed by the crystal structure of a neuronal calcium sensor, guanylate cyclase-activating protein 1. *Structure* **15**, 1392-1402
169. Bereta, G., Wang, B., Kiser, P. D., Baehr, W., Jang, G. F., and Palczewski, K. (2010) A functional kinase homology domain is essential for the activity of photoreceptor guanylate cyclase 1. *J Biol Chem* **285**, 1899-1908
170. Pichlo, M., Bungert-Plumke, S., Weyand, I., Seifert, R., Bonigk, W., Strunker, T., Kashikar, N. D., Goodwin, N., Muller, A., Pelzer, P., Van, Q., Enderlein, J., Klemm, C., Krause, E., Trotschel, C., Poetsch, A., Kremmer, E., Kaupp, U. B., Korschen, H. G., and Collienne, U. (2014) High density and ligand affinity confer ultrasensitive signal detection by a guanylyl cyclase chemoreceptor. *J Cell Biol* **206**, 541-557
171. Steinhelper, M. E., Cochrane, K. L., and Field, L. J. (1990) Hypotension in transgenic mice expressing atrial natriuretic factor fusion genes. *Hypertension* **16**, 301-307
172. Ogawa, Y., Itoh, H., Yoshitake, Y., Inoue, M., Yoshimasa, T., Serikawa, T., and Nakao, K. (1994) Molecular cloning and chromosomal assignment of the mouse C-type natriuretic peptide (CNP) gene (Nppc): comparison with the human CNP gene (NPPC). *Genomics* **24**, 383-387
173. Oliver, P. M., John, S. W., Purdy, K. E., Kim, R., Maeda, N., Goy, M. F., and Smithies, O. (1998) Natriuretic peptide receptor 1 expression influences blood pressures of mice in a dose-dependent manner. *Proc Natl Acad Sci U S A* **95**, 2547-2551
174. Holtwick, R., Gotthardt, M., Skryabin, B., Steinmetz, M., Potthast, R., Zetsche, B., Hammer, R. E., Herz, J., and Kuhn, M. (2002) Smooth muscle-selective deletion of guanylyl cyclase-A prevents the acute but not chronic effects of ANP on blood pressure. *Proc Natl Acad Sci U S A* **99**, 7142-7147
175. Sabrane, K., Kruse, M. N., Fabritz, L., Zetsche, B., Mitko, D., Skryabin, B. V., Zwiener, M., Baba, H. A., Yanagisawa, M., and Kuhn, M. (2005) Vascular endothelium is critically involved in the hypotensive and hypovolemic actions of atrial natriuretic peptide. *J Clin Invest* **115**, 1666-1674
176. Franco, F., Dubois, S. K., Peshock, R. M., and Shohet, R. V. (1998) Magnetic resonance imaging accurately estimates LV mass in a transgenic mouse model of cardiac hypertrophy. *Am J Physiol* **274**, H679-683
177. Barbee, R. W., Perry, B. D., Re, R. N., Murgo, J. P., and Field, L. J. (1994) Hemodynamics in transgenic mice with overexpression of atrial natriuretic factor. *Circ Res* **74**, 747-751
178. Kishimoto, I., Rossi, K., and Garbers, D. L. (2001) A genetic model provides evidence that the receptor for atrial natriuretic peptide (guanylyl cyclase-A)

inhibits cardiac ventricular myocyte hypertrophy. *Proc Natl Acad Sci U S A* **98**, 2703-2706.
179. Knowles, J. W., Esposito, G., Mao, L., Hagaman, J. R., Fox, J. E., Smithies, O., Rockman, H. A., and Maeda, N. (2001) Pressure-independent enhancement of cardiac hypertrophy in natriuretic peptide receptor A-deficient mice. *J Clin Invest* **107**, 975-984
180. Holtwick, R., Van Eickels, M., Skryabin, B. V., Baba, H. A., Bubikat, A., Begrow, F., Schneider, M. D., Garbers, D. L., and Kuhn, M. (2003) Pressure-independent cardiac hypertrophy in mice with cardiomyocyte-restricted inactivation of the atrial natriuretic peptide receptor guanylyl cyclase-A. *J Clin Invest* **111**, 1399-1407
181. Masciarelli, S., Horner, K., Liu, C., Park, S. H., Hinckley, M., Hockman, S., Nedachi, T., Jin, C., Conti, M., and Manganiello, V. (2004) Cyclic nucleotide phosphodiesterase 3A-deficient mice as a model of female infertility. *J Clin Invest* **114**, 196-205
182. Norris, R. P., Ratzan, W. J., Freudzon, M., Mehlmann, L. M., Krall, J., Movsesian, M. A., Wang, H., Ke, H., Nikolaev, V. O., and Jaffe, L. A. (2009) Cyclic GMP from the surrounding somatic cells regulates cyclic AMP and meiosis in the mouse oocyte. *Development* **136**, 1869-1878
183. Zhang, M., Su, Y. Q., Sugiura, K., Xia, G., and Eppig, J. J. (2010) Granulosa cell ligand NPPC and its receptor NPR2 maintain meiotic arrest in mouse oocytes. *Science* **330**, 366-369
184. Robinson, J. W., Zhang, M., Shuhaibar, L. C., Norris, R. P., Geerts, A., Wunder, F., Eppig, J. J., Potter, L. R., and Jaffe, L. A. (2012) Luteinizing hormone reduces the activity of the NPR2 guanylyl cyclase in mouse ovarian follicles, contributing to the cyclic GMP decrease that promotes resumption of meiosis in oocytes. *Dev Biol* **366**, 308-316
185. Egbert, J. R., Shuhaibar, L. C., Edmund, A. B., Van Helden, D. A., Robinson, J. W., Uliasz, T. F., Baena, V., Geerts, A., Wunder, F., Potter, L. R., and Jaffe, L. A. (2014) Dephosphorylation and inactivation of NPR2 guanylyl cyclase in granulosa cells contributes to the LH-induced decrease in cGMP that causes resumption of meiosis in rat oocytes. *Development* **141**, 3594-3604
186. Shuhaibar, L. C., Egbert, J. R., Edmund, A. B., Uliasz, T. F., Dickey, D. M., Yee, S. P., Potter, L. R., and Jaffe, L. A. (2016) Dephosphorylation of juxtamembrane serines and threonines of the NPR2 guanylyl cyclase is required for rapid resumption of oocyte meiosis in response to luteinizing hormone. *Dev Biol* **409**, 194-201
187. Jaffe, L. A., and Egbert, J. R. (2017) Regulation of Mammalian Oocyte Meiosis by Intercellular Communication Within the Ovarian Follicle. *Annu Rev Physiol* **79**, 237-260
188. Egbert, J. R., Robinson, J. W., Uliasz, T. F., Potter, L. R., and Jaffe, L. A. (2021) Cyclic AMP links luteinizing hormone signaling to dephosphorylation and inactivation of the NPR2 guanylyl cyclase in ovarian follicles. *Biol Reprod*
189. Yasoda, A., Ogawa, Y., Suda, M., Tamura, N., Mori, K., Sakuma, Y., Chusho, H., Shiota, K., Tanaka, K., and Nakao, K. (1998) Natriuretic peptide regulation of endochondral ossification. Evidence for possible roles of the C-type natriuretic peptide/guanylyl cyclase-B pathway. *J Biol Chem* **273**, 11695-11700
190. Geister, K. A., Brinkmeier, M. L., Hsieh, M., Faust, S. M., Karolyi, I. J., Perosky, J. E., Kozloff, K. M., Conti, M., and Camper, S. A. (2013) A novel loss-of-function mutation in Npr2 clarifies primary role in female reproduction and reveals a

potential therapy for acromesomelic dysplasia, Maroteaux type. *Hum Mol Genet* **22**, 345-357
191. Kılıç, E., Çavdarlı, B., Büyükyılmaz, G., and Kılıç, M. (2021) Acromesomelic dysplasia-Maroteaux type, nine patients with two novel. *J Pediatr Endocrinol Metab* **34**, 1115-1121
192. Wang, W., Song, M. H., Miura, K., Fujiwara, M., Nawa, N., Ohata, Y., Kitaoka, T., Kubota, T., Namba, N., Jin, D. K., Kim, O. H., Ozono, K., and Cho, T. J. (2016) Acromesomelic dysplasia, type maroteaux caused by novel loss-of-function mutations of the NPR2 gene: Three case reports. *Am J Med Genet A* **170**, 426-434
193. Olney, R. C., Bükülmez, H., Bartels, C. F., Prickett, T. C., Espiner, E. A., Potter, L. R., and Warman, M. L. (2006) Heterozygous mutations in natriuretic peptide receptor-B (NPR2) are associated with short stature. *J Clin Endocrinol Metab* **91**, 1229-1232
194. Wang, S. R., Jacobsen, C. M., Carmichael, H., Edmund, A. B., Robinson, J. W., Olney, R. C., Miller, T. C., Moon, J. E., Mericq, V., Potter, L. R., Warman, M. L., Hirschhorn, J. N., and Dauber, A. (2015) Heterozygous Mutations in Natriuretic Peptide Receptor-B (NPR2) Gene as a Cause of Short Stature. *Hum Mutat* **36**, 474-481
195. Jacob, M., Menon, S., Botti, C., and Marshall, I. (2018) Heterozygous NPR2 Mutation in Two Family Members with Short Stature and Skeletal Dysplasia. *Case Rep Endocrinol* **2018**, 7658496
196. Hannema, S. E., van Duyvenvoorde, H. A., Premsler, T., Yang, R. B., Mueller, T. D., Gassner, B., Oberwinkler, H., Roelfsema, F., Santen, G. W., Prickett, T., Kant, S. G., Verkerk, A. J., Uitterlinden, A. G., Espiner, E., Ruivenkamp, C. A., Oostdijk, W., Pereira, A. M., Losekoot, M., Kuhn, M., and Wit, J. M. (2013) An activating mutation in the kinase homology domain of the natriuretic peptide receptor-2 causes extremely tall stature without skeletal deformities. *J Clin Endocrinol Metab* **98**, E1988-1998
197. Miura, K., Namba, N., Fujiwara, M., Ohata, Y., Ishida, H., Kitaoka, T., Kubota, T., Hirai, H., Higuchi, C., Tsumaki, N., Yoshikawa, H., Sakai, N., Michigami, T., and Ozono, K. (2012) An overgrowth disorder associated with excessive production of cGMP due to a gain-of-function mutation of the natriuretic peptide receptor 2 gene. *PLoS One* **7**, e42180
198. Miura, K., Kim, O. H., Lee, H. R., Namba, N., Michigami, T., Yoo, W. J., Choi, I. H., Ozono, K., and Cho, T. J. (2014) Overgrowth syndrome associated with a gain-of-function mutation of the natriuretic peptide receptor 2 (NPR2) gene. *Am J Med Genet A* **164A**, 156-163
199. Hirota, K., Furuya, M., Morozumi, N., Yoshikiyo, K., Yotsumoto, T., Jindo, T., Nakamura, R., Murakami, K., Ueda, Y., Hanada, T., Sade, H., Yoshida, S., Enomoto, K., Kanai, Y., Yamauchi, I., Yamashita, T., Ueda-Sakane, Y., Fujii, T., Yasoda, A., and Inagaki, N. (2018) Exogenous C-type natriuretic peptide restores normal growth and prevents early growth plate closure in its deficient rats. *PLoS One* **13**, e0204172
200. Schmidt, H., Dickey, D. M., Dumoulin, A., Octave, M., Robinson, J. W., Kühn, R., Feil, R., Potter, L. R., and Rathjen, F. G. (2018) Regulation of the natriuretic peptide receptor 2 (Npr2) by phosphorylation of juxtamembrane serine and threonine residues is essential for bifurcation of sensory axons. *J Neurosci*

201. Ornitz, D. M., and Legeai-Mallet, L. (2017) Achondroplasia: Development, pathogenesis, and therapy. *Dev Dyn* **246**, 291-309
202. Shiang, R., Thompson, L. M., Zhu, Y. Z., Church, D. M., Fielder, T. J., Bocian, M., Winokur, S. T., and Wasmuth, J. J. (1994) Mutations in the transmembrane domain of FGFR3 cause the most common genetic form of dwarfism, achondroplasia. *Cell* **78**, 335-342
203. Rousseau, F., Bonaventure, J., Legeai-Mallet, L., Pelet, A., Rozet, J. M., Maroteaux, P., Le Merrer, M., and Munnich, A. (1994) Mutations in the gene encoding fibroblast growth factor receptor-3 in achondroplasia. *Nature* **371**, 252-254
204. Heuertz, S., Le Merrer, M., Zabel, B., Wright, M., Legeai-Mallet, L., Cormier-Daire, V., Gibbs, L., and Bonaventure, J. (2006) Novel FGFR3 mutations creating cysteine residues in the extracellular domain of the receptor cause achondroplasia or severe forms of hypochondroplasia. *Eur J Hum Genet* **14**, 1240-1247
205. Naski, M. C., Colvin, J. S., Coffin, J. D., and Ornitz, D. M. (1998) Repression of hedgehog signaling and BMP4 expression in growth plate cartilage by fibroblast growth factor receptor 3. *Development* **125**, 4977-4988
206. Wang, Y., Spatz, M. K., Kannan, K., Hayk, H., Avivi, A., Gorivodsky, M., Pines, M., Yayon, A., Lonai, P., and Givol, D. (1999) A mouse model for achondroplasia produced by targeting fibroblast growth factor receptor 3. *Proc Natl Acad Sci U S A* **96**, 4455-4460
207. Lee, Y. C., Song, I. W., Pai, Y. J., Chen, S. D., and Chen, Y. T. (2017) Knock-in human FGFR3 achondroplasia mutation as a mouse model for human skeletal dysplasia. *Sci Rep* **7**, 43220
208. Mugniery, E., Dacquin, R., Marty, C., Benoist-Lasselin, C., de Vernejoul, M. C., Jurdic, P., Munnich, A., Geoffroy, V., and Legeai-Mallet, L. (2012) An activating Fgfr3 mutation affects trabecular bone formation via a paracrine mechanism during growth. *Hum Mol Genet* **21**, 2503-2513
209. Yasoda, A., Komatsu, Y., Chusho, H., Miyazawa, T., Ozasa, A., Miura, M., Kurihara, T., Rogi, T., Tanaka, S., Suda, M., Tamura, N., Ogawa, Y., and Nakao, K. (2004) Overexpression of CNP in chondrocytes rescues achondroplasia through a MAPK-dependent pathway. *Nat Med* **10**, 80-86
210. Yasoda, A., Kitamura, H., Fujii, T., Kondo, E., Murao, N., Miura, M., Kanamoto, N., Komatsu, Y., Arai, H., and Nakao, K. (2009) Systemic administration of C-type natriuretic peptide as a novel therapeutic strategy for skeletal dysplasias. *Endocrinology* **150**, 3138-3144
211. Lorget, F., Kaci, N., Peng, J., Benoist-Lasselin, C., Mugniery, E., Oppeneer, T., Wendt, D. J., Bell, S. M., Bullens, S., Bunting, S., Tsuruda, L. S., O'Neill, C. A., Di Rocco, F., Munnich, A., and Legeai-Mallet, L. (2012) Evaluation of the therapeutic potential of a CNP analog in a Fgfr3 mouse model recapitulating achondroplasia. *Am J Hum Genet* **91**, 1108-1114
212. Wendt, D. J., Dvorak-Ewell, M., Bullens, S., Lorget, F., Bell, S. M., Peng, J., Castillo, S., Aoyagi-Scharber, M., O'Neill, C. A., Krejci, P., Wilcox, W. R., Rimoin, D. L., and Bunting, S. (2015) Neutral endopeptidase-resistant C-type natriuretic peptide variant represents a new therapeutic approach for treatment of fibroblast growth factor receptor 3-related dwarfism. *J Pharmacol Exp Ther* **353**, 132-149
213. Savarirayan, R., Tofts, L., Irving, M., Wilcox, W., Bacino, C. A., Hoover-Fong, J., Ullot Font, R., Harmatz, P., Rutsch, F., Bober, M. B., Polgreen, L. E., Ginebreda,

I., Mohnike, K., Charrow, J., Hoernschmeyer, D., Ozono, K., Alanay, Y., Arundel, P., Kagami, S., Yasui, N., White, K. K., Saal, H. M., Leiva-Gea, A., Luna-González, F., Mochizuki, H., Basel, D., Porco, D. M., Jayaram, K., Fisheleva, E., Huntsman-Labed, A., and Day, J. (2020) Once-daily, subcutaneous vosoritide therapy in children with achondroplasia: a randomised, double-blind, phase 3, placebo-controlled, multicentre trial. *Lancet* **396**, 684-692

214. Ozasa, A., Komatsu, Y., Yasoda, A., Miura, M., Sakuma, Y., Nakatsuru, Y., Arai, H., Itoh, N., and Nakao, K. (2005) Complementary antagonistic actions between C-type natriuretic peptide and the MAPK pathway through FGFR-3 in ATDC5 cells. *Bone* **36**, 1056-1064
215. Krejci, P., Masri, B., Fontaine, V., Mekikian, P. B., Weis, M., Prats, H., and Wilcox, W. R. (2005) Interaction of fibroblast growth factor and C-natriuretic peptide signaling in regulation of chondrocyte proliferation and extracellular matrix homeostasis. *J Cell Sci* **118**, 5089-5100
216. Robinson, J. W., Egbert, J. R., Davydova, J., Schmidt, H., Jaffe, L. A., and Potter, L. R. (2017) Dephosphorylation is the mechanism of fibroblast growth factor inhibition of guanylyl cyclase-B. *Cell Signal* **40**, 222-229
217. Shuhaibar, L. C., Robinson, J. W., Vigone, G., Shuhaibar, N. P., Egbert, J. R., Baena, V., Uliasz, T. F., Kaback, D., Yee, S. P., Feil, R., Fisher, M. C., Dealy, C. N., Potter, L. R., and Jaffe, L. A. (2017) Dephosphorylation of the NPR2 guanylyl cyclase contributes to inhibition of bone growth by fibroblast growth factor. *Elife* **6**
218. Hagiwara, H., Inoue, A., Yamaguchi, A., Yokose, S., Furuya, M., Tanaka, S., and Hirose, S. (1996) cGMP produced in response to ANP and CNP regulates proliferation and differentiation of osteoblastic cells. *Am J Physiol* **270**, C1311-1318
219. Suda, M., Tanaka, K., Fukushima, M., Natsui, K., Yasoda, A., Komatsu, Y., Ogawa, Y., Itoh, H., and Nakao, K. (1996) C-type natriuretic peptide as an autocrine/paracrine regulator of osteoblast. Evidence for possible presence of bone natriuretic peptide system. *Biochem Biophys Res Commun* **223**, 1-6
220. Holliday, L. S., Dean, A. D., Greenwald, J. E., and Glucks, S. L. (1995) C-type natriuretic peptide increases bone resorption in 1,25- dihydroxyvitamin D3-stimulated mouse bone marrow cultures. *J Biol Chem* **270**, 18983-18989
221. Dong, S. S., Williams, J. P., Jordan, S. E., Cornwell, T., and Blair, H. C. (1999) Nitric oxide regulation of cGMP production in osteoclasts. *J Cell Biochem* **73**, 478-487
222. Yeh, L. C., Zavala, M. C., and Lee, J. C. (2006) C-type natriuretic peptide enhances osteogenic protein-1-induced osteoblastic cell differentiation via Smad5 phosphorylation. *J Cell Biochem* **97**, 494-500
223. Lenz, A., Bennett, M., Skelton, W. P., and Vesely, D. L. (2010) Vessel dilator and C-type natriuretic peptide enhance the proliferation of human osteoblasts. *Pediatr Res* **68**, 405-408
224. Ayturk, U. M., Jacobsen, C. M., Christodoulou, D. C., Gorham, J., Seidman, J. G., Seidman, C. E., Robling, A. G., and Warman, M. L. (2013) An RNA-seq protocol to identify mRNA expression changes in mouse diaphyseal bone: applications in mice with bone property altering Lrp5 mutations. *J Bone Miner Res* **28**, 2081-2093
225. Thumbigere-Math, V., Foster, B. L., Bachu, M., Yoshii, H., Brooks, S. R., Coulter, A., Chavez, M. B., Togi, S., Neely, A. L., Deng, Z., Mansky, K. C., Ozato, K., and Somerman, M. J. (2019) Inactivating Mutation in IRF8 Promotes Osteoclast

Transcriptional Programs and Increases Susceptibility to Tooth Root Resorption. *J Bone Miner Res*

226. Kanai, Y., Yasoda, A., Mori, K. P., Watanabe-Takano, H., Nagai-Okatani, C., Yamashita, Y., Hirota, K., Ueda, Y., Yamauchi, I., Kondo, E., Yamanaka, S., Sakane, Y., Nakao, K., Fujii, T., Yokoi, H., Minamino, N., Mukoyama, M., Mochizuki, N., and Inagaki, N. (2017) Circulating osteocrin stimulates bone growth by limiting C-type natriuretic peptide clearance. *J Clin Invest* **127**, 4136-4147
227. Watanabe-Takano, H., Ochi, H., Chiba, A., Matsuo, A., Kanai, Y., Fukuhara, S., Ito, N., Sako, K., Miyazaki, T., Tainaka, K., Harada, I., Sato, S., Sawada, Y., Minamino, N., Takeda, S., Ueda, H. R., Yasoda, A., and Mochizuki, N. (2021) Mechanical load regulates bone growth via periosteal Osteocrin. *Cell Rep* **36**, 109380
228. Robinson, J. W., Blixt, N. C., Norton, A., Mansky, K. C., Ye, Z., Aparicio, C., Wagner, B. M., Benton, A. M., Warren, G. L., Khosla, S., Gaddy, D., Suva, L. J., and Potter, L. R. (2020) Male mice with elevated C-type natriuretic peptide-dependent guanylyl cyclase-B activity have increased osteoblasts, bone mass and bone strength. *Bone* **135**, 115320
229. Potter, L. R., Abbey-Hosch, S., and Dickey, D. M. (2006) Natriuretic peptides, their receptors, and cyclic guanosine monophosphate-dependent signaling functions. *Endocr Rev* **27**, 47-72
230. Kuhn, M. (2016) Molecular Physiology of Membrane Guanylyl Cyclase Receptors. *Physiol Rev* **96**, 751-804
231. Kishimoto, I., Dubois, S. K., and Garbers, D. L. (1996) The heart communicates with the kidney exclusively through the guanylyl cyclase-A receptor: acute handling of sodium and water in response to volume expansion. *Proc Natl Acad Sci U S A* **93**, 6215-6219
232. Lopez, M. J., Garbers, D. L., and Kuhn, M. (1997) The guanylyl cyclase-deficient mouse defines differential pathways of natriuretic peptide signaling. *J Biol Chem* **272**, 23064-23068
233. Li, Y., Kishimoto, I., Saito, Y., Harada, M., Kuwahara, K., Izumi, T., Takahashi, N., Kawakami, R., Tanimoto, K., Nakagawa, Y., Nakanishi, M., Adachi, Y., Garbers, D. L., Fukamizu, A., and Nakao, K. (2002) Guanylyl cyclase-A inhibits angiotensin II type 1A receptor-mediated cardiac remodeling, an endogenous protective mechanism in the heart. *Circulation* **106**, 1722-1728
234. Scott, N. J., Ellmers, L. J., Lainchbury, J. G., Maeda, N., Smithies, O., Richards, A. M., and Cameron, V. A. (2009) Influence of natriuretic peptide receptor-1 on survival and cardiac hypertrophy during development. *Biochim Biophys Acta* **1792**, 1175-1184
235. Shuhaibar, L. C., Egbert, J. R., Norris, R. P., Lampe, P. D., Nikolaev, V. O., Thunemann, M., Wen, L., Feil, R., and Jaffe, L. A. (2015) Intercellular signaling via cyclic GMP diffusion through gap junctions restarts meiosis in mouse ovarian follicles. *Proc Natl Acad Sci U S A* **112**, 5527-5532
236. Wagner, B. M., Robinson, J. W., Lin, Y. W., Lee, Y. C., Kaci, N., Legeai-Mallet, L., and Potter, L. R. (2021) Prevention of guanylyl cyclase-B dephosphorylation rescues achondroplastic dwarfism. *JCI Insight* **6**
237. Suda, M., Ogawa, Y., Tanaka, K., Tamura, N., Yasoda, A., Takigawa, T., Uehira, M., Nishimoto, H., Itoh, H., Saito, Y., Shiota, K., and Nakao, K. (1998) Skeletal overgrowth in transgenic mice that overexpress brain natriuretic peptide.

Proceedings of the National Academy of Sciences of the United States of America **95**, 2337-2342
238. Coué, M., Badin, P. M., Vila, I. K., Laurens, C., Louche, K., Marquès, M. A., Bourlier, V., Mouisel, E., Tavernier, G., Rustan, A. C., Galgani, J. E., Joanisse, D. R., Smith, S. R., Langin, D., and Moro, C. (2015) Defective Natriuretic Peptide Receptor Signaling in Skeletal Muscle Links Obesity to Type 2 Diabetes. *Diabetes* **64**, 4033-4045
239. Miyashita, K., Itoh, H., Tsujimoto, H., Tamura, N., Fukunaga, Y., Sone, M., Yamahara, K., Taura, D., Inuzuka, M., Sonoyama, T., and Nakao, K. (2009) Natriuretic peptides/cGMP/cGMP-dependent protein kinase cascades promote muscle mitochondrial biogenesis and prevent obesity. *Diabetes* **58**, 2880-2892
240. Dickey, D. M., Yoder, A. R., and Potter, L. R. (2009) A familial mutation renders atrial natriuretic Peptide resistant to proteolytic degradation. *The Journal of biological chemistry* **284**, 19196-19202
241. Domino, S. E., Tubb, D. J., and Garbers, D. L. (1991) Assay of guanylyl cyclase catalytic activity. *Methods Enzymol* **195**, 345-355
242. Asirvatham-Jeyaraj, N., Gauthier, M. M., Banek, C. T., Ramesh, A., Garver, H., Fink, G. D., and Osborn, J. W. (2021) Renal Denervation and Celiac Ganglionectomy Decrease Mean Arterial Pressure Similarly in Genetically Hypertensive Schlager (BPH/2J) Mice. *Hypertension* **77**, 519-528
243. O'Connell, T. D., Swigart, P. M., Rodrigo, M. C., Ishizaka, S., Joho, S., Turnbull, L., Tecott, L. H., Baker, A. J., Foster, E., Grossman, W., and Simpson, P. C. (2006) Alpha1-adrenergic receptors prevent a maladaptive cardiac response to pressure overload. *J Clin Invest* **116**, 1005-1015
244. O'Connell, T. D., Ishizaka, S., Nakamura, A., Swigart, P. M., Rodrigo, M. C., Simpson, G. L., Cotecchia, S., Rokosh, D. G., Grossman, W., Foster, E., and Simpson, P. C. (2003) The alpha(1A/C)- and alpha(1B)-adrenergic receptors are required for physiological cardiac hypertrophy in the double-knockout mouse. *J Clin Invest* **111**, 1783-1791
245. Keppler, A., Gretz, N., Schmidt, R., Kloetzer, H.-M., Groene, H.-J., Lelongt, B., Meyer, M., Sadick, M., and Pill, J. (2007) Plasma creatinine determination in mice and rats: An enzymatic method compares favorably with a high-performance liquid chromatography assay. *Kidney International* **71**, 74-78
246. Marin-Grez, M., Fleming, J. T., and Steinhausen, M. (1986) Atrial natriuretic peptide causes pre-glomerular vasodilatation and post-glomerular vasoconstriction in rat kidney. *Nature* **324**, 473-476
247. Schewe, J., Seidel, E., Forslund, S., Marko, L., Peters, J., Muller, D. N., Fahlke, C., Stölting, G., and Scholl, U. (2019) Elevated aldosterone and blood pressure in a mouse model of familial hyperaldosteronism with ClC-2 mutation. *Nat Commun* **10**, 5155
248. Li, Y., Kishimoto, I., Saito, Y., Harada, M., Kuwahara, K., Izumi, T., Hamanaka, I., Takahashi, N., Kawakami, R., Tanimoto, K., Nakagawa, Y., Nakanishi, M., Adachi, Y., Garbers, D. L., Fukamizu, A., and Nakao, K. (2004) Androgen contributes to gender-related cardiac hypertrophy and fibrosis in mice lacking the gene encoding guanylyl cyclase-A. *Endocrinology* **145**, 951-958
249. Pandey, K. N., Oliver, P. M., Maeda, N., and Smithies, O. (1999) Hypertension associated with decreased testosterone levels in natriuretic peptide receptor-A gene-knockout and gene-duplicated mutant mouse models. *Endocrinology* **140**, 5112-5119

250. Yan, Z. P., Li, J. T., Zeng, N., and Ni, G. X. (2020) Role of extracellular signal-regulated kinase 1/2 signaling underlying cardiac hypertrophy. *Cardiol J*
251. Ueyama, T., Kawashima, S., Sakoda, T., Rikitake, Y., Ishida, T., Kawai, M., Yamashita, T., Ishido, S., Hotta, H., and Yokoyama, M. (2000) Requirement of activation of the extracellular signal-regulated kinase cascade in myocardial cell hypertrophy. *J Mol Cell Cardiol* **32**, 947-960
252. Rose, B. A., Force, T., and Wang, Y. (2010) Mitogen-activated protein kinase signaling in the heart: angels versus demons in a heart-breaking tale. *Physiol Rev* **90**, 1507-1546
253. Hayashi, D., Kudoh, S., Shiojima, I., Zou, Y., Harada, K., Shimoyama, M., Imai, Y., Monzen, K., Yamazaki, T., Yazaki, Y., Nagai, R., and Komuro, I. (2004) Atrial natriuretic peptide inhibits cardiomyocyte hypertrophy through mitogen-activated protein kinase phosphatase-1. *Biochem Biophys Res Commun* **322**, 310-319
254. Sugimoto, T., Kikkawa, R., Haneda, M., and Shigeta, Y. (1993) Atrial natriuretic peptide inhibits endothelin-1-induced activation of mitogen-activated protein kinase in cultured rat mesangial cells. *Biochem Biophys Res Commun* **195**, 72-78
255. Pandey, K. N., Nguyen, H. T., Li, M., and Boyle, J. W. (2000) Natriuretic peptide receptor-A negatively regulates mitogen-activated protein kinase and proliferation of mesangial cells: role of cGMP-dependent protein kinase. *Biochem Biophys Res Commun* **271**, 374-379
256. Hodgson-Zingman, D. M., Karst, M. L., Zingman, L. V., Heublein, D. M., Darbar, D., Herron, K. J., Ballew, J. D., de Andrade, M., Burnett, J. C., Jr., and Olson, T. M. (2008) Atrial natriuretic peptide frameshift mutation in familial atrial fibrillation. *N Engl J Med* **359**, 158-165
257. Chen, Y., Schaefer, J. J., Iyer, S. R., Harders, G. E., Pan, S., Sangaralingham, S. J., Chen, H. H., Redfield, M. M., and Burnett, J. C. (2020) Long-term blood pressure lowering and cGMP-activating actions of the novel ANP analog MANP. *Am J Physiol Regul Integr Comp Physiol* **318**, R669-R676
258. Nushiro, N., Abe, K., Seino, M., Itoh, S., and Yoshinaga, K. (1987) The effects of atrial natriuretic peptide on renal function and the renin-aldosterone system in anesthetized rabbits. *Tohoku J Exp Med* **152**, 301-310
259. Vellaichamy, E., Das, S., Subramanian, U., Maeda, N., and Pandey, K. N. (2014) Genetically altered mutant mouse models of guanylyl cyclase/natriuretic peptide receptor-A exhibit the cardiac expression of proinflammatory mediators in a gene-dose-dependent manner. *Endocrinology* **155**, 1045-1056
260. Otani, K., Tokudome, T., Kamiya, C. A., Mao, Y., Nishimura, H., Hasegawa, T., Arai, Y., Kaneko, M., Shioi, G., Ishida, J., Fukamizu, A., Osaki, T., Nagai-Okatani, C., Minamino, N., Ensho, T., Hino, J., Murata, S., Takegami, M., Nishimura, K., Kishimoto, I., Miyazato, M., Harada-Shiba, M., Yoshimatsu, J., Nakao, K., Ikeda, T., and Kangawa, K. (2020) Deficiency of Cardiac Natriuretic Peptide Signaling Promotes Peripartum Cardiomyopathy-Like Remodeling in the Mouse Heart. *Circulation* **141**, 571-588
261. Huang, P. L., Huang, Z., Mashimo, H., Bloch, K. D., Moskowitz, M. A., Bevan, J. A., and Fishman, M. C. (1995) Hypertension in mice lacking the gene for endothelial nitric oxide synthase. *Nature* **377**, 239-242
262. Tsai, E. J., and Kass, D. A. (2009) Cyclic GMP signaling in cardiovascular pathophysiology and therapeutics. *Pharmacol Ther* **122**, 216-238

263. Lee, D. I., Zhu, G., Sasaki, T., Cho, G. S., Hamdani, N., Holewinski, R., Jo, S. H., Danner, T., Zhang, M., Rainer, P. P., Bedja, D., Kirk, J. A., Ranek, M. J., Dostmann, W. R., Kwon, C., Margulies, K. B., Van Eyk, J. E., Paulus, W. J., Takimoto, E., and Kass, D. A. (2015) Phosphodiesterase 9A controls nitric-oxide-independent cGMP and hypertrophic heart disease. *Nature* **519**, 472-476
264. Suhasini, M., Li, H., Lohmann, S. M., Boss, G. R., and Pilz, R. B. (1998) Cyclic-GMP-dependent protein kinase inhibits the Ras/Mitogen-activated protein kinase pathway. *Mol Cell Biol* **18**, 6983-6994
265. Lukowski, R., Rybalkin, S. D., Loga, F., Leiss, V., Beavo, J. A., and Hofmann, F. (2010) Cardiac hypertrophy is not amplified by deletion of cGMP-dependent protein kinase I in cardiomyocytes. *Proc Natl Acad Sci U S A* **107**, 5646-5651
266. Patrucco, E., Domes, K., Sbroggió, M., Blaich, A., Schlossmann, J., Desch, M., Rybalkin, S. D., Beavo, J. A., Lukowski, R., and Hofmann, F. (2014) Roles of cGMP-dependent protein kinase I (cGKI) and PDE5 in the regulation of Ang II-induced cardiac hypertrophy and fibrosis. *Proc Natl Acad Sci U S A* **111**, 12925-12929
267. Hofmann, F. (2018) A concise discussion of the regulatory role of cGMP kinase I in cardiac physiology and pathology. *Basic Res Cardiol* **113**, 31
268. Nakamura, M., and Sadoshima, J. (2018) Mechanisms of physiological and pathological cardiac hypertrophy. *Nat Rev Cardiol* **15**, 387-407
269. Purcell, N. H., Wilkins, B. J., York, A., Saba-El-Leil, M. K., Meloche, S., Robbins, J., and Molkentin, J. D. (2007) Genetic inhibition of cardiac ERK1/2 promotes stress-induced apoptosis and heart failure but has no effect on hypertrophy in vivo. *Proc Natl Acad Sci U S A* **104**, 14074-14079
270. Kehat, I., and Molkentin, J. D. (2010) Extracellular signal-regulated kinase 1/2 (ERK1/2) signaling in cardiac hypertrophy. *Ann N Y Acad Sci* **1188**, 96-102
271. Bueno, O. F., De Windt, L. J., Tymitz, K. M., Witt, S. A., Kimball, T. R., Klevitsky, R., Hewett, T. E., Jones, S. P., Lefer, D. J., Peng, C. F., Kitsis, R. N., and Molkentin, J. D. (2000) The MEK1-ERK1/2 signaling pathway promotes compensated cardiac hypertrophy in transgenic mice. *EMBO J* **19**, 6341-6350
272. Lips, D. J., Bueno, O. F., Wilkins, B. J., Purcell, N. H., Kaiser, R. A., Lorenz, J. N., Voisin, L., Saba-El-Leil, M. K., Meloche, S., Pouysségur, J., Pagès, G., De Windt, L. J., Doevendans, P. A., and Molkentin, J. D. (2004) MEK1-ERK2 signaling pathway protects myocardium from ischemic injury in vivo. *Circulation* **109**, 1938-1941
273. Chen, Y., Liu, F., Chen, B. D., Li, X. M., Huang, Y., Yu, Z. X., Gao, X. L., He, C. H., Yang, Y. N., Ma, Y. T., and Gao, X. M. (2020) rAAV9-Mediated MEK1 Gene Expression Restores Post-conditioning Protection Against Ischemia Injury in Hypertrophic Myocardium. *Cardiovasc Drugs Ther* **34**, 3-14
274. Silberbach, M., Gorenc, T., Hershberger, R. E., Stork, P. J., Steyger, P. S., and Roberts, C. T. (1999) Extracellular signal-regulated protein kinase activation is required for the anti-hypertrophic effect of atrial natriuretic factor in neonatal rat ventricular myocytes. *J Biol Chem* **274**, 24858-24864
275. Babiker, F. A., De Windt, L. J., van Eickels, M., Thijssen, V., Bronsaer, R. J., Grohé, C., van Bilsen, M., and Doevendans, P. A. (2004) 17beta-estradiol antagonizes cardiomyocyte hypertrophy by autocrine/paracrine stimulation of a guanylyl cyclase A receptor-cyclic guanosine monophosphate-dependent protein kinase pathway. *Circulation* **109**, 269-276

276. van Eickels, M., Grohé, C., Cleutjens, J. P., Janssen, B. J., Wellens, H. J., and Doevendans, P. A. (2001) 17beta-estradiol attenuates the development of pressure-overload hypertrophy. *Circulation* **104**, 1419-1423
277. Tiemann-Boege, I., Navidi, W., Grewal, R., Cohn, D., Eskenazi, B., Wyrobek, A. J., and Arnheim, N. (2002) The observed human sperm mutation frequency cannot explain the achondroplasia paternal age effect. *Proc Natl Acad Sci U S A* **99**, 14952-14957
278. Naski, M. C., Wang, Q., Xu, J., and Ornitz, D. M. (1996) Graded activation of fibroblast growth factor receptor 3 by mutations causing achondroplasia and thanatophoric dysplasia. *Nat Genet* **13**, 233-237
279. Su, W. C., Kitagawa, M., Xue, N., Xie, B., Garofalo, S., Cho, J., Deng, C., Horton, W. A., and Fu, X. Y. (1997) Activation of Stat1 by mutant fibroblast growth-factor receptor in thanatophoric dysplasia type II dwarfism. *Nature* **386**, 288-292
280. Murakami, S., Balmes, G., McKinney, S., Zhang, Z., Givol, D., and de Crombrugghe, B. (2004) Constitutive activation of MEK1 in chondrocytes causes Stat1-independent achondroplasia-like dwarfism and rescues the Fgfr3-deficient mouse phenotype. *Genes Dev* **18**, 290-305
281. Potter, L. R. (2011) Natriuretic Peptide Metabolism, Clearance and Degradation. *The FEBS Journal* **278**, 1808-1817
282. Moffatt, P., Thomas, G., Sellin, K., Bessette, M. C., Lafreniere, F., Akhouayri, O., St-Arnaud, R., and Lanctot, C. (2007) Osteocrin is a specific ligand of the natriuretic Peptide clearance receptor that modulates bone growth. *J Biol Chem* **282**, 36454-36462
283. Thomas, G. P., Sellin, K., Bessette, M., Lafreniere, F., Lanctot, C., and Moffatt, P. (2004) Osteocrin, a Local Mediator of the Natriuretic System. In *26th Annual Meeting of the American Society for Bone and Mineral Research*, American Society for Bone and Mineral Research, Seattle, WA
284. Thomas, G., Moffatt, P., Salois, P., Gaumond, M. H., Gingras, R., Godin, E., Miao, D., Goltzman, D., and Lanctot, C. (2003) Osteocrin, a novel bone-specific secreted protein that modulates the osteoblast phenotype. *J Biol Chem* **278**, 50563-50571
285. Olney, R. C., Prickett, T. C., Espiner, E. A., Mackenzie, W. G., Duker, A. L., Ditro, C., Zabel, B., Hasegawa, T., Kitoh, H., Aylsworth, A. S., and Bober, M. B. (2015) C-type natriuretic peptide plasma levels are elevated in subjects with achondroplasia, hypochondroplasia, and thanatophoric dysplasia. *J Clin Endocrinol Metab* **100**, E355-359
286. Agoston, H., Khan, S., James, C. G., Gillespie, J. R., Serra, R., Stanton, L. A., and Beier, F. (2007) C-type natriuretic peptide regulates endochondral bone growth through p38 MAP kinase-dependent and -independent pathways. *BMC Dev Biol* **7**, 18
287. Esapa, C. T., Piret, S. E., Nesbit, M. A., Loh, N. Y., Thomas, G., Croucher, P. I., Brown, M. A., Brown, S. D., Cox, R. D., and Thakker, R. V. (2016) Mice with an N-Ethyl-N-Nitrosourea (ENU) Induced Tyr209Asn Mutation in Natriuretic Peptide Receptor 3 (NPR3) Provide a Model for Kyphosis Associated with Activation of the MAPK Signaling Pathway. *PLoS One* **11**, e0167916
288. Kamemura, N., Murakami, S., Komatsu, H., Sawanoi, M., Miyamoto, K., Ishidoh, K., Kishimoto, K., Tsuji, A., and Yuasa, K. (2017) Type II cGMP-dependent protein kinase negatively regulates fibroblast growth factor signaling by

phosphorylating Raf-1 at serine 43 in rat chondrosarcoma cells. *Biochem Biophys Res Commun* **483**, 82-87
289. Hirota, K., Yasoda, A., Kanai, Y., Ueda, Y., Yamauchi, I., Yamashita, T., Sakane, Y., Fujii, T., and Inagaki, N. (2018) Live imaging analysis of the growth plate in a murine long bone explanted culture system. *Sci Rep* **8**, 10332
290. Ueda, Y., Hirota, K., Yamauchi, I., Hakata, T., Yamashita, T., Fujii, T., Yasoda, A., and Inagaki, N. (2020) Is C-type natriuretic peptide regulated by a feedback loop? A study on systemic and local autoregulatory effect. *PLoS One* **15**, e0240023
291. Ganel, A., and Horoszowski, H. (1996) Limb lengthening in children with achondroplasia. Differences based on gender. *Clin Orthop Relat Res*, 179-183
292. Pannier, S., Mugniery, E., Jonquoy, A., Benoist-Lasselin, C., Odent, T., Jais, J. P., Munnich, A., and Legeai-Mallet, L. (2010) Delayed bone age due to a dual effect of FGFR3 mutation in Achondroplasia. *Bone* **47**, 905-915
293. Shuhaibar, L. C., Kaci, N., Egbert, J. R., Horville, T., Loisay, L., Vigone, G., Uliasz, T. F., Dambroise, E., Swingle, M. R., Honkanen, R. E., Biosse Duplan, M., Jaffe, L. A., and Legeai-Mallet, L. (2021) Phosphatase inhibition by LB-100 enhances BMN-111 stimulation of bone growth. *JCI Insight* **6**
294. Bartels, C. F., Bukulmez, H., Padayatti, P., Rhee, D. K., van Ravenswaaij-Arts, C., Pauli, R. M., Mundlos, S., Chitayat, D., Shih, L. Y., Al-Gazali, L. I., Kant, S., Cole, T., Morton, J., Cormier-Daire, V., Faivre, L., Lees, M., Kirk, J., Mortier, G. R., Leroy, J., Zabel, B., Kim, C. A., Crow, Y., Braverman, N. E., van den Akker, F., and Warman, M. L. a. (2004) Mutations in the transmembrane natriuretic peptide receptor NPR-B impair skeletal growth and cause acromesomelic dysplasia, type Maroteaux. *Am J Hum Genet* **75**, 27-34
295. Hachiya, R., Ohashi, Y., Kamei, Y., Suganami, T., Mochizuki, H., Mitsui, N., Saitoh, M., Sakuragi, M., Nishimura, G., Ohashi, H., Hasegawa, T., and Ogawa, Y. (2007) Intact kinase homology domain of natriuretic peptide receptor-B is essential for skeletal development. *J Clin Endocrinol Metab* **92**, 4009-4014
296. Holmes, G., Zhang, L., Rivera, J., Murphy, R., Assouline, C., Sullivan, L., Oppeneer, T., and Jabs, E. W. (2018) C-type natriuretic peptide analog treatment of craniosynostosis in a Crouzon syndrome mouse model. *PLoS One* **13**, e0201492
297. Morozumi, N., Yotsumoto, T., Yamaki, A., Yoshikiyo, K., Yoshida, S., Nakamura, R., Jindo, T., Furuya, M., Maeda, H., Minamitake, Y., and Kangawa, K. (2019) ASB20123: A novel C-type natriuretic peptide derivative for treatment of growth failure and dwarfism. *PLoS One* **14**, e0212680
298. Savarirayan, R., Irving, M., Bacino, C. A., Bostwick, B., Charrow, J., Cormier-Daire, V., Le Quan Sang, K. H., Dickson, P., Harmatz, P., Phillips, J., Owen, N., Cherukuri, A., Jayaram, K., Jeha, G. S., Larimore, K., Chan, M. L., Huntsman Labed, A., Day, J., and Hoover-Fong, J. (2019) C-Type Natriuretic Peptide Analogue Therapy in Children with Achondroplasia. *N Engl J Med* **381**, 25-35
299. Krejci, P. (2019) C-Type Natriuretic Peptide Analogue Therapy in Children with Achondroplasia. *N Engl J Med* **381**, 1291
300. Teixeira, C. C., Agoston, H., and Beier, F. (2008) Nitric oxide, C-type natriuretic peptide and cGMP as regulators of endochondral ossification. *Dev Biol* **319**, 171-178
301. Pejchalova, K., Krejci, P., and Wilcox, W. R. (2007) C-natriuretic peptide: an important regulator of cartilage. *Mol Genet Metab* **92**, 210-215

302. Prickett, T. C., and A Espiner, E. (2020) Circulating products of C-type natriuretic peptide and links with organ function in health and disease. *Peptides* **132**, 170363
303. Joshua, J., Schwaerzer, G. K., Kalyanaraman, H., Cory, E., Sah, R. L., Li, M., Vaida, F., Boss, G. R., and Pilz, R. B. (2014) Soluble guanylate cyclase as a novel treatment target for osteoporosis. *Endocrinology* **155**, 4720-4730
304. Kalyanaraman, H., Ramdani, G., Joshua, J., Schall, N., Boss, G. R., Cory, E., Sah, R. L., Casteel, D. E., and Pilz, R. B. (2017) A Novel, Direct NO Donor Regulates Osteoblast and Osteoclast Functions and Increases Bone Mass in Ovariectomized Mice. *J Bone Miner Res* **32**, 46-59
305. Bouxsein, M. L., Boyd, S. K., Christiansen, B. A., Guldberg, R. E., Jepsen, K. J., and Müller, R. (2010) Guidelines for assessment of bone microstructure in rodents using micro-computed tomography. *J Bone Miner Res* **25**, 1468-1486
306. Dudakovic, A., Camilleri, E. T., Riester, S. M., Paradise, C. R., Gluscevic, M., O'Toole, T. M., Thaler, R., Evans, J. M., Yan, H., Subramaniam, M., Hawse, J. R., Stein, G. S., Montecino, M. A., McGee-Lawrence, M. E., Westendorf, J. J., and van Wijnen, A. J. (2016) Enhancer of Zeste Homolog 2 Inhibition Stimulates Bone Formation and Mitigates Bone Loss Caused by Ovariectomy in Skeletally Mature Mice. *J Biol Chem* **291**, 24594-24606
307. Prickett, T. C., Bothwell, J. C., Yandle, T. G., Richards, A. M., and Espiner, E. A. (2012) Pharmacodynamic responses of plasma and tissue C-type natriuretic peptide to GH: correlation with linear growth in GH-deficient rats. *J Endocrinol* **212**, 217-225
308. Wagner, B. M., Robinson, J. W., Healy, C. L., Gauthier, M., Dickey, D. M., Yee, S. P., Osborn, J. W., O'Connell, T. D., and Potter, L. R. (2022) Guanylyl cyclase-A phosphorylation decreases cardiac hypertrophy and improves systolic function in male, but not female, mice. *FASEB J* **36**, e22069
309. Yang, L., Tsang, K. Y., Tang, H. C., Chan, D., and Cheah, K. S. (2014) Hypertrophic chondrocytes can become osteoblasts and osteocytes in endochondral bone formation. *Proc Natl Acad Sci U S A* **111**, 12097-12102
310. Touaitahuata, H., Cres, G., de Rossi, S., Vives, V., and Blangy, A. (2014) The mineral dissolution function of osteoclasts is dispensable for hypertrophic cartilage degradation during long bone development and growth. *Dev Biol* **393**, 57-70
311. Oliveira, M. H., Antunes-Rodrigues, J., Leal, A. M., Elias, L. L., and Moreira, A. C. (1993) Circadian variations of plasma atrial natriuretic peptide and corticosterone in rats with continuous or restricted access to food. *Life Sci* **53**, 1795-1801
312. Schipke, J., Roloff, K., Kuhn, M., and Mühlfeld, C. (2015) Systemic, but not cardiomyocyte-specific, deletion of the natriuretic peptide receptor guanylyl cyclase A increases cardiomyocyte number in neonatal mice. *Histochem Cell Biol* **144**, 365-375